

THE UNIVERSITY OF CALGARY

Experimental and Theoretical Studies of the Products from the
Reactions of Silylated Amidines with Organosulfur Chlorides

by

Ignacio Vargas-Baca

A DISSERTATION

SUBMITTED TO THE FACULTY OF GRADUATE STUDIES
IN PARTIAL FULFILLMENT OF THE REQUIREMENTS FOR THE
DEGREE OF DOCTOR OF PHILOSOPHY

DEPARTMENT OF CHEMISTRY

CALGARY, ALBERTA

SEPTEMBER, 1996

© Ignacio Vargas-Baca 1996

THE UNIVERSITY OF CALGARY
FACULTY OF GRADUATE STUDIES

The undersigned certify they have read, and recommend to the Faculty of Graduate Studies for acceptance, a dissertation entitled " Experimental and Theoretical Studies of the Products from the Reactions of Silylated Amidines with Organosulfur Chlorides" submitted by Ignacio Vargas-Baca in partial fulfillment of the requirements for the degree of Doctor of Philosophy.

T. Chivers

Supervisor, Dr. T. Chivers, Department of Chemistry

Tom Ziegler

Dr. T. Ziegler, Department of Chemistry

P. M. Boorman

Dr. P.M. Boorman, Department of Chemistry

R. E. Huber

Dr. R.E. Huber, Department of Biological Sciences

R. Oakley

Dr. R. Oakley, University of Guelph

Sept 6, 1996

Date

Abstract

The discovery of low temperature superconductivity in the inorganic polymer $(SN)_x$ in 1975 motivated vigorous research activity on sulfur-nitrogen chemistry. Comprehensive investigations revealed in a relatively short period of time a rich family of compounds which includes rings, cages and radicals. Carbon, phosphorus, and other elements were incorporated to reinforce and give flexibility to those structures. The intention, in part, is to prepare materials (e.g. molecular conductors) that take advantage of the unique polarity and π -electron richness of the S-N bond. The chemistry of the hybrid systems, and the natural extension to the heavier chalcogens Se and Te, is still under development. The subject still poses many questions about structure, bonding and reactivity. The reaction of trisilylated carbamidines, $R'CN_2(SiMe_3)_3$, with organosulfur chlorides, $RSCl$, affords a rich variety of products. These include mono- and tri- thiolato-substituted amidines, $R'C(NSR)[N(SiMe_3)_2]$ and $RCN_2(SR)_3$; radicals of the type $R'C(NSR)_2$; intensely coloured diazenes, $RSN=C(R')N=NC(R')=NSR$; S,S'-diorgano-1,5-dithiatetrazocines, $(R'C)_2N_4(SR)_2$; and a sixteen-membered ring, $(R'C)_4N_8(SR)_4$. This dissertation describes a series of experimental and theoretical (Density Functional Theory) studies on these systems, designed to provide an understanding of their structures, properties and the relationships between them.

The diazenes $RSN=C(R')N=NC(R')=NSR$ are shown to exist in several geometries. Three different structures have been characterized by X-ray diffraction, one of them as a part of this dissertation. The most stable structures involve close $S\cdots N$ contacts. They are stabilized by donation of a chalcogen lone pair into the $\pi^*(N=N)$ molecular orbital and steric

repulsion is alleviated by donation of a nitrogen lone pair into $\sigma^*(\text{N-S})$ orbitals. This bonding scheme can be extended to related organoselenium and organotellurium systems. Variable temperature nuclear magnetic resonance studies of $\text{PhSN}=\text{C}(\text{H})\text{N}=\text{NC}(\text{H})=\text{NSPh}$ in solution demonstrate that structural interconversion of isomers is possible.

The thiolato-substituted amidines, $\text{RC}(\text{NSR})[\text{N}(\text{SiMe}_3)_2]$, are readily hydrolyzed to form $\text{RC}(\text{NSR})(\text{NH}_2)$. The Se analogs were shown to exist in a tautomeric equilibrium with the purple imino isomer $\text{RC}[\text{NH}(\text{SeR})](\text{NH})$.

The kinetics of the decomposition of $\text{HCN}_2(\text{SPh})_3$ to $\text{PhSN}=\text{C}(\text{H})\text{N}=\text{NC}(\text{H})=\text{NPh}$ were studied. This process involves formation of the radical $\text{HC}(\text{NSPh})_2\cdot$, which decays with a second order rate law. Theoretical calculations and qualitative experiments suggest that the process is catalyzed by the $\text{PhS}\cdot$ radical. Theoretical calculations predict an asymmetric *E,Z* geometry for the radicals $\text{R}'\text{C}(\text{NSR})_2\cdot$.

Theoretical studies of the $(\text{R}'\text{C})_2\text{N}_4(\text{SR})_2$ rings provide an explanation for the experimentally observed folded C_{2v} geometry and the photochemical isomerization to the $\text{RSN}=\text{C}(\text{R}')\text{N}=\text{NC}(\text{R}')=\text{NR}$ diazenes.

The 1,4,5,7-dithiadiazepinyl radicals, $\text{C}_2\text{S}_2\text{N}_2\text{C}\cdot$, were investigated. Calculations on model systems suggest useful properties of these rings, such as low dimerization energies, for the preparation of molecular conductors. The silylated precursor $\text{S}(\text{C}_6\text{Cl}_4)\text{SN}(\text{SiMe}_3)\text{C}(4\text{-CH}_3\text{C}_6\text{H}_4)=\text{N}$ was isolated and structurally characterized. However, the preparation of the radicals is complicated by the instability of the radical and especially the cation. There is evidence that the 10 π -electron anionic heterocycle is stable.

Acknowledgments

I am grateful to the many people who during the last four years, helped me to go through the graduate program and to complete this dissertation. I thank:

Dr. T. Chivers for his support and advice, and especially for his leadership in research.

Dr. T. Ziegler for his guidance in the theoretical aspects of this work, the stimulating discussions, and all his help.

Dr. B. McGarvey (University of Windsor) for the ESR spectroscopic studies.

Dr. M. Parvez for the determination of the crystal structures by X-ray diffraction.

The members of the Chivers' group, past and present, for their collaboration and for providing the questions that motivated this investigation. Special thanks to Dr. K. McGregor and Dr. X. Gao, from whom I learned some of their many skills; and to P. Zoricak for his help and entertaining discussions.

The members of the Ziegler group, for their advice on the practical application of Density Functional Theory.

Dr. R. Yamdagni, D. Fox and Q. Wu for their services at the instrumentation laboratory.

The Department of Chemistry for all the help given to me. The assistance and support of Ms. G. Prihodko, Dr. H. Wieser, Dr. B.A. Keay and Dr. C.A Lucy are gratefully acknowledged.

The *Universidad Nacional Autónoma de México* (UNAM), which has funded my studies with a Graduate Scholarship, and Dr. L. Ruiz, my closest link with UNAM, for all her support and encouragement.

The University of Calgary for additional financial support in the form of the Graduate Council Scholarship, the J.B. Hyne Scholarship, a Graduate Teaching Assistantship and a Graduate Conference Travel Grant.

Dr. P.M. Boorman for kindly hosting me in his laboratory during my first months at the University of Calgary.

My fellow students and other members of the Department of Chemistry for all their help.

I am also grateful to my mother and my brothers, Carlos and Rosa Elvira, for being always close. Finally, I am indebted to Peter, Eva, Georg, Ulrike, Nicole and Sim, for a friendship that will never be forgotten.

Table of Contents

Approval Page.....	ii
Abstract	iii
Acknowledgments	v
Table of Contents	vii
List of Tables	xvi
List of Figures	xviii
List of Abbreviations	xxi
Formula Index	xxiii
1. Introduction	1
1.1. Synthetic Methods for Inorganic Heterocycles.....	2
1.1.1. Direct Combination of the Constituent Elements.....	2
1.1.2. Cycloaddition	3
1.1.3. Condensation Reactions.....	4
1.1.4. Modification of Existing Rings.....	5
1.1.5. Ring Expansion and Contraction.....	6
1.1.6. Other Methods	7
1.1.7. Kinetic vs. Thermodynamic Control of Products	9
1.2. Use of Si-N Reagents for the Synthesis of E-N (R = S, Se, Te) Compounds.....	11

1.2.1. The Reaction of MeSeCl ₃ with PhCN ₂ (Si(CH ₃) ₃) ₃	14
1.3. Objectives of this Dissertation	16
2. Molecular and Electronic Structures of the Diazenes of the Type	
REN=C(R')N=NC(R')=NER (E = S, Se, Te) (28)	18
2.1. Intramolecular D···E (D = O, N; E = S, Se, Te) Interactions.....	18
2.2. Molecular Structures of RSN=C(R')N=NC(R')=NSR (28)	21
2.2.1. Structurally Characterized Examples.....	21
2.2.1.1. Preparation of PhSN=C(H)N=NC(H)=NSPh (28f).....	21
2.2.1.2. X-ray Structure of PhSN=C(H)N=NC(H)=NSPh (28f)	21
2.2.1.3. Comparison with Other Structures	22
2.2.2. Relative Stabilities of the Geometrical Isomers of the Model Diazenes	
HSN=C(H)N=NC(H)=NSH (28i).....	24
2.2.3. Comparison Between Calculated and Experimental Structures	25
2.2.4. VT ¹ H NMR Spectra of PhSN=C(H)N=NC(H)=NSPh (28f).....	26
2.3. Electronic Structure	28
2.3.1. Frontier Orbitals of HSN=C(H)N=NC(H)=NSH (28i)	28
2.3.2. Electronic spectrum of RSN=C(R')N=NC(R')=NSR (28).....	29
2.3.3. Bonding in HEN=C(H)N=NC(H)=NEH (E = S, Se, Te) (28)	30
2.3.3.1. Analysis of the Total Atomization Energy.....	30
2.3.3.2. Fragment Orbital Analysis.	31

2.4.. Considerations for the synthesis of $\text{RTeN}=\text{C}(\text{R}')\text{N}=\text{NC}(\text{R}')=\text{NTeR}$ (28m).....	36
2.5. Summary.....	37
2.6. Computational Method and Calculations Details.....	38
2.7. Experimental Section	39
2.7.1. Reagents and General Procedures.....	39
2.7.2. Instrumentation	39
2.7.3. Preparation of $\text{PhSN}=\text{C}(\text{H})\text{N}=\text{NC}(\text{H})=\text{NSPh}$ (28f)	40
2.7.4. Attempted Preparation of $\text{MesTeN}=\text{C}(4\text{-CH}_3\text{C}_6\text{H}_4)\text{N}=\text{NC}(4\text{-CH}_3\text{C}_6\text{H}_4)=\text{NTeMes}$ (28m) (Mes = 2,4,6-($\text{CH}_3\text{C}_6\text{H}_2$))	40
3. Molecular and Electronic Structures of $\text{RC}(\text{NH}_2)(\text{NEPh})$ (R=H, 4- $\text{CH}_3\text{C}_6\text{H}_4$; E=S, Se) 41	
3.1. Preamble.....	41
3.2. Properties of 4- $\text{CH}_3\text{C}_6\text{H}_4\text{C}[\text{N}(\text{SiMe}_3)_2](\text{NEPh})$ (E = S, Se) (38a,b).....	42
3.3. Preparation and Characterization of $\text{HC}(\text{NH}_2)(\text{NSePh})$ (40e).....	43
3.3.1. X-ray Structure $\text{HC}(\text{NH}_2)(\text{NSePh})$ (40e)	44
3.4. Hydrolysis of 4- $\text{CH}_3\text{C}_6\text{H}_4\text{C}(\text{NEPh})[\text{N}(\text{SiMe}_3)_2]$ (E = S, Se) (38a, 38b).....	47
3.5. DFT Calculations for $\text{HC}(\text{NH}_2)(\text{NER})$ and $\text{HC}(\text{NH})[\text{NH}(\text{ER})]$ (E = S, Se; R = H, Ph) (40d-e' , 40d-e'').....	48
3.6. Summary.....	51
3.7. Experimental Section	52
3.7.1. Preparation of 4- $\text{CH}_3\text{C}_6\text{H}_4\text{C}[\text{N}(\text{SiMe}_3)_2](\text{SPh})$ (38a).....	52

3.7.2. Preparation of 4-CH ₃ C ₆ H ₄ C[N(SiMe ₃) ₂](SePh) (38b)	53
3.7.3. Preparation of 4-CH ₃ C ₆ H ₄ C(NH ₂)(SPh) (40c)	53
3.7.4. Reaction of HCN ₂ (SiMe ₃) ₃ with PhSeCl	54
3.7.5. Preparation of 4-CH ₃ C ₆ H ₄ C(NH ₂)(SePh) (40f)	54
4. Mechanistic Studies of the Formation of the Diazenes of the Type	
RSN=C(R')N=NC(R')=NSR (28)	56
4.1. CSN Radicals.....	56
4.1.1. Non-Cyclic CSN Radicals.....	56
4.2. The PhCN ₂ (ER) ₂ · (E = S, Se) Radical (29).....	58
4.3. Preparation of HCN ₂ (SPh) ₃	59
4.3.1. X-ray Structure of HCN ₂ (SPh) ₃ (31d)	60
4.4. Mechanism and Thermodynamics of the Formation of RSN=C(R')N=NC(R')=NSR	
(28)	63
4.4.1. Mechanism of the Thermolysis of HCN ₂ (SH) ₃ (31f).....	63
4.4.2. Thermodynamics: N-S Homolysis versus HS· Abstraction.....	66
4.5. Thermolysis of HCN ₂ (SPh) ₃ (31d)	68
4.5.1. Preliminary Visible and ¹ H NMR Spectroscopy Studies.....	68
4.5.2. Kinetic Study.....	69
4.5.3. NMR Study	71
4.5.4. ESR Study.....	71

4.6. Molecular Modeling of the Free Radical $\text{HC}(\text{NSH})_2\cdot$ (29e).....	73
4.6.1. Structure	75
4.6.2. Rotational Barrier and Interconversion.....	75
4.6.3. Electronic Structure, ESR and Visible Spectra.....	75
4.7. Decay of $\text{HCN}(\text{SPh})_2\cdot$ (29c).....	76
4.8. Effect of $\text{PhS}\cdot$ Radicals on the Thermolysis of $\text{HCN}_2(\text{SPh})_3$ (31d)	77
4.8.1.1. Effect of PhSSPh	78
4.8.1.2. Effect of PhSCl	78
4.8.1.3. Attempted Reaction of $\text{PhCN}_2(\text{SCCl}_3)_3$ (31b) with $4\text{-CH}_3\text{C}_6\text{H}_4\text{SCl}$	79
4.9. Summary.....	80
4.10. Details of Calculations.....	80
4.11. Experimental Section	81
4.11.1. Preparation of $\text{HCN}_2(\text{SPh})_3$	81
4.11.2. Visible Spectroscopy Studies of the Thermolysis of $\text{HCN}_2(\text{SPh})_3$	82
4.11.3. ^1H NMR Spectroscopy Studies of the Thermolysis of $\text{HCN}_2(\text{SPh})_3$	84
4.11.4. ESR Spectroscopy Studies of the Thermolysis of $\text{HCN}_2(\text{SPh})_3$	85
4.11.5. Visible Spectroscopy Studies of the Effect of PhSSPh on the Thermolysis of $\text{HCN}_2(\text{SPh})_3$	85
4.11.6. ^1H NMR Spectroscopy Studies of the Effect of PhSCl on the Thermolysis of $\text{HCN}_2(\text{SPh})_3$	86
4.11.7. Attempted Reaction of $\text{PhCN}_2(\text{SCCl}_3)_3$ (31b) with $4\text{-CH}_3\text{C}_6\text{H}_4\text{SCl}$	87

5. Theoretical Study of the $(R'C)_2N_4(SR)_2$ Ring.....	88
5.1. The Electronic Structure of Dithiatetrazocines	88
5.2. Molecular Structure of $(HC)_2N_4(SH)_2$ (27h).....	90
5.3. Relative Thermodynamic Stabilities of $(R'C)_2N_4(SR)_2$ and the Diazene Isomers $RSN=C(R')N=NC(R')=NSR$	93
5.4. Electronic Structure of $(HC)_2N_4(SH)_2$	94
5.4.1. Frontier Orbitals	94
5.4.2. Calculated Structure of the Anion $(HC)_2N_4(SH)_2^{2-}$ (51).....	94
5.4.3. Theoretical Basis for the Photochemical Isomerization of $(R'C)_2N_4(SR)_2$ Ring Systems	95
5.5. Summary.....	98
5.6. Details of Calculations.....	99
6. Studies on 1,4,5,7-Dithiadiazepinyl Radicals.....	100
6.1. Cyclic CSN Radicals	100
6.1.1. Four-Membered Rings.....	100
6.1.2. Five-Membered Rings.....	101
6.1.3. Larger Rings.....	102
6.2. Singly Occupied Molecular Orbitals (SOMOs)	104
6.3. Molecular Conductors Based on CSN radicals	104
6.4. 1,4,5,7-Dithiadiazepinyl Radicals.....	106

6.4.1. Molecular Structures of the Neutral Radicals $(\text{HC})_2\text{E}_2\text{N}_2\text{CH}\cdot$ (E = S, Se).....	107
6.4.2. Electronic Structures of the Radicals $(\text{HC})_2\text{E}_2\text{N}_2\text{CH}\cdot$ (E = S, Se)	108
6.4.3. The $[(\text{HC})_2\text{E}_2\text{N}_2\text{CH}]^+$ Cation and $[(\text{HC})_2\text{E}_2\text{N}_2\text{CH}]^-$ Anion (E = S, Se): Disproportionation Enthalpies	108
6.4.4. Dimers: Structures and Dimerization Energies	110
6.5. Attempted Synthesis of Cyclic $\text{C}_2\text{S}_2\text{N}_2\text{C}\cdot$ Radicals: Reaction of 1,2- $\text{C}_6\text{H}_4(\text{SCl})_2$ with $\text{PhCN}_2(\text{SiMe}_3)_3$ and PhSeCl	112
6.6. Isolation of $\overbrace{\text{S}(\text{C}_6\text{Cl}_4)\text{S}(\text{NSiMe}_3)(4\text{-CH}_3\text{C}_6\text{H}_4\text{C})=\text{N}}$ (74)	114
6.6.1. X-ray Structure of $\overbrace{\text{S}(\text{C}_6\text{Cl}_4)\text{S}(\text{NSiMe}_3)(4\text{-CH}_3\text{C}_6\text{H}_4\text{C})=\text{N}}$ (74)	115
6.6.2. By-products of the Synthesis of $\overbrace{\text{S}(\text{C}_6\text{Cl}_4)\text{S}(\text{NSiMe}_3)(4\text{-CH}_3\text{C}_6\text{H}_4\text{C})=\text{N}}$	118
6.7. Reactions of $\overbrace{\text{S}(\text{C}_6\text{Cl}_4)\text{S}(\text{NSiMe}_3)(4\text{-CH}_3\text{C}_6\text{H}_4\text{C})=\text{N}}$ (74).....	122
6.7.1. Attempted Reactions with ArECl (E = S, Se).....	122
6.7.2. Oxidation with Cl_2	122
6.7.3. Thermodynamics of the Ring Contraction	124
6.7.4. Attempts to Prepare the Anion $[\text{C}_6\text{Cl}_4\text{S}_2\text{N}_2\text{C}(4\text{-CH}_3\text{C}_6\text{H}_4)]^-$: Reaction of $\overbrace{\text{S}(\text{C}_6\text{Cl}_4)\text{S}(\text{NSiMe}_3)(4\text{-CH}_3\text{C}_6\text{H}_4\text{C})=\text{N}}$ with CsF	125
6.8. X-ray Structures of $(\text{C}_6\text{X}_4\text{S}_2)_2$ (X = F, Cl) (81a,b).....	126
6.9. Summary.....	131
6.10. Details of Calculations.....	131
6.11. Experimental Part.....	132
6.11.1. Reaction of 1,2- $\text{C}_6\text{H}_4(\text{SCl})_2$ with $\text{PhCN}_2(\text{SiMe}_3)_3$ and PhSeCl	132

6.11.2. Reaction of 4-RC ₆ H ₃ -1,2(SCl) ₂ (R = H, Me) with 4-CH ₃ C ₆ H ₄ CN ₂ (SiMe ₃) ₃	133
6.11.3. Reaction of C ₆ Cl ₆ with Na ₂ S and Fe: Preparation of C ₆ Cl ₄ -1,2-(SH) ₂	133
6.11.4. Chlorination of C ₆ Cl ₅ SH and C ₆ Cl ₄ (SH) ₂	134
6.11.5. Preparation of 4-CH ₃ C ₆ H ₄ C(NSC ₆ Cl ₅)(N(SiMe ₃) ₂) (38b).....	135
6.11.6. Reaction of C ₆ Cl ₄ -5,6-(SCl) ₂ with 4-CH ₃ C ₆ H ₄ CN ₂ (SiMe ₃) ₃	135
6.11.7. Attempted Reaction of $\overline{\text{S}(\text{C}_6\text{Cl}_4)\text{S}(\text{NSiMe}_3)(4\text{-CH}_3\text{C}_6\text{H}_4\text{C})=\text{N}}$ with PhSeCl	137
6.11.8. Attempted Reaction of $\overline{\text{S}(\text{C}_6\text{Cl}_4)\text{S}(\text{NSiMe}_3)(4\text{-CH}_3\text{C}_6\text{H}_4\text{C})=\text{N}}$ with 4-CH ₃ C ₆ H ₄ SCl	137
6.11.9. Reaction of $\overline{\text{S}(\text{C}_6\text{Cl}_4)\text{SN}(\text{SiMe}_3)\text{C}(4\text{-CH}_3\text{C}_6\text{H}_4)=\text{N}}$ with Cl ₂	138
6.11.10. Reaction of $\overline{\text{S}(\text{C}_6\text{Cl}_4)\text{S}(\text{NSiMe}_3)(4\text{-CH}_3\text{C}_6\text{H}_4\text{C})=\text{N}}$ with CsF.....	139
6.11.11. Crystallization of (C ₆ Cl ₄ S ₂) ₂ (81b)	140
6.11.12. Preparation of 2,3,4,5-F ₄ C ₆ H(SH).....	140
6.11.13. Preparation of 3,4,5,6-F ₄ C ₆ -1,2-(SH) ₂	141
6.11.14. Attempted Chlorination of 3,4,5,6-F ₄ C ₆ -1,2-(SH) ₂ . Preparation of (C ₆ F ₄ S ₂) ₂ (81a).....	141
 7. Concluding Remarks and Suggestions for Future Research	 142
7.1. The RSN=C(R')N=NC(R')=NR Diazenes and Related Close D··E (D = O, N; E = S, Se, Te) Contacts.....	142
7.1.1. Intermolecular Interactions	142
7.1.2. Materials with Potentially Useful Optical Properties.....	144

7.2. Mechanism of Formation of the Diazenes of the Type 28 . Properties of the RC(NPh) ₂ · (29) Radicals.....	148
7.2.1. Stable Radicals of the Type 29	148
7.2.2. Formation of Cyclic Products	149
7.3. The (R'C) ₂ N ₄ (SR) ₂ Rings	150
7.4. The 1,4,5,7-Dithiadiazepinyl Radicals.....	151

List of Tables

Table 2.1. Crystallographic data for <i>Z,E,Z</i> -PhSNC(H)N=NC(H)NSPh (28f).....	22
Table 2.2. Comparison of selected experimental bond lengths (Å) and bond angles (°) for 28f , 28g , and 28h , and the calculated values for model 28i in the geometries I-V	25
Table 2.3. Calculated contributions to the total atomization energy (kJ mol ⁻¹) of the exchange repulsions and orbital interactions for the model diazenes HEN=C(H)-N=N-(H)C=NEH (corrections not included).....	32
Table 2.4. Population of selected fragment orbitals in the model diazenes HEN=C(H)-N=N-(H)C=NEH	34
Table 3.1. Crystal data for HC(NH ₂)(NSePh) (40e).....	45
Table 3.2. Experimental and calculated values of selected bond distances (Å) and bond angles (°) for HC(NH ₂)(NSePh) (40e).....	45
Table 3.3. Total atomization energies (TAE) and electronic transition energies (ΔE) for HC(NH ₂)(NER) and HC(NH)[NH(ER)] (E = S, Se; R = H, Ph) (40a' , b' , d' , e' , 40a'' , b'' , d'' , e'').....	49
Table 4.1. Crystallographic data for HCN ₂ (SPh) ₃ (31d).....	61
Table 4.2. Selected bond lengths (Å), bond angles and torsion angles (°) for HCN ₂ (SPh) ₃ (31d).....	62

Table 4.3. Absorbances at 820 and 450 nm during the decomposition of $\text{HCN}_2(\text{SPh})_3$ (31d) 1.4×10^{-4} M in toluene solution, at 95°C ; $\text{Abs}_{820\text{nm}}^2$, and $\Delta\text{Abs}_{470\text{nm}} = [\text{Abs}_{470\text{nm},t} - \text{Abs}_{470\text{nm},t-1200\text{s}}]/1200\text{s}$	82
Table 4.4. Absorbance at 820 and 470 nm of the mixture $\text{HCN}_2(\text{SPh})_3$ 1.4×10^{-4} M, PhSSPh 1.3×10^{-3} M in toluene solution, at 95°C	85
Table 5.1. Comparison of molecular dimensions calculated for the model ring $(\text{HC})_2\text{N}_4(\text{SH})_2$ (27h), experimental data, and the calculated anion $(\text{HC})_2\text{N}_4(\text{SH})_2^{2-}$ (51).....	91
Table 6.1. Calculated bond distances (Å) and bond angles ($^\circ$) of $(\text{HC})_2\text{E}_2\text{N}_2(\text{CH})$ (E = S, Se).....	107
Table 6.2. Calculated (DFT) and experimental Vertical Ionization Potentials of 1,2,3,5- $(\text{HC})\text{N}_2\text{E}_2$ (E = S, Se) radicals (eV).	110
Table 6.3. Comparison of calculated properties of cyclic CSN and CSeN radicals (in kJ mol^{-1}).....	111
Table 6.4. Crystallographic data for $\overline{\text{S}(\text{C}_6\text{Cl}_4)\text{S}(\text{NSiMe}_3)(4\text{-CH}_3\text{C}_6\text{H}_4\text{C})=\text{N}}$ (74).....	116
Table 6.5. Bond lengths (Å), bond angles and torsion angles ($^\circ$) for $\overline{\text{S}(\text{C}_6\text{Cl}_4)\text{S}(\text{NSiMe}_3)(4\text{-CH}_3\text{C}_6\text{H}_4\text{C})=\text{N}}$ (74).....	117
Table 6.6. Crystallographic data for $(\text{C}_6\text{X}_4\text{S}_2)_2$ (X = F, Cl) (81a,b).	128
Table 6.7 Selected bond distances (Å) bond angles and torsion angles ($^\circ$) for $(\text{C}_6\text{F}_4\text{S}_2)_2$ (81a).....	129
Table 6.8. Selected bond distances (Å) bond angles and torsion angles ($^\circ$) for $(\text{C}_6\text{Cl}_4\text{S}_2)_2$ (81b).	130

List of Figures

Figure 2.1. ORTEP diagram for <i>Z,E,Z</i> -PhSN=C(H)N=NC(H)=NSPh (28f).	22
Figure 2.2. Relative energies (kJ mol ⁻¹) of geometrical isomers of HSN=C(H)N=NC(H)=NSH (28i).	24
Figure 2.3. Variable temperature ¹ H NMR spectra of PhSN=C(H)-N=N-C(H)=NSPh (28-f) in (a) toluene-d ₈ , (b) dichloromethane-d ₂	27
Figure 2.4. Relevant molecular orbitals of HSN=C(H)N=NC(H)=NSH (28i-I).	29
Figure 2.5. Orbital interactions for the N=N...S close contact: (a) donation (b) repulsion (c) backdonation.	30
Figure 2.6. Orbital interactions for the fragments (HS-N=C(H)·) ₂ and ·N=N·.	35
Figure 3.1. ORTEP diagram for HC(NH ₂)(NSePh) (40e) showing atom labeling (50% probability ellipsoids are shown for non-hydrogen atoms).	46
Figure 3.2. Packing diagram for HC(NH ₂)(NSePh) (40e).	46
Figure 3.3. Correlation diagram for the π orbitals of HC(NH ₂)(NEH) and HC(NH)[NH(EH)] (E = S, Se) (40a,d' , 40a,d'').	51
Figure 4.1. ORTEP diagram for HCN ₂ (SPh) ₃ (31d).	61
Figure 4.2. Evolution of the absorption spectrum during the decomposition of HCN ₂ (SPh) ₃ in toluene solution.	68

Figure 4.3. Time dependence of the absorbances at 820 and 450 nm during the decomposition of $\text{HCN}_2(\text{SPh})_3$ (31d) 1.4×10^{-4} M in toluene solution, at 95°C .	70
Figure 4.4. Dependence of the slope of $\Delta\text{Abs}_{450\text{nm}}$ on $\text{Abs}_{820\text{nm}}$ during the decomposition of $\text{HCN}_2(\text{SPh})_3$ (31d) 1.4×10^{-4} M in toluene solution, at 95°C . $r = 0.991$, slope: $3.6 \pm 0.1 \times 10^{-4} \text{ s}^{-1}$, y-intercept: $-2.1 \pm 0.4 \times 10^{-6} \text{ s}^{-1}$.	70
Figure 4.5. a) Integrated (absorption) ESR spectrum for the decomposition of $\text{HCN}_2(\text{SPh})_3$ (31d) in toluene solution. b) difference spectrum. c) calculated three line spectrum.	72
Figure 4.6. Potential energy diagram for the isomers of $\text{HC}(\text{NSH})_2$. Relative energy differences are given in kJ/mol.	74
Figure 4.7. SOMO for $\text{HCN}_2(\text{SH})_2 \cdot \mathbf{I}$.	76
Figure 4.8. Time dependence of the absorbances at 820 and 450 nm of the mixture $\text{HCN}_2(\text{SPh})_3$ 1.4×10^{-4} M, PhSSPh 1.3×10^{-3} M in toluene solution, at 95°C .	79
Figure 5.1. Mixing of molecular orbitals of dithiatetrazocines in D_{2h} and C_{2v} geometries.	89
Figure 5.2. Optimized structure of the model ring $(\text{HC})_2\text{N}_4(\text{SH})_2$ (27h).	90
Figure 5.3. Qualitative correlation diagram for $(\text{HC})_2\text{N}_4(\text{SH})_2$ in D_{2h} and C_{2v} geometries.	93
Figure 5.4 Qualitative correlation diagram for the isomerization of $(\text{HC})_2\text{N}_4(\text{SH})_2$ (27h) into $\text{HSN}=\text{C}(\text{H})-\text{N}=\text{N}-\text{C}(\text{H})=\text{NSH}$ (28i) based on the calculated energies of MOs I-IV.	97
Figure 6.1. SOMOs of some common CSN cyclic free radicals.	104
Figure 6.2. a) Radical plate. b) Uniform stack. c) dimer formation. d) crystal packing (Adapted from Figure 5 in reference 127c and Figure 1 in reference 128a).	105

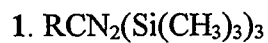
Figure 6.3. Calculated SOMO of the model ring $(\text{HC})_2\text{S}_2\text{N}_2(\text{CH})\cdot$ (68a).....	108
Figure 6.4. ORTEP diagram for $\text{S}(\text{C}_6\text{Cl}_4)\text{S}(\text{NSiMe}_3)(4\text{-CH}_3\text{C}_6\text{H}_4\text{C})=\text{N}$ (74).....	116
Figure 6.5. ^1H NMR spectrum for the second fraction of the product from the reaction of $\text{C}_6\text{Cl}_4\text{-5,6}(\text{SCL})_2$ with $4\text{-CH}_3\text{C}_6\text{H}_4\text{CN}_2(\text{SiMe}_3)_3$	120
Figure 6.6. ORTEP diagram for $(\text{C}_6\text{F}_4\text{S}_2)_2$ (81a).....	129
Figure 6.7. ORTEP diagram for the $(\text{C}_6\text{Cl}_4\text{S}_2)_2$ (81b).....	130

List of Abbreviations

DFT	Density Functional Theory
<i>E</i>	<i>Entgegen</i> , opposite. Used to designate a diastereomer in which the two groups of higher priority are on opposite sides of a double bond.
EA	Electron Affinity
EIMS	Electron Impact Mass Spectrometry
ESR	Electron Spin Resonance
Et	ethyl group, CH ₃ CH ₂
FABMS	Fast Atom Bombardment Mass Spectrometry
GCMS	Gas Chromatography Mass Spectrometry
HOMO	Highest Occupied Molecular Orbital
I.R.	Infrared
IP	Ionization Potential
<i>i</i> -Pr	<i>iso</i> -propyl group, (CH ₃) ₂ CH
LDA	Local Density Approximation
LUMO	Lowest Unoccupied Molecular Orbital
Me	methyl group, CH ₃
Mes	mesityl group, 2,4,6-(CH ₃) ₃ C ₆ H ₂
Mp.	Melting Point
NMR	Nuclear Magnetic Resonance
Ph	phenyl group, C ₆ H ₅

p-Tol	<i>para</i> -tolyl group, 4-CH ₃ C ₆ H ₄
SOMO	Singly Occupied Molecular Orbital
STO	Slater Type Orbital
TAE	Total Atomization Energy
TASF	[((CH ₃) ₂ N) ₃ S][F·FSi(CH ₃) ₃]
<i>t</i> -Bu	<i>tert</i> -butyl group, (CH ₃) ₃ C
THF	Tetrahydrofuran, C ₄ H ₈ O
<i>t</i> -Oct	<i>tert</i> -octyl group, ((CH ₃) ₃ C)(CH ₃) ₂ C
UV-vis	Ultraviolet-visible
VT	Variable Temperature
Z	<i>Zusammen</i> , together. Used to designate a diastereomer in which the two groups of higher priority are on the same side of a double bond.

Formula Index



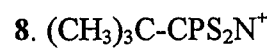
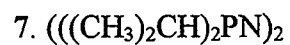
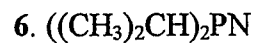
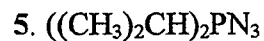
- a. $\text{R} = \text{C}_6\text{H}_5$
- b. $\text{R} = 4\text{-CH}_3\text{C}_6\text{H}_4$
- c. $\text{R} = 4\text{-CF}_3\text{C}_6\text{H}_4$
- d. $\text{R} = 4\text{-NO}_2\text{C}_6\text{H}_4$
- e. $\text{R} = \text{H}$

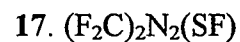
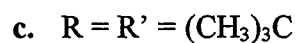
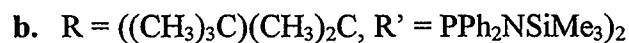
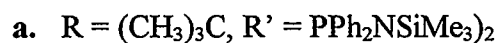
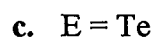
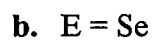
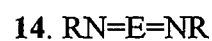
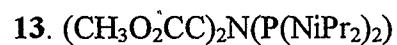
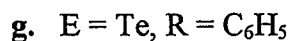
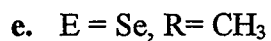
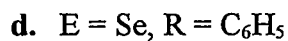
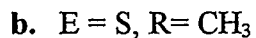
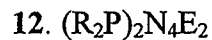
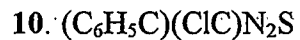


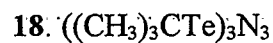
- a. $\text{X} = \text{F}$
- b. $\text{X} = \text{Cl}$



- a. $\text{R} = \text{CH}_3$
- b. $\text{R} = \text{CH}_3\text{CH}_2$
- c. $\text{R} = (\text{CH}_3)_2(\text{H})\text{C}$



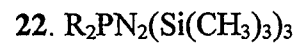




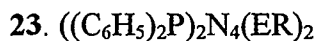
- a. $\text{E} = \text{S}, \text{R} = \text{C}_6\text{H}_5$
- b. $\text{E} = \text{S}, \text{R} = 4\text{-CH}_3\text{C}_6\text{H}_4$
- c. $\text{E} = \text{S}, \text{R} = 4\text{-CF}_3\text{C}_6\text{H}_4$
- d. $\text{E} = \text{S}, \text{R} = 4\text{-NO}_2\text{C}_6\text{H}_4$
- e. $\text{E} = \text{Se}, \text{R} = \text{C}_6\text{H}_5$
- f. $\text{E} = \text{Te}, \text{R} = \text{C}_6\text{H}_5$
- g. $\text{E} = \text{S}, \text{R} = \text{N}(\text{CH}_3)_2$



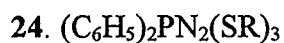
- a. $\text{R} = \text{C}_6\text{H}_5, \text{E} = \text{S}$



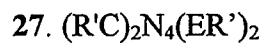
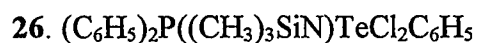
- a. $\text{R} = \text{C}_6\text{H}_5$
- b. $\text{R} = \text{CH}_3$
- c. $\text{R} = \text{CH}_3\text{CH}_2$



- a. $\text{E} = \text{Se}, \text{R} = \text{C}_6\text{H}_5$
- b. $\text{E} = \text{Se}, \text{R} = \text{CH}_3$
- c. $\text{E} = \text{Se}, \text{R} = \text{CH}_3\text{CH}_2$
- d. $\text{E} = \text{S}, \text{R} = \text{C}_6\text{H}_5$
- e. $\text{E} = \text{S}, \text{R} = 2,4\text{-(NO}_2)_2\text{C}_6\text{H}_3$
- f. $\text{E} = \text{Te}, \text{R} = \text{C}_6\text{H}_5$



- a. $\text{R} = \text{C}_6\text{H}_5$
- b. $\text{R} = 2,4\text{-(NO}_2)_2\text{C}_6\text{H}_3$



- a. $\text{E} = \text{Se}, \text{R} = \text{C}_6\text{H}_5, \text{R}' = \text{CH}_3$
- b. $\text{E} = \text{Se}, \text{R} = \text{C}_6\text{H}_5, \text{R}' = \text{C}_6\text{H}_5$
- c. $\text{E} = \text{S}, \text{R} = \text{C}_6\text{H}_5, \text{R}' = \text{C}_6\text{H}_5$
- d. $\text{E} = \text{S}, \text{R} = \text{C}_6\text{H}_5, \text{R}' = 4\text{-CF}_3\text{C}_6\text{H}_4$
- e. $\text{E} = \text{S}, \text{R} = \text{CCl}_3, \text{R}' = \text{C}_6\text{H}_5$
- f. $\text{E} = \text{S}, \text{R} = 2,4\text{-(NO}_2)_2\text{C}_6\text{H}_3, \text{R}' = \text{C}_6\text{H}_5$
- g. $\text{E} = \text{S}, \text{R} = \text{C}_6\text{H}_5, \text{R}' = 4\text{-BrC}_6\text{H}_4$
- h. $\text{E} = \text{S}, \text{R}' = \text{H}, \text{R} = \text{H}$

28. $\text{REN}=\text{C}(\text{R}')\text{N}=\text{NC}(\text{R}')=\text{NER}$

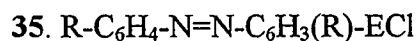
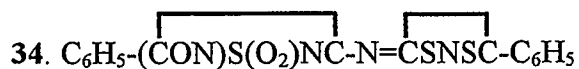
- a. $\text{E} = \text{Se}, \text{R} = \text{CH}_3, \text{R}' = \text{C}_6\text{H}_5$
- b. $\text{E} = \text{Se}, \text{R} = \text{C}_6\text{H}_5, \text{R}' = \text{C}_6\text{H}_5$
- c. $\text{E} = \text{S}, \text{R} = \text{C}_6\text{H}_5, \text{R}' = \text{C}_6\text{H}_5$
- d. $\text{E} = \text{S}, \text{R} = \text{C}_6\text{H}_5, \text{R}' = 4\text{-CH}_3\text{C}_6\text{H}_4$
- e. $\text{E} = \text{O}, \text{R} = \text{H}, \text{R}' = \text{H}$
- f. $\text{E} = \text{S}, \text{R} = \text{C}_6\text{H}_5, \text{R}' = \text{H}$
- g. $\text{E} = \text{S}, \text{R} = 4\text{-CH}_3\text{C}_6\text{H}_4, \text{R}' = 4\text{-CH}_3\text{C}_6\text{H}_4$
- h. $\text{E} = \text{S}, \text{R} = \text{C}_6\text{H}_5, \text{R}' = 2\text{-BrC}_6\text{H}_4$
- i. $\text{E} = \text{S}, \text{R} = \text{H}, \text{R}' = \text{H}$
- j. $\text{E} = \text{S}, \text{R} = \text{C}_6\text{H}_5, \text{R}' = 4\text{-BrC}_6\text{H}_4$
- k. $\text{E} = \text{S}, \text{R} = \text{C}_6\text{H}_5, \text{R}' = 2\text{-CF}_3\text{C}_6\text{H}_4$
- l. $\text{E} = \text{Se}, \text{R} = \text{H}, \text{R}' = \text{H}$
- m. $\text{E} = \text{Te}, \text{R} = \text{H}, \text{R}' = \text{H}$
- n. $\text{E} = \text{Te}, \text{R} = 2,3,6\text{-(CH}_3)_3\text{C}_6\text{H}_2, \text{R}' = 4\text{-CH}_3\text{C}_6\text{H}_4$

29. $\text{RCN}_2(\text{ER}')_2$

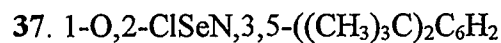
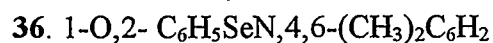
- a. $\text{E} = \text{S}, \text{R} = \text{C}_6\text{H}_5, \text{R}' = \text{C}_6\text{H}_5$
- b. $\text{E} = \text{Se}, \text{R} = \text{C}_6\text{H}_5, \text{R}' = \text{C}_6\text{H}_5$
- c. $\text{E} = \text{S}, \text{R} = \text{H}, \text{R}' = \text{C}_6\text{H}_5$
- d. $\text{E} = \text{S}, \text{R} = \text{H}, \text{R}' = \text{H}$
- e. $\text{E} = \text{S}, \text{R} = 2,4,6\text{-(C}_6\text{H}_5)_3\text{C}_6\text{H}_2, \text{R}' = 4\text{-ClC}_6\text{H}_4$



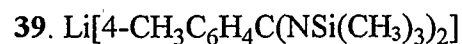
- a. $\text{E} = \text{S}, \text{R} = \text{C}_6\text{H}_5, \text{R}' = \text{C}_6\text{H}_5$
- b. $\text{E} = \text{S}, \text{R} = \text{C}_6\text{H}_5, \text{R}' = \text{SCCl}_3$
- c. $\text{E} = \text{S}, \text{R} = \text{C}_6\text{H}_5, \text{R}' = 2,4\text{-(NO}_2)_2\text{C}_6\text{H}_3$
- d. $\text{E} = \text{S}, \text{R} = \text{H}, \text{R}' = \text{C}_6\text{H}_5$
- e. $\text{E} = \text{Se}, \text{R} = \text{C}_6\text{H}_5, \text{R}' = \text{C}_6\text{H}_5$
- f. $\text{E} = \text{S}, \text{R} = \text{H}, \text{R}' = \text{H}$



- a. $\text{E} = \text{Se}, \text{R} = \text{CH}_3$
- b. $\text{E} = \text{Te}, \text{R} = \text{H}$



- a. $\text{E} = \text{S}, \text{R} = \text{C}_6\text{H}_5$
- b. $\text{E} = \text{Se}, \text{R} = \text{C}_6\text{H}_5$
- c. $\text{E} = \text{S}, \text{R} = \text{C}_6\text{Cl}_5$



40. $\text{RC}(\text{NER}')(\text{NH}_2)$

- a. $\text{E} = \text{S}, \text{R} = \text{R}' = \text{H}$
- b. $\text{E} = \text{S}, \text{R} = \text{H}, \text{R}' = \text{C}_6\text{H}_5$
- c. $\text{E} = \text{S}, \text{R} = 4\text{-CH}_3\text{C}_6\text{H}_4, \text{R}' = \text{C}_6\text{H}_5$
- d. $\text{E} = \text{Se}, \text{R} = \text{R}' = \text{H}$
- e. $\text{E} = \text{Se}, \text{R} = \text{H}, \text{R}' = \text{C}_6\text{H}_5$
- f. $\text{E} = \text{Se}, \text{R} = 4\text{-CH}_3\text{C}_6\text{H}_4, \text{R}' = \text{C}_6\text{H}_5$

41. $\text{R}_2\text{N-S}\cdot$

42. $\text{R}_2\text{N-S(O)}\cdot$

43. $[(\text{RN})_2\text{S}]^{\cdot-}$

44. $[\text{RNSNRR}']\cdot$

45. $[\text{RSNR}']\cdot$

46. $[(\text{RE})_2\text{N}]\cdot$

- a. $\text{E} = \text{S}, \text{R} = \text{C}_6\text{H}_5$
- b. $\text{E} = \text{Se}, \text{R} = \text{C}_6\text{H}_5$

47. $[((\text{CH}_3)_3\text{CN})_3\text{S}]^{\cdot-}$

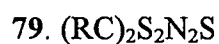
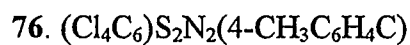
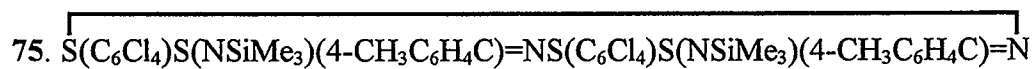
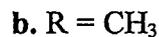
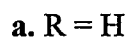
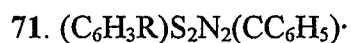
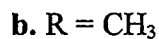
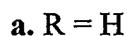
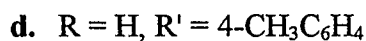
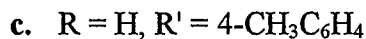
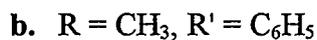
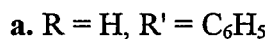
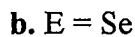
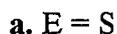
48. $[(((\text{CH}_3)_3\text{CN})_3\text{S})\text{Li}_2]_2$

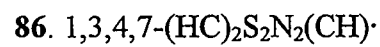
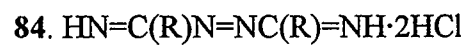
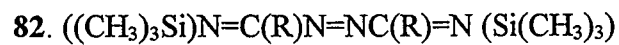
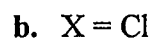
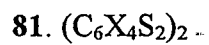
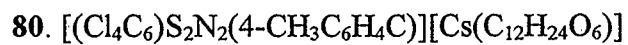
49. $(\text{C}_6\text{H}_5\text{E})_3\text{N}$

- a. $\text{E} = \text{S}$
- b. $\text{E} = \text{Se}$

50. $((\text{CH}_3)_3\text{CN})_2\text{Se}_6$

51. $(\text{HC})_2\text{N}_4(\text{SH})_2^{2-}$
52. $((\text{CH}_3)_3\text{CN})_2\text{S}(\text{Si}(\text{CH}_3)_2)$
53. $(\text{C}_6\text{H}_5\text{C})\text{N}_2\text{S}$
54. $((\text{C}_6\text{H}_5)_2\text{P})\text{N}_2\text{Se}$
55. $(\text{RC})_2\text{S}_2\text{N}$
- a. $\text{R} = \text{H}$
56. 1,3,2- $(\text{H}_4\text{C}_6)\text{S}_2\text{N}$
57. $(\text{H}_4\text{C}_6)\text{N}_2\text{S}$
58. 1,2,3- $(\text{H}_4\text{C}_6)\text{S}_2\text{N}$
59. $(\text{H}_{10}\text{C}_7)\text{S}_2\text{N}$
60. 1,3,2,4- $(\text{RC})\text{N}_2\text{S}_2$
61. 1,2,3,5- $(\text{RC})\text{N}_2\text{E}_2$
- a. $\text{E} = \text{S}, \text{R} = \text{H}$
- b. $\text{E} = \text{Se}, \text{R} = \text{H}$
62. $(\text{H}_6\text{C}_{10})\text{N}_2\text{S}$
63. $(\text{RC})_2\text{N}_3\text{S}$
64. $((\text{C}_6\text{H}_5)_2\text{P})_2\text{N}_3\text{S}$
65. $((\text{C}_6\text{H}_5)_2\text{P})(\text{RC})\text{N}_3\text{S}$
66. $((\text{C}_6\text{H}_5)_2\text{P})_3\text{N}_4\text{S}$
67. C_{13}H_9
68. 1,4,5,7- $(\text{HC})_2\text{E}_2\text{N}_2(\text{CH})$





1. Introduction

One of the areas of fastest development in contemporary Inorganic Chemistry is that concerned with the study of inorganic rings and cages. There has been an extensive discussion on the potential application of inorganic heterocycles and cluster structures as precursors of useful materials, such as new polymers [1] and electronic devices [2], to mention just two examples. Nevertheless the main interest in such chemical systems resides in their fundamental chemistry: researchers find it appealing to explore the properties of hitherto unknown species. Moreover, the synthesis of novel inorganic rings is still considered an area of “genuine synthetic challenge” [3].

Modern structural characterization techniques have reduced to, perhaps, two the key factors that limit progress in the field: (a) the availability of suitable precursor materials and (b) a full understanding of their reactivity patterns. For instance amidines, nitrogen containing compounds of the general formula $RC(=NH)NH_2$, have been known for nearly 120 years [4], and the trisilylated benzamidine derivative $PhCN_2(SiMe_3)_3$ (**1a**) was first prepared in 1973 [5]. However, the use of amidines in inorganic synthesis was studied comprehensively only after an improved preparation of **1a**, and several substituted derivatives, was published in 1987 [6]. Subsequently, chemists have established that reagents of the type **1** are useful in the preparation of both inorganic heterocycles and metal complexes [7, 8] and they are able to employ them to design the synthesis of new compounds. Notwithstanding this progress, there are a few cases in which the outcome of the reactions has been puzzling if not surprising. A remarkable example is the reaction of

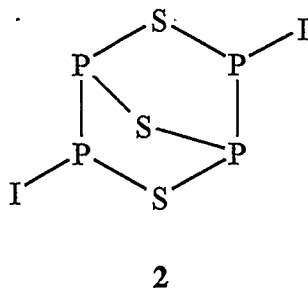
type 1 reagents with organosulfur and organoselenium chlorides, which affords, depending on the conditions, a variety of products including the simple derivatives of methathesis, persistent radicals, heterocycles and/or diazenes (*vide infra*). This dissertation is concerned with the properties of these compounds and the relationships between them. The end goal is to achieve control of the factors that select the formation of a certain product. To place this investigation in context, the rest of the chapter includes a general discussion of the methods employed in the synthesis of inorganic heterocycles, with some examples from recent publications. This is followed by a presentation of the background to the research topic and, finally, the specific objectives of this dissertation.

1.1. Synthetic Methods for Inorganic Heterocycles

Despite their diversity, most of the methods for the synthesis of inorganic rings can be classified into a few groups [9]:

1.1.1. Direct Combination of the Constituent Elements

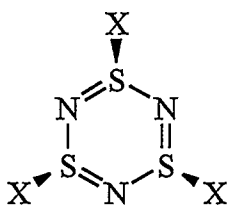
This method is of limited application since little control is exerted on the structure of the end products. It can be applied in few cases, especially for the synthesis of P,S-containing cages. For example, $P_4S_3I_2$ (**2**) is formed when equivalent amounts of P, S, and I are allowed to react in a homogeneous mixture at 120°C [10].



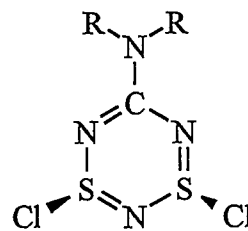
1.1.2. Cycloaddition

Some heterocycles that are composed of a regular alternating sequence of atoms can be prepared by the cycloaddition of the appropriate monomers. For example $\text{N}\equiv\text{S}-\text{F}$ is a gas that can be stored at room temperature in copper or Teflon vessels; at pressures above 1 atm it trimerizes to the heterocycle $(\text{NSF})_3$ (**3a**). The corresponding chloride, $\text{N}\equiv\text{S}-\text{Cl}$, is more reactive and forms $(\text{NSCl})_3$ (**3b**) rapidly at room temperature. This process is reversible both in solution and the gas phase [11], and $\text{N}\equiv\text{S}-\text{Cl}$ is best obtained by vacuum pyrolysis of $(\text{NSCl})_3$ [12].

The method of cycloaddition can be extended to incorporate other units in S-N heterocycles. The reaction of dialkylcyanamides with NSCl , generated from **3b**, produces $(\text{R}_2\text{NCN})(\text{NSCl})_2$ (**4**) [13].

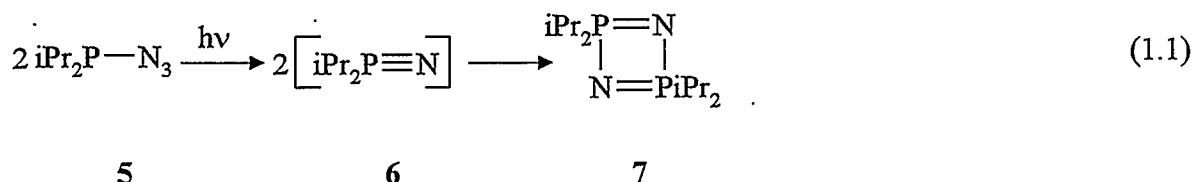


3 (a: X = F, b: X = Cl)

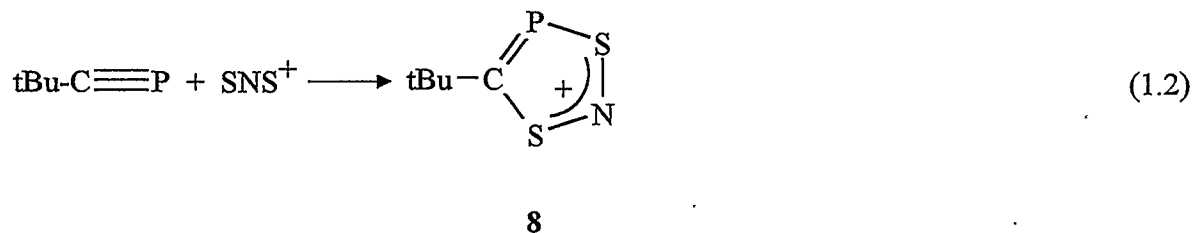


4 (R = Me, Et, *i*-Pr)

Due to their reactivity, some monomers must be prepared *in situ*. Photolysis of the phosphanyl azide **5** produces the phosphonitrile **6**, which dimerizes to produce the diazadiphosphete **7**, in the absence of trapping agents [14] (eq. 1.1).



Cycloaddition of two different reagents is also a useful technique. Usually each molecule contains two or more of the ring-forming atoms. For example, the linear cation SNS^+ undergoes cycloaddition reactions with unsaturated bonds. This approach allows the preparation of several heterocycles such as the 1,3,2,4-dithiazaphospholium cation **8** (eq. 1.2) [15].

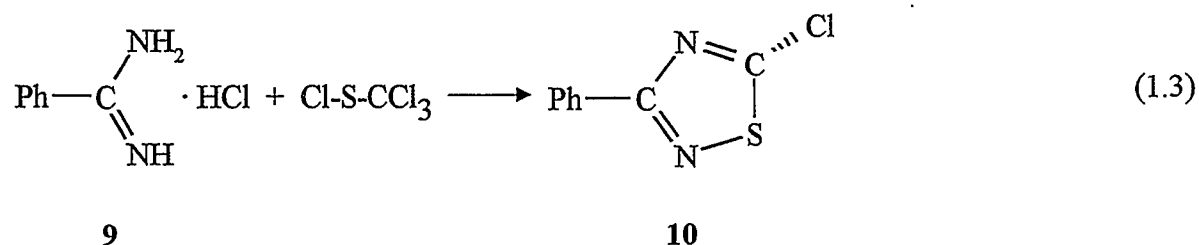


1.1.3. Condensation Reactions

In a condensation reaction two functional groups undergo methathesis to form new chemical bonds. One of them is the “target bond” that couples two fragments or closes the ring, while the other corresponds to a by-product. This type of reaction may involve the same type of functional groups (homofunctional condensation) or two different groups (heterofunctional condensation). Homofunctional condensation is limited to a few cases. The

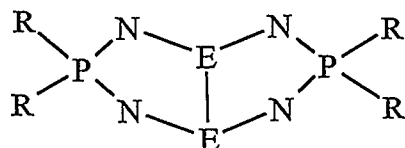
unstable silicon diols, $(R_2Si(OH)_2)$, condense to form cyclosiloxanes $(R_2SiO)_x$. Sulfamide, $SO_2(NH_2)_2$, produces the cyclic trimer $(SO_2NH)_3$; similar behavior has been observed for some phosphorus (V) oxoamides and thioamides [9].

Heterofunctional condensation is more versatile. It is the most commonly considered method when the synthesis of new heterocycles is designed. Usually the reagents are chosen so that the formation of the by-product is the thermodynamic driving force; precipitation of alkali-metal chlorides from organic media and evolution of HCl or Me_3SiX ($X = F, Cl$) are frequently used for this purpose. When benzamidine (**9**), as the hydrochloride, reacts with trichloromethanesulfonyl chloride, the elimination of HCl is so favorable that the 1,2,4-thiadiazole (**10**) is obtained (eq. 1.3) [16].

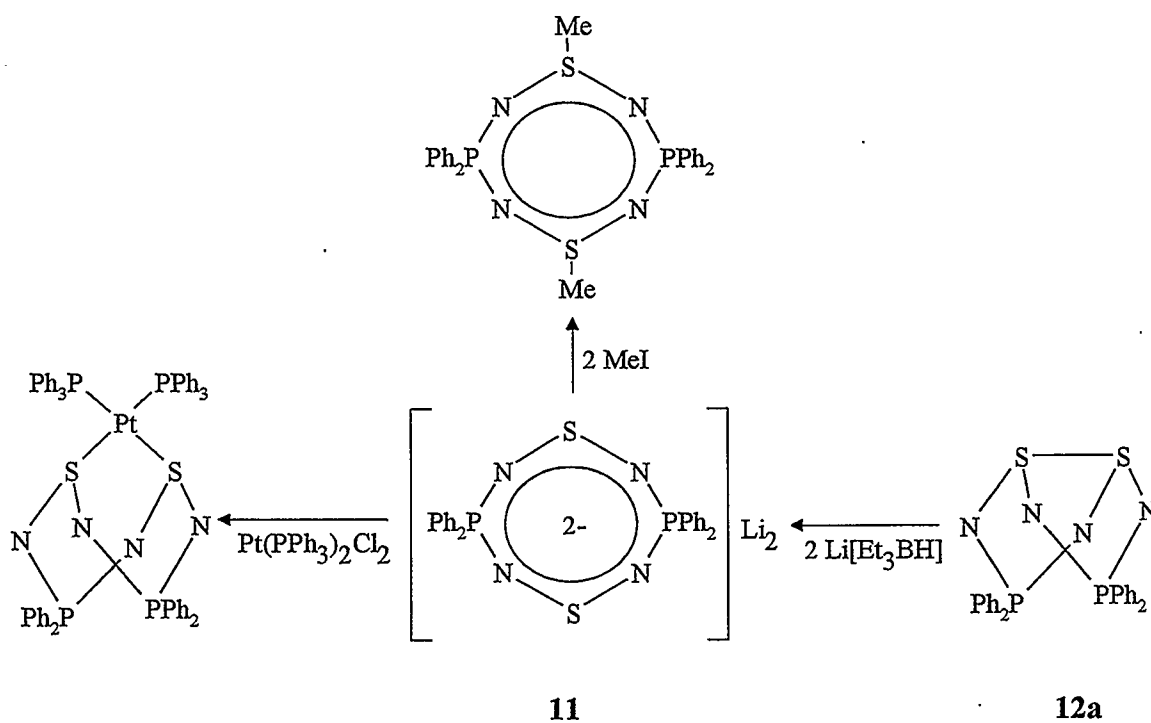


1.1.4. Modification of Existing Rings

Inorganic heterocycles can also be used as the starting materials for other rings. Addition of substituent groups, coordination to transition metals and change of oxidation state are processes that sometimes can be accomplished with preservation of the ring backbone. The chemistry of the dianionic derivative (**11**) of the 1,5-diphosphadithia-tetrazocine (**12a**) illustrates those reactions (see Scheme 1.1) [17].



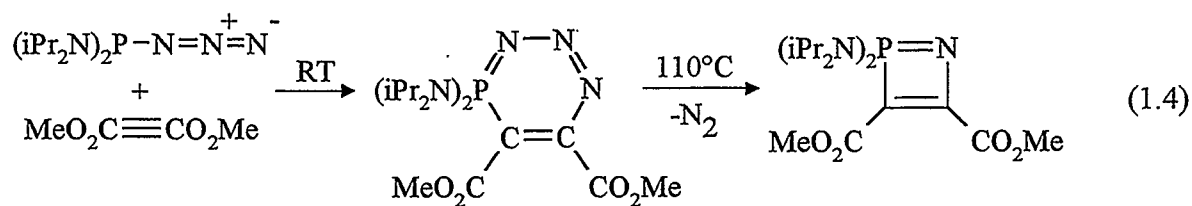
12 (a: E = S, R = C₆H₅; b: E = S, R = CH₃; c: E = S, R = CH₃CH₂; d: E = Se, R = C₆H₅,
e: E = Se, R = CH₃; f: E = Se, R = CH₃CH₂; g: E = Te, R = C₆H₅).



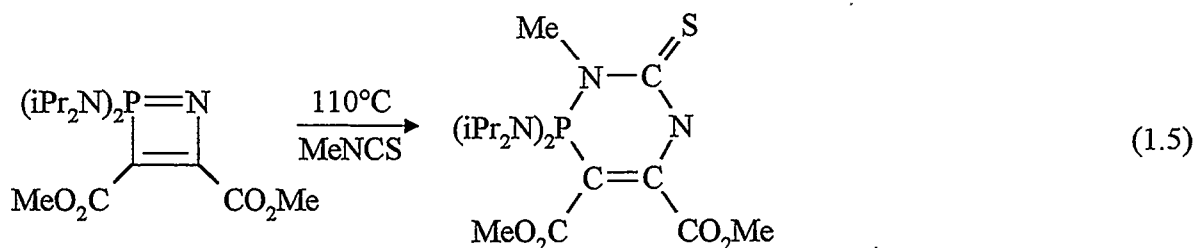
Scheme 1.1

1.1.5. Ring Expansion and Contraction

Several inorganic rings are thermally unstable and they may allow insertion or extrusion of ring fragments. The 1,2-azaphosphete **13** is conveniently prepared by contraction of a six-membered ring (eq. 1.4) [18]. On the other hand it can also undergo a ring expansion to form other six-membered cycles (eq. 1.5) [19].



13

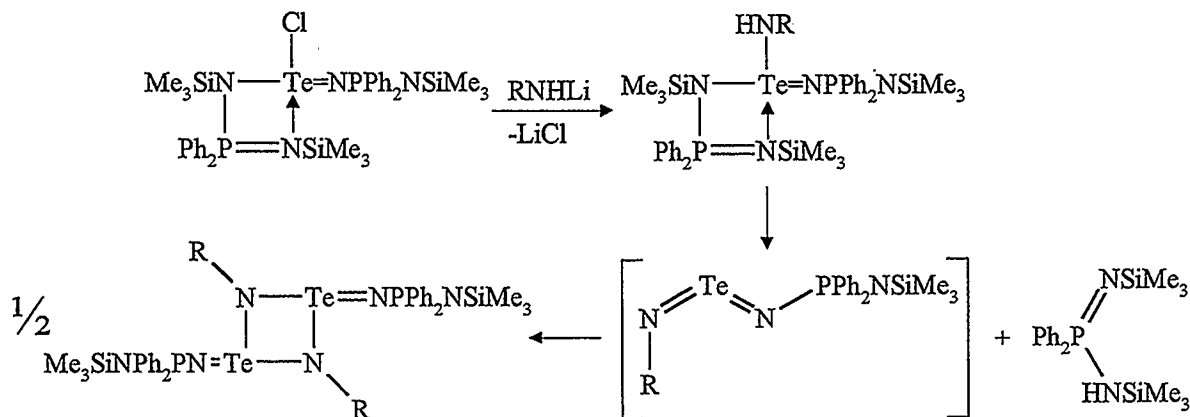


13

1.1.6. Other Methods

The synthetic methods illustrated above are understood well enough to be applied in the synthesis of new rings. However, some reactions lead to the formation of rings as an unexpected outcome.

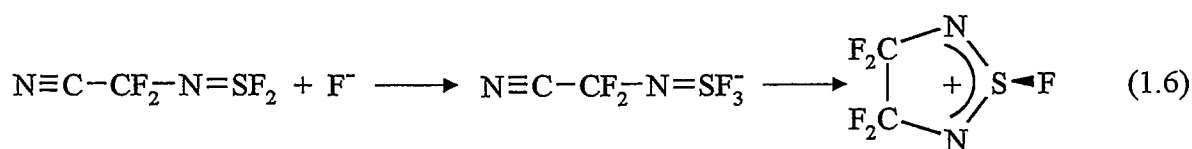
The most simple case would be that of an unanticipated cycloaddition. Until recently chalcogen diimides ($\text{RN}=\text{E}=\text{NR}$) (14) were only known, with certainty, for sulfur and selenium. Both are monomeric species. While the S species (14a) are thermally stable, the Se compounds (14b) decompose slowly at room temperature [20]. The first tellurium diimides (14c), prepared as depicted in Scheme 1.2, were found to exist as dimers (15a,b) both in solution and in the solid state. This feature offers an explanation for their remarkable thermal stability [21].



15 (a: R = ^tBu, b: ^tOct)

Scheme 1.2

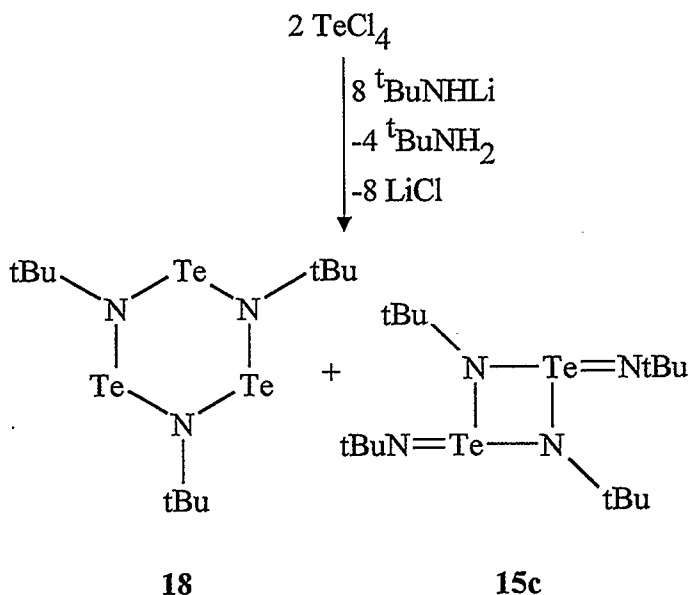
An interesting example of cyclization as the outcome of a rearrangement has been observed when F⁻, as [(Me₂N)₃S]⁺[Me₃SiF₃]⁻ (TASF), is added to N≡C-CF₂-N=SF₂ (**16**). The fluoride ion usually reacts with sulfur difluoride imides (R_FNSF₂) to yield sulfur trifluoride imide anions (R_FNSF₃⁻); such an anion is formed initially in the case of **16**, and then a rearrangement occurs to yield the cyclic bis(imino)fluorosulfinate **17** (eq. 1.6) [22].



16

17

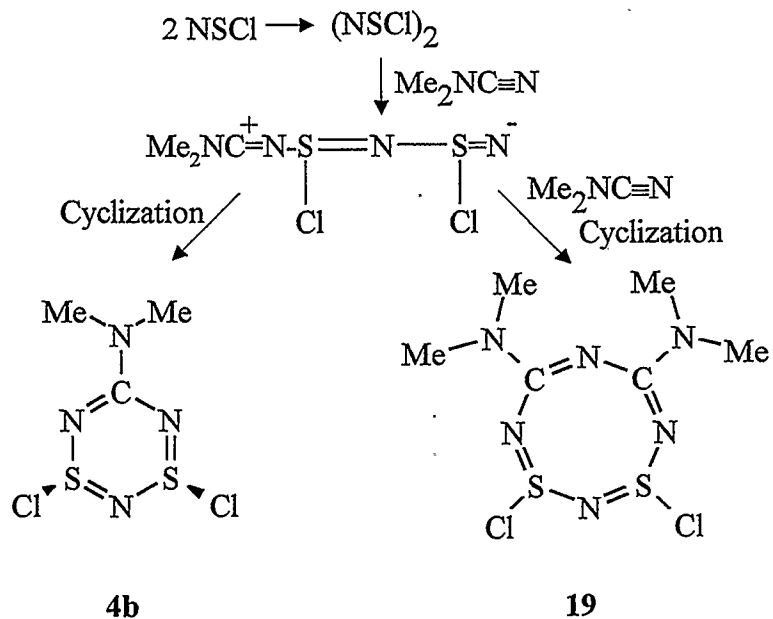
Some rearrangements are very complicated and all the steps in the reaction mechanism are not readily evident. That is the case of the reaction of TeCl₄ with lithium *tert*-butylamide, in a 1:4 ratio (Scheme 1.3). The dimer of a tellurium (IV) diimide (**15c**) is produced together with the six-membered Te (II) ring **18** [23]



Scheme 1.3

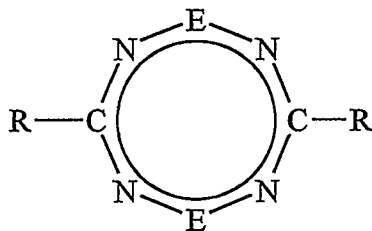
1.1.7. Kinetic vs. Thermodynamic Control of Products

Scheme 1.3 illustrates a problem commonly encountered in the synthesis of inorganic rings. Significant amounts of other products, either cyclic or acyclic, may be obtained simultaneously. In some cases it is possible to set the conditions deliberately to favor the formation of either the kinetic or the thermodynamic product. The preparation of the eight-membered ring $(\text{Me}_2\text{NCN})_2(\text{NSCl})_2$ (**19**) is linked to that of **4b**. It is proposed that NSCl readily dimerizes in CCl_4 solution and then dimethylcyanamide adds to the dimer to form a linear intermediate. The ring closure to form **4b** is relatively slow; if, at this point, a large excess of Me_2NCN is quickly added, a second cyanamide molecule links to the intermediate and subsequent cyclization produces **19** (See Scheme 1.4) (13).

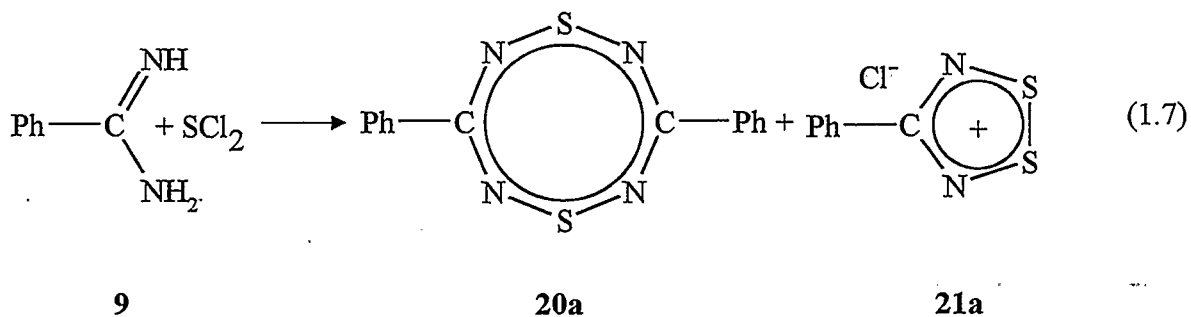


Scheme 1.4

When the reaction mechanism is not clear, kinetic control can only be attempted by lowering the temperature. Some reactions have to be carried out under thermodynamic control and the products must be separated from a complex mixture. For example, the reaction between benzamidine (9) and SCl_2 (eq. 1.7) affords 7.4% of the 1,5-dithiatetrazocine **20a** and 15% of the 1,2,3,5-dithiadiazolium cation **21a** [24].



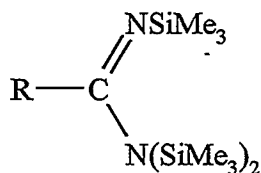
20 (a: E = S, R = C_6H_5 ; b: E = S, R = 4- $\text{CH}_3\text{C}_6\text{H}_4$; c: E = S, R = 4- $\text{CF}_3\text{C}_6\text{H}_4$; d: E = S, R = 4- $\text{NO}_2\text{C}_6\text{H}_4$; e: E = Se, R = C_6H_5 ; f: E = Te, R = C_6H_5).



1.2. Use of Si-N Reagents for the Synthesis of E-N (R = S, Se, Te) Compounds

In older synthesis the main sources of nitrogen for inorganic heterocycles were ammonia, organic amines, etc., usually in condensation reactions with main-group element halides. These reagents have been replaced by derivatives in which silicon substituents (usually the trimethylsilyl group) are present instead of hydrogen. The use of these compounds has several advantages: There is no production of hydrogen halides that may further react with the rings. Instead, less reactive trimethylsilyl halides are obtained and these by-products can easily be removed by *in vacuo* distillation; Si-X bond formation from the Si-N bond is a very strong driving force and some of these N-Si reagents are more stable or even more soluble than the parent (NH-containing) compounds.

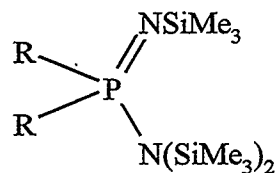
The use of substituted derivatives of the trisilylated reagents $\text{RCN}_2(\text{SiMe}_3)_3$ (**1**) and the lithium salts $[\text{RCN}_2(\text{SiMe}_3)_2]\text{Li}^+$ instead of the parent benzamidine in eq. 1.7, has permitted the preparation of a number of substituted dithiatetrazocines (**20a--d**), [25, 26].



1 (a: R = C₆H₅; b: R = 4-CH₃C₆H₄;

c: R = 4-CF₃C₆H₄; d: R = 4-NO₂C₆H₄;

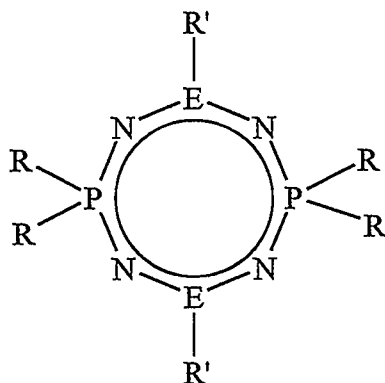
e: R = H)



22 (a: R = C₆H₅; b: R = CH₃;

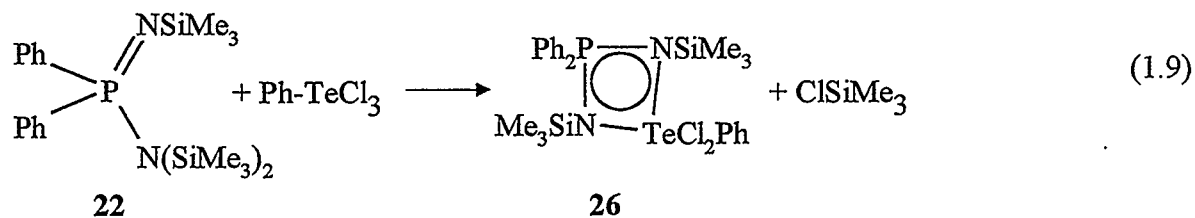
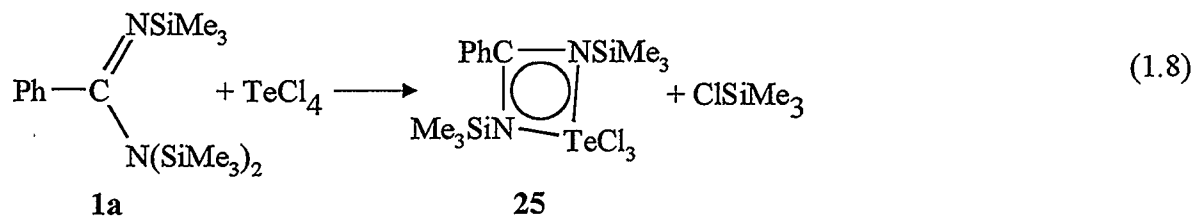
c: R = CH₃CH₂)

In the same way that the trisilylated benzamidines are useful reagents to incorporate the -N-C=N- unit in inorganic rings, the trisilylated phosphamidines (**22**) provide the -N-P=N- unit. The chemistry of these two families of reagents is similar. The reaction of **22** with SCl₂ produces the 1,5-diphosphadithiatetrazocines **12a,b** [27]; the yield is improved by using SOCl₂ instead of SCl₂; this also allows for the preparation of the ethyl derivative **12c**. The selenium analogs are prepared by reaction of **22** with "SeCl₃" [28]. Reaction of **22** with RSeCl₃ affords the Se,Se'-organo-substituted rings (**23a-c**) [29]. The sulfur analog **23d** is prepared by reaction of **22** with three equivalents of PhSCl [29b]. The reaction is thought to proceed through the thermally unstable Ph₂PN₂(SPh)₃ (**24a**).

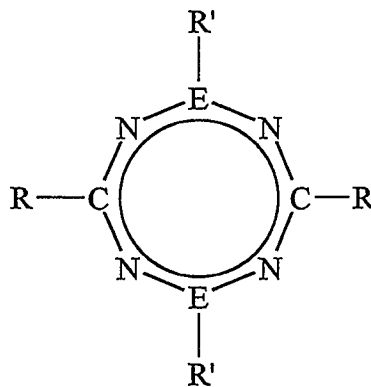


23 (a: E = Se, R = C₆H₅; b: E = Se, R = CH₃; c: E = Se, R = CH₃CH₂; d: E = S, R = C₆H₅; e: E = S, R = 2,4-(NO₂)₂C₆H₃; f: E = Te, R = C₆H₅).

The corresponding ditelluratetrazocines (**20f**) or diphosphaditelluratetrazocines (**12g**, **23f**) cannot be prepared by this method since Te-Cl bonds are less reactive than S-Cl and Se-Cl. The products of the cyclocondensation reactions of **1a** or **22a** with tellurium (IV) halides or organotellurium (IV) halides (eq. 1.8 and 1.9) are four-membered rings (**25**, **26**) in which the benzamidines and phosphamidines retain two trimethylsilyl groups [30, 31]. With respect to this behavior, the chemistry of tellurium resembles that of some transition-metal halides [8, 32].

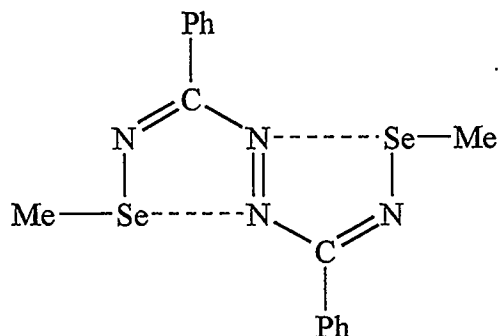


1.2.1. The Reaction of MeSeCl₃ with PhCN₂(Si(CH₃)₃)₃

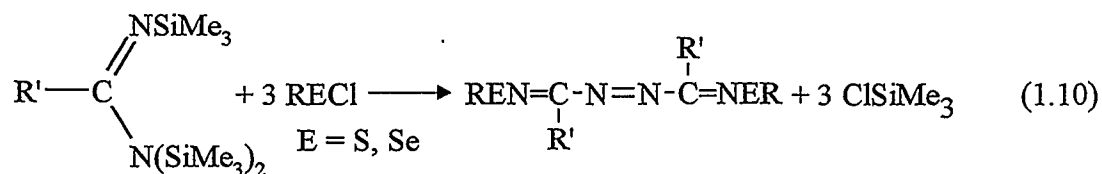


27 (a: E = Se, R = C₆H₅, R' = CH₃; b: E = Se, R = C₆H₅, R' = C₆H₅ c: E = S, R = C₆H₅, R' = C₆H₅; d: E = S, R = C₆H₅, R' = 4-CF₃C₆H₄; e: E = S, R = CCl₃, R' = C₆H₅; f: E = S, R = 2,4-(NO₂)₂C₆H₃, R' = C₆H₅; g: E = S, R = C₆H₅, R' = 4-BrC₆H₄; h: E = S, R' = H, R = H).

In view of the result of the reaction of **22** with RSeCl₃, the preparation of the 1,5-diselenatetrazocines **27a** and **27b** was attempted by reaction of **1a** with MeSeCl₃ and PhSeCl₃. Instead of the expected eight-membered ring, intensely purple coloured ($\lambda_{\text{max}} = 530\text{-}550\text{ nm}$) materials were obtained. Single crystal X-ray diffraction of the methyl derivative revealed the product to be the diazene **28a**, an isomer of **27a**. Remarkably the planar *Z,E,Z* structure exhibits two intramolecular Se...N contacts of 2.65 Å (the sum of van der Waals radii is 3.5 Å) [33].

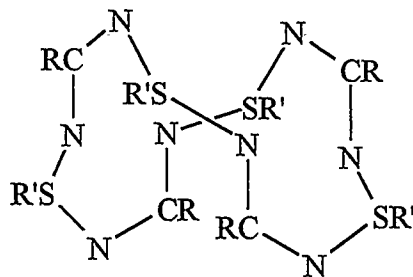
**28a**

Further study demonstrated that this type of diazene can also be obtained by reaction of the trisilylated reagents **1 a-c** with 3 equivalents of RSeCl or RSCl (eq. 1.10). This method allowed the preparation of several S and Se containing diazenes (**28a-d**). On the basis of spectroscopic characterization it was assumed they are isostructural with **28a** [34].

**1a-c****28a-d**

ESR spectra of the reaction mixtures of **1a** and PhECl (E= S, Se) suggested the presence of the radicals $\text{PhC}(\text{NEPh})_2\cdot$ (**29**), which can be envisioned as intermediates in the formation of the diazenes **28** (See Chapter 4).

In some cases, other products were obtained in addition to the diazenes. They were identified, on the basis of elemental analysis and molecular weight determinations, as the eight-membered rings **27d-f** [34]. Later it was shown that the reaction between $4\text{-BrC}_6\text{H}_4\text{CN}_2(\text{SiMe}_3)_3$ and PhSCl affords the eight-membered ring **27g**, the diazene **28j**, and even a sixteen-membered ring $(4\text{-BrC}_6\text{H}_4\text{C})_4\text{N}_8(\text{SC}_6\text{H}_5)_4$ (**30**) [35].



30 (R = 4-BrC₆H₄, R' = Ph)

1.3. Objectives of this Dissertation

The study of the reaction mixtures of trisilylated benzamidines (1) with RSCl, RSeCl, and RSeCl₃ is interesting for a number of reasons. It is apparent that a complicated set of factors exert kinetic and/or thermodynamic control to determine the outcome of the reaction; understanding such factors would permit the choice of the appropriate conditions to enhance the production of either the rings or the diazenes. These diazenes are interesting species to study due to the close E··N interactions. Finally, a novel type of radical, RC(NEPh)₂· has been added to the family of free radicals that frequently appear in organo-chalcogen-nitrogen chemistry [36], whose study is appealing by itself.

Dr. Chivers' group has implemented a wide investigation of the rich chemistry of these systems. The present dissertation is a part of those studies. Its objectives, as initially proposed, include the study of:

- The structure of the type **28** diazenes, including the nature of the E...N interactions and structural characterization of other examples.
- The properties of the free-radicals **29** and their role in the mechanism of diazene formation.
- The thermodynamic and/or kinetic relationship between the rings, free radicals and diazenes.
- The preparation of a novel family of cyclic free radicals, related to **29**.

The different aspects of this study required a combined experimental and theoretical approach. Approximate Density Functional Theory (DFT) has proven to be an efficient method for modeling the structures and properties of many electron systems such as transition metal complexes [37] and it can be a useful tool for the study of chalcogen-nitrogen compounds [38], especially in the case of the heavy chalcogens.

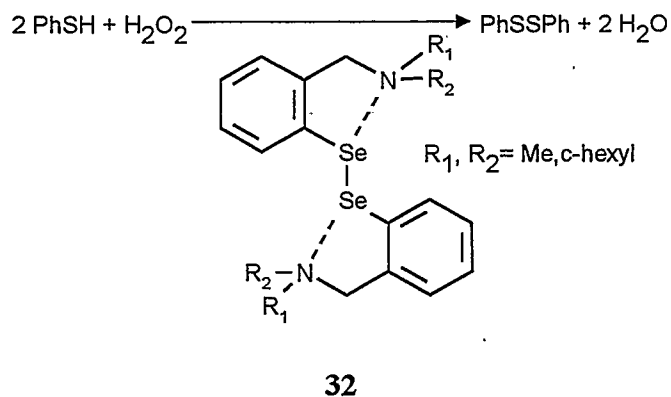
2. Molecular and Electronic Structures of the Diazenes of the Type



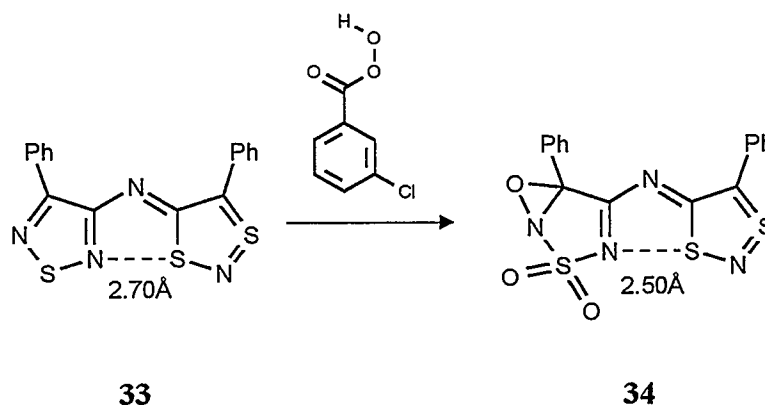
2.1. Intramolecular D...E (D = O, N; E = S, Se, Te) Interactions

In the structures of some main group compounds, especially the heavy ones, two atoms approach each other to a distance shorter than the sum of their corresponding van der Waals radii. These interactions have attracted interest because they are clearly weaker than covalent single bonds. The case most extensively studied is that of the *adducts* of dihalogen (X_2) molecules with both σ and π donors [40].

In organo-chalcogen chemistry this phenomenon is manifested as intramolecular close contacts between the chalcogen and an atom possessing lone pairs (D), usually nitrogen or oxygen. This sort of *intramolecular coordination* is known to have an important influence on the structures, properties and reactivity of certain chalcogen-nitrogen compounds [41]. For example, $\text{Se}\cdots\text{N}$ interactions are thought to play an important role in the reduction of peroxides by glutathione peroxidase, an essential selenium-containing antioxidant enzyme, and its synthetic mimics (see Scheme 2.1) [42]. On the other hand, a sulfur (II) center involved in an interannular contact with nitrogen displays a remarkable inertness towards oxidation with *meta*-chloroperbenzoic acid (Scheme 2.2) [43].



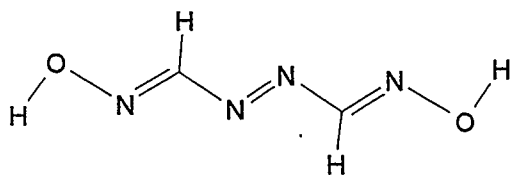
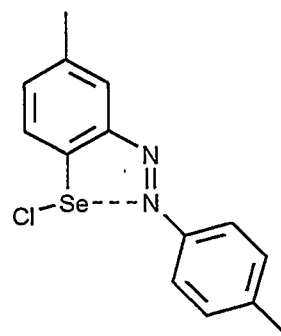
Scheme 2.1



Scheme 2.2

It is evident that a variety of geometrical isomers is possible for diazenes of the type $\text{REN}=\text{C}(\text{R}')\text{N}=\text{NC}(\text{R}')=\text{NER}$ (**28**). The structure that can be assumed *a priori* to be the most stable would be that which minimizes the repulsion between multiple lone pairs. This is the *E,E,E* configuration known for the azodialdehyde dioxime **28e** [44]. However, no other geometries have been characterized for these oxygen derivatives. This is in contrast to the previously described X-ray structure of $\text{MeSeN}=\text{C}(\text{Ph})\text{N}=\text{NC}(\text{Ph})=\text{NSeMe}$ (**28a**) with the short 2.65 Å $\text{Se}\cdots\text{N}$ contact (see Section 1.2.1). Very recently, a related, but much stronger, selenium-diazene interaction [$d(\text{Se}\cdots\text{N}) = 2.025$ Å] has been reported for the selenenyl

halide **35a** [45]. Since the sulfur derivatives **28c** and **28d** exhibit intense visible absorption bands similar to those of their Se analogues ($\lambda_{\text{max}} = 500\text{-}550\text{ nm}$, $\epsilon = 1 \times 10^4\text{ L mol}^{-1}\text{ cm}^{-1}$), it was assumed that they are also structurally related, but no X-ray structures were obtained [34].

**28e****35a**

These considerations raise a number of important questions about the structures and properties of this interesting class of type **28** diazenes: (a) What is the relative stability of the various possible geometrical and conformational isomers? (b) Is it possible to isolate and structurally characterize other geometrical isomers? (c) Can these isomers undergo interconversion? (d) What is the nature of the intramolecular E \cdots N interaction and why is it stronger in the halogeno derivative **35a** compared to **28a**?

2.2. Molecular Structures of $\text{RSN}=\text{C}(\text{R}')\text{N}=\text{NC}(\text{R}')=\text{NSR}$ (**28**)

2.2.1. Structurally Characterized Examples

2.2.1.1. Preparation of $\text{PhSN}=\text{C}(\text{H})\text{N}=\text{NC}(\text{H})=\text{NSPh}$ (**28f**)

This species can only be obtained as a pure crystalline sample, in low yield, from mixtures of $\text{HCN}_2(\text{SiMe}_3)_3$ and PhSCl which have been heated for several hours. The other sulfur analogs are usually obtained in high yields, but the isolation and purification of **28f** is complicated by solubility properties similar to those of PhSSPh . Hydrolysis of the material precluded purification by chromatography, which has been successful in the separation of related compounds [46]. No indication of the formation of rings was observed.

2.2.1.2. X-ray Structure of $\text{PhSN}=\text{C}(\text{H})\text{N}=\text{NC}(\text{H})=\text{NSPh}$ (**28f**)

The compound was crystallized from diethyl ether at -20°C , and its structure was determined by X-ray crystallography. An ORTEP diagram is presented in Figure 2.1. Relevant crystallographic data are included in Table 2.1. Selected bond distances and angles for **28f** are given in Table 2.2. The molecule is nearly planar, with fairly localized single and double bonds (*vide infra*). It is *Z* with respect to the $\text{C}=\text{N}$ bonds, *E* for the $\text{N}=\text{N}$ bond, and *anti* with respect to the single bonds. This structure is slightly different from that of **28a**, which is *syn* with respect to the $\text{C}-\text{N}$ single bond. This geometry leads to a $\text{S}\cdots\text{N}$ close contact (2.83 Å), so that the intramolecular $\text{S}\cdots\text{N}$ interaction gives rise to a four-membered rather than a five-membered ring.

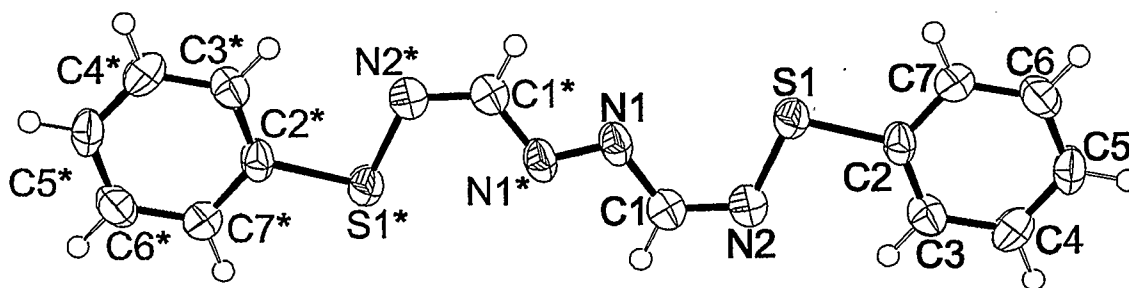


Figure 2.1. ORTEP diagram for *Z,E,Z*-PhSN=C(H)N=NC(H)=NSPh (**28f**).

Table 2.1. Crystallographic data for *Z,E,Z*-PhSNC(H)N=NC(H)NSPh (**28f**).

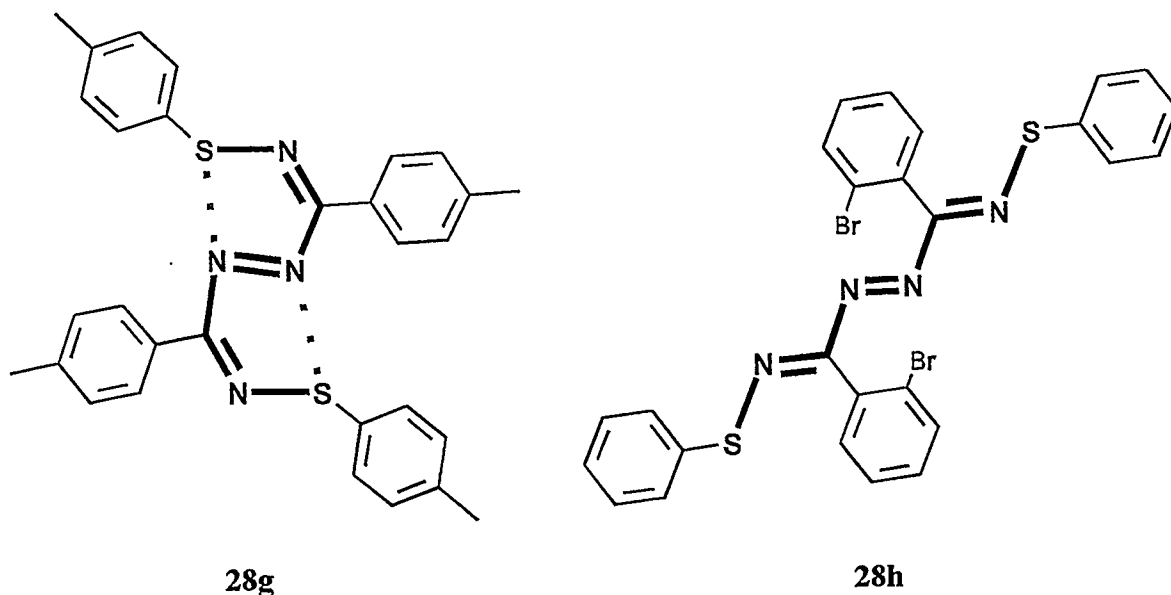
formula	C ₁₄ H ₁₂ N ₄ S ₂	Z	2
fw	300.40	T (°C)	-103
space group	P2 ₁ /n	λ (Å)	0.71069
a (Å)	5.897(6)	ρ _{calc} (g cm ⁻³)	1.392
b (Å)	18.458(10)	μ (cm ⁻¹)	3.66
c (Å)	7.050(8)	R	0.075
β (°)	110.97(5)	R _w	0.085
V (Å ³)	716 (1)	dimensions (mm)	0.63×0.33×0.15

2.2.1.3. Comparison with Other Structures

In the course of this study, other structures of diazenes of the type **28** were characterized in the Chivers' group. Diazenes **28g** and **28h** were prepared I.H. Krouse [47] and P. Zoricak [46], respectively. The derivative **28g** is a dark solid that yields purple solutions ($\lambda_{\text{max}} = 550$ nm) whereas **28h** forms dark red crystals ($\lambda_{\text{max}} = 469$ nm). The molecular geometries of these compounds are depicted in Scheme 2.3, which shows that

28g adopts the planar *Z,E,Z* structure previously established for the selenium analogue **28a**.

By contrast, **28h** exists as the *E,E,E* isomer (c.f. the oxygen derivative **28e**).



Scheme 2.3

The bond lengths and bond angles for the nearly planar SNCNNCNS chains are compared in Table 2.2 for all three derivatives. The bond lengths indicate essentially localized bonding with C-N single bonds in the range 1.39-1.41 Å, C=N double bonds in the range 1.30-1.32 Å, and an N=N double bond with a value of 1.25-1.29 Å (cf. 1.25 Å for azobenzenes) [48]. Significantly, the longest N=N bond [1.294(14) Å] is observed for **28g** in which the intramolecular S...N interaction [2.607(10) Å] is significantly stronger than in **28f**.

No X-ray structure has been determined for other derivatives of diazenes of the type **28**. However, if it is assumed that the colour is indicative of a specific geometric arrangement, the purple diazenes **28c**, **28d** [34], and **28j** [46] would have a structure like that of **28a**, and the red diazenes a geometry like that of **28h**.

2.2.2. Relative Stabilities of the Geometrical Isomers of the Model Diazenes

HSN=C(H)N=NC(H)=NSH (28i)

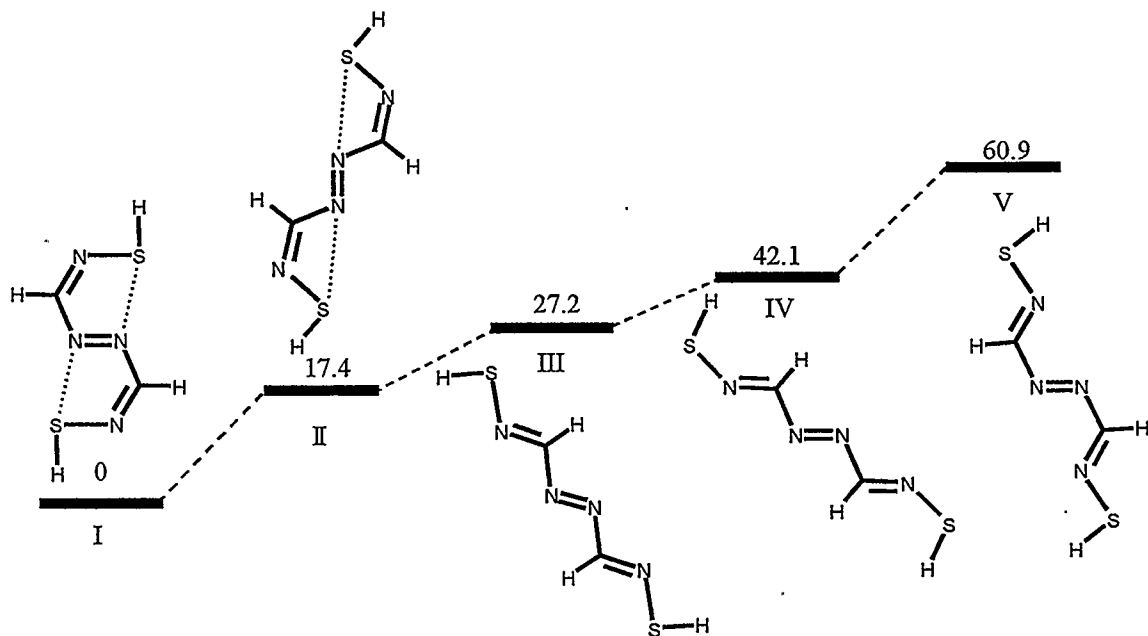


Figure 2.2. Relative energies (kJ mol^{-1}) of geometrical isomers of $\text{HSN}=\text{C}(\text{H})\text{N}=\text{NC}(\text{H})=\text{NSH}$ (**28i**).

In order to gain some insight into the relative stabilities of the geometrical isomers of the model diazene **28i**, DFT calculations were carried out for the five structures shown in Figure 2.2: **I** (cf. **28g**) and **II** (cf. **28f**) are *Z,E,Z* isomers, while **III** (cf. **28h**), **IV** and **V** are *E,E,E* isomers. The pair of *Z,E,Z* isomers **I** and **II** and the pair of *E,E,E* isomers **III** and **IV** are rotamers related to each other by rotation about the C-N single bonds. In view of the preference of diazenes for a *trans* (*E*) geometry [49], isomers with a *cis* (*Z*) orientation at the -N=N- bond were not considered. All structures were fully optimized assuming C_{2h}

symmetry. A total atomization energy analysis showed that isomer **I** is the most stable. However, isomer **II** is only 17.4 kJ mol⁻¹ higher in energy than **I** for the model system and isomer **III** is 27.2 kJ mol⁻¹ above **I**. Thus it is not surprising that examples of the three most stable geometrical isomers of these sulfur-substituted diazenes have now been isolated and structurally characterized.

2.2.3. Comparison Between Calculated and Experimental Structures

Table 2.2. Comparison of selected experimental bond lengths (Å) and bond angles (°) for **28f**, **28g**, and **28h**, and the calculated values for model **28i** in the geometries **I-V**.

Bond	28g	I	28f	II	28h	III	IV	V
N=N	1.294(14)	1.277	1.254(8)	1.292	1.26(1)	1.285	1.277	1.272
N-C	1.415(11)	1.367	1.392(7)	1.377	1.41(1)	1.381	1.363	1.393
C=N	1.303(11)	1.290	1.296(7)	1.296	1.32(1)	1.293	1.286	1.274
N-S	1.641(8)	1.680	1.658(5)	1.706	1.627(8)	1.696	1.646	1.672
S-C	1.779(7)		1.780(5)		1.74(1)			
N...S	2.607(10)	2.448	2.83	2.946				
Bond Angle								
NSC	100.3(4)		100.2(3)		100.9(5)			
SNC	124.7(7)	121.1	118.0(2)	120.0	118.5(6)	118.2	122.8	117.0
NCN	126.9(10)	126.9	122.4(5)	124.5	114.7(8)	115.0	118.4	124.9
CNN	112.2(7)	112.6	112.4(6)	112.2	113.5(9)	111.7	112.5	115.0

The calculated molecular dimensions of the isomers of **28i**, **I-V**, are compared with the experimental data for **28f-h** in Table 2.2. Although there is a reasonably good agreement between the calculated and the experimental data, this comparison is of limited validity in view of the inability of the model system to mimic the steric and/or electronic effects of the substituents on C and S in **28f-h**.

2.2.4. VT ^1H NMR Spectra of $\text{PhSN}=\text{C}(\text{H})\text{N}=\text{NC}(\text{H})=\text{NSPh}$ (**28f**)

Evidence for the co-existence and interconversion of several geometric isomers of **28f** in solution has been obtained from VT ^1H NMR studies in toluene- d_8 and CD_2Cl_2 . As indicated in Figure 2.3a the spectrum in toluene- d_8 at 300 K displays four singlets in the region δ 8.5-9.5 ppm. This spectrum is reproducibly obtained for different samples of **28f**. The relative intensities of these four resonances are independent, suggesting that each one corresponds to the formamidinic proton of a symmetrical, geometrical isomer of **28f**. It is evident that the red colour of the solutions of **28f** ($\lambda_{\text{max}} = 470$ nm) is due to the superposition of the absorptions from the different isomers.

When the solution is heated the middle two signals broaden and coalesce at 330 K, while the outer two signals also broaden. At higher temperatures all four resonances collapse to give a singlet. It is proposed that these observations may be attributed to the exchange between the *E,E,E*-rotamers **III** and **V** (via a C-N bond rotation) and, subsequently, an exchange with the *Z,E,Z*-isomers **I** and **II**. The higher energy of this second exchange process is ascribed to the intramolecular $\text{S}\cdots\text{N}$ interactions in **I** and **II**. The reverse of these changes is observed upon cooling the solution to 300 K.

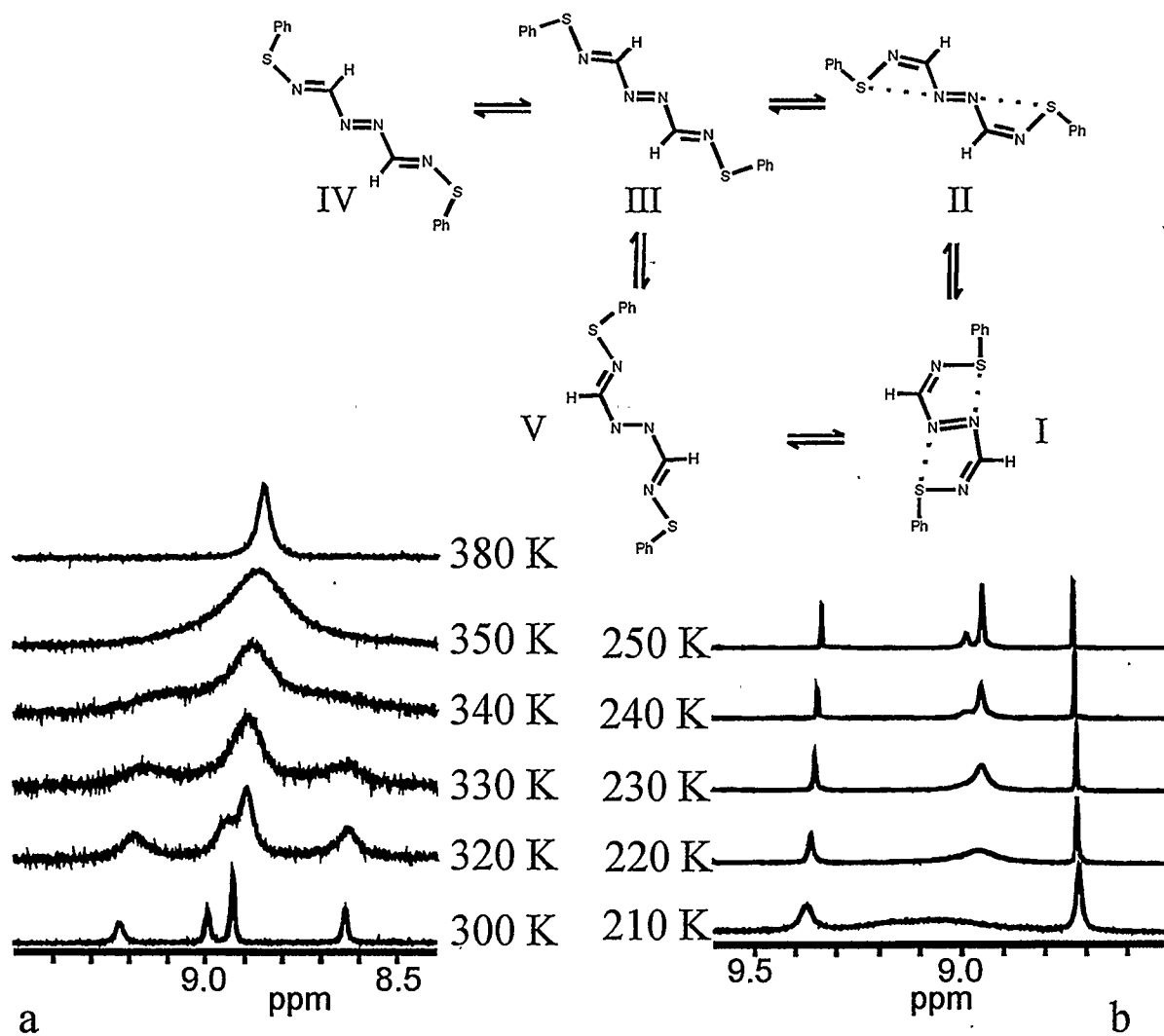


Figure 2.3. Variable temperature ^1H NMR spectra of PhSN=C(H)-N=N-C(H)=NSPh (**28-f**) in (a) toluene- d_8 , (b) dichloromethane- d_2 .

^1H NMR spectra of **28-f** below room temperature revealed a second exchange process. As indicated in Figure 2.3b these spectra were recorded in CD_2Cl_2 owing to the limited solubility of the sample in toluene- d_8 . Small changes in chemical shifts are observed upon changing the solvent, but the overall appearance of the NMR spectrum is unaltered. On cooling the solution, the outer two resonances do not change consistent with the

assignment of these signals to the thermodynamically most stable isomers **I** and **II** (see Figure 2.3b). However, the middle two resonances broaden to give a new set of poorly resolved signals at 210K, indicating that a very low energy exchange process is occurring even at this temperature. It is tentatively suggested that this process involves rotation about the S-N single bonds in the way that rotamers **III** and **IV** are related. The reverse of these changes is observed on warming the solution to room temperature.

No other diazene of the type **28** has been observed to exhibit the coexistence and dynamic equilibrium between different isomers. However, it is significant that in the synthesis and purification of the purple diazene $\text{PhSN}=\text{C}(4\text{-BrC}_6\text{H}_4)\text{N}=\text{NC}(4\text{-BrC}_6\text{H}_4)=\text{NSPh}$ (**28j**) an additional dark red product is present, but it quickly transforms into the purple product and cannot be isolated [46].

2.3. Electronic Structure

2.3.1. Frontier Orbitals of $\text{HSN}=\text{C}(\text{H})\text{N}=\text{NC}(\text{H})=\text{NSH}$ (**28i**)

The compositions of some molecular orbitals of diazenes type **28** are illustrated in Figure 2.4 for the model **28i** in the geometry **I**, under C_{2h} symmetry. The LUMO ($3b_g$) is a π orbital that can be identified with the $\pi^*(\text{N}=\text{N})$ orbital as the main contribution. The HOMO ($9a_g$) is a σ orbital involving primarily the lone pairs on the diazene nitrogen atoms.

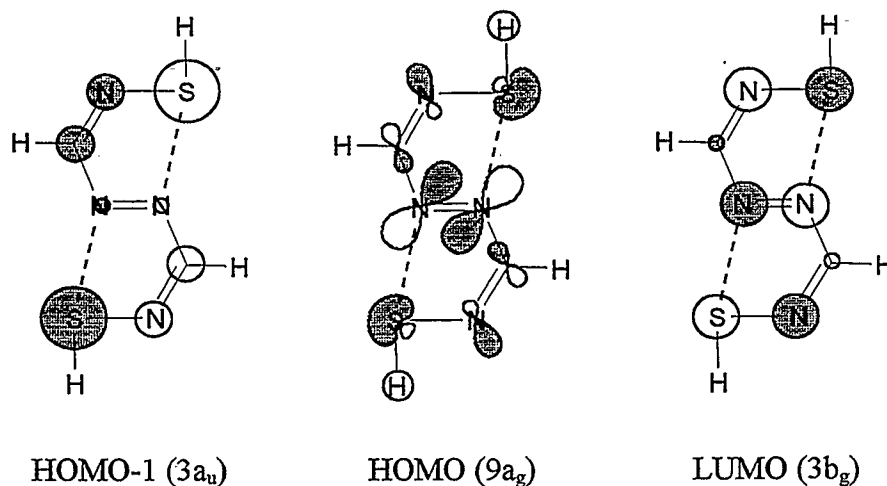


Figure 2.4. Relevant molecular orbitals of $\text{HSN}=\text{C}(\text{H})\text{N}=\text{NC}(\text{H})=\text{NSH}$ (**28i-I**).

2.3.2. Electronic spectrum of $\text{RSN}=\text{C}(\text{R}')\text{N}=\text{NC}(\text{R}')=\text{NSR}$ (**28**)

The determination of the electronic structure of the model diazene $\text{HSN}=\text{C}(\text{H})\text{N}=\text{NC}(\text{H})=\text{NSH}$ permits the identification of the first symmetry-allowed electronic transition as $\text{HOMO-1} (3a_u) \rightarrow \text{LUMO} (3b_g)$. The former MO is a π orbital which corresponds to a chalcogen-centered lone pair. Thus the intense colour of the type-**28** compounds is attributed to the excitation of an electron from a chalcogen lone pair to the $\pi^*(\text{N}=\text{N})$ orbital.

2.3.3. Bonding in HEN=C(H)N=NC(H)=NEH (E = S, Se, Te) (28)

2.3.3.1. Analysis of the Total Atomization Energy

It is apparent from the DFT calculations that the intramolecular S \cdots N interactions observed for the *Z,E,Z*-isomers **28g** and **28f** have a stabilizing influence. Frequently this “intramolecular coordination” is explained, on the basis of qualitative arguments, as donation of the nitrogen lone pair ($\sigma(\text{N})\text{lp}$) into the $\sigma^*(\text{S-X})$ orbitals (Figure 2.5a) [45]. However this simplistic picture neglects a lone pair of the chalcogen ($\sigma(\text{S})\text{lp}$) which also has an orientation suitable to interact repulsively with $\sigma(\text{N})\text{lp}$ (Figure 2.5b) and is even closer in energy than the $\sigma^*(\text{S-X})$ orbitals. Another neglected interaction is π -“backdonation” of a chalcogen lone pair ($\pi(\text{S})\text{lp}$) into a suitable orbital, such as $\pi^*(\text{N=N})$ (Figure 2.5c).

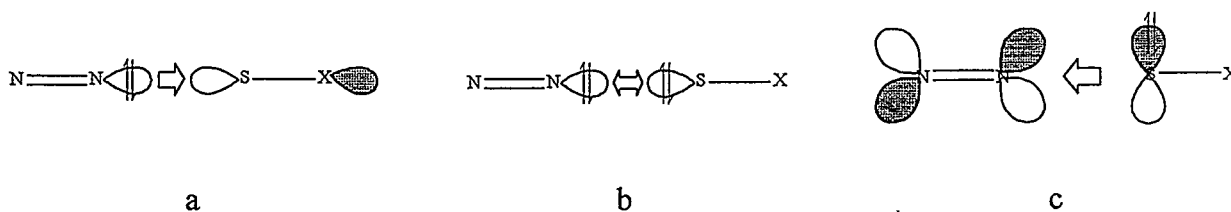


Figure 2.5. Orbital interactions for the N=N \cdots S close contact: (a) donation (b) repulsion (c) backdonation.

This balance of interactions was studied by comparing the contributions to the total atomization energy in models **28iII** and **28iV**, analyzed by the transition state method. This treatment also allows for a detailed energy decomposition of the total bonding energy into steric (electrostatic, $\delta_{\text{Exchange-Correlation}}$, electron-exchange repulsion) and single orbital

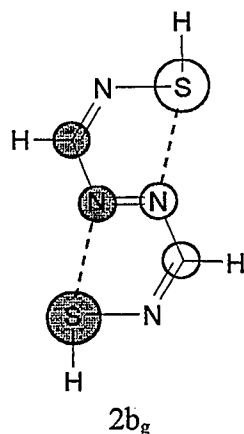
contributions [50]. The exchange-repulsion and orbital-interaction contributions to the total energy are quoted in Table 2.3. Comparative analysis shows that while the σ interactions (a_g and b_u) are destabilizing, the π interactions (b_g and a_u) stabilize **I** with respect to **V**. The same analysis was repeated for the model diazenes $\text{HEN}=\text{C}(\text{H})-\text{N}=\text{N}-\text{C}(\text{H})=\text{NEH}$ [$\text{E} = \text{Se}$ (**28l**), Te (**28m**)]. The calculations showed that **I** is more stable than **V** by 74.4 and 114.4 kJ mol^{-1} for $\text{E} = \text{Se}$ and Te , respectively.

2.3.3.2. Fragment Orbital Analysis.

The model diazenes **28i**, **28l**, and **28m** were separated into the fragments $\cdot\text{N}=\text{N}\cdot$ and $(\text{HE}-\text{N}=\text{C}(\text{H})\cdot)_2$ to evaluate the extent of donation into the empty orbitals of each fragment (Table 2.4). Electron donation to both $\sigma^*(\text{E}-\text{H})(a_g$ and $b_u)$ orbitals is negligible in all cases. Donation into $\pi^*(\text{N}=\text{N})(b_g)$ is considerable and increases for $\text{E} = \text{Te}$ since the energy of $\pi(\text{Te})\text{lp}$ is closer to that of the acceptor orbital. Donation to $\sigma^*(\text{E}-\text{N})(a_g)$ is also noticeable. Donation into $\sigma^*(\text{E}-\text{N})(b_u)$ becomes important only for $\text{E} = \text{Te}$. On the basis of this analysis, the chalcogen-diazene close contact is better described as a weak bonding interaction involving donation from a chalcogen lone pair $\pi(\text{E})\text{lp}$ to the $\pi^*(\text{N}=\text{N})$ orbital. The molecular orbital that best represents this interaction is $2b_g$ (Figure 2.4).

Table 2.3. Calculated contributions to the total atomization energy (kJ mol^{-1}) of the exchange repulsions and orbital interactions for the model diazenes $\text{HEN}=\text{C}(\text{H})-\text{N}=\text{N}-(\text{H})\text{C}=\text{NEH}$ (corrections not included).

	E = S (28i)		E = Se (28l)		E = Te (28m)					
	Geometry		Geometry		Geometry					
	I	V	I	V	I	V				
Exchange Repulsion (ER)										
a_g	17217.5	16849.7	16612.5	16325.1	16473.8	15987.1				
b_g	240.5	264.8	222.3	238.4	216.4	234.2				
a_u	852.3	806.2	824.9	787.6	814.8	764.9				
b_u	14746.8	14666.9	14160.2	14112.0	13967.8	13818.9				
Orbital Interaction (OI)										
a_g	-11917.0	-11740.6	-11416.8	-11249.3	-11242.3	-10933.3				
b_g	-1406.8	-1409.8	-1346.4	-1346.3	-1319.8	-1309.5				
a_u	-2635.4	-2535.0	-2585.0	-2479.1	-2518.0	-2378.5				
b_u	-12272.5	-12275.1	-11744.3	-11811.4	-11517.2	-11543.5				
ER + OI			Δ		Δ		Δ		Δ	
a_g	5300.5	5109.1	191.5	5195.7	5075.8	119.9	5231.5	5053.8	177.7	
b_g	-1166.4	-1145.1	-21.3	-1124.1	-1107.8	-16.2	-1103.4	-1075.3	-28.1	
a_u	-1783.1	-1728.9	-54.2	-1760.2	-1691.5	-68.7	-1703.1	-1613.6	-89.6	
b_u	2474.3	2391.8	82.5	2416.0	2300.6	115.4	2450.6	2275.4	175.1	

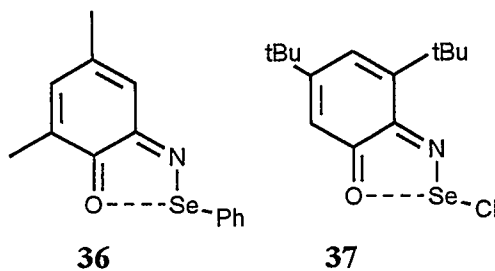


While the acceptor ability of the $\sigma^*(\text{S-X})$ orbitals of the SX_2 ligand in transition metal complexes is well established [51], in the present case the nitrogen lone pair is well below the energy of the metal valence electrons; consequently, the interaction with the σ^* levels is less effective and only alleviates the repulsive forces. Additional stabilization by the π (a_u) orbitals can be interpreted as the result of delocalization of electron density in two incipient five-membered rings. An interaction diagram that summarizes these effects is presented in Figure 2.6.

Table 2.4. Population of selected fragment orbitals in the model diazenes
 $\text{HEN}=\text{C}(\text{H})-\text{N}=\text{N}-(\text{H})\text{C}=\text{NEH}$

Orbital	E = S (28i)			E = Se (28l)			E = Te (28m)		
	Geometry			Geometry			Geometry		
	V	I	Δ	V	I	Δ	V	I	Δ
$\sigma^*(\text{H-E}) a_g$	0.01	0.06	0.05	0.04	0.09	0.05	0.05	0.07	0.02
$\sigma^*(\text{H-E}) b_u$	0.02	0.01	-0.01	0.07	0.01	-0.06	0.07	0.01	-0.06
$\sigma^*(\text{N-E}) a_g$	0.01	0.19	0.18	0.05	0.17	0.12	0.07	0.26	0.19
$\sigma^*(\text{N-E}) b_u$	0.01	0.08	0.07	0.04	0.09	0.05	0.08	0.30	0.22
$\pi^*(\text{N=N}) b_g$	0.29	0.47	0.18	0.31	0.49	0.18	0.31	0.58	0.27

It follows from the bonding description that intramolecular interactions of the type considered in this study would be enhanced by increasing the degree of donation into the $\pi^*(\text{N=N})$ and/or $\sigma^*(\text{E-X})$ orbitals. The acceptor ability of the $\sigma^*(\text{E-X})$ orbitals is improved by increasing the electronegativity of X (c.f. **35a**). Similar $\text{O}\cdots\text{Se}$ close-contacts have been observed in the quinone derivatives **36** and **37**. The $\text{O}\cdots\text{Se}$ distance is reduced from 2.575(3) to 2.079(3) Å by replacing the phenyl group with a chlorine atom [52].



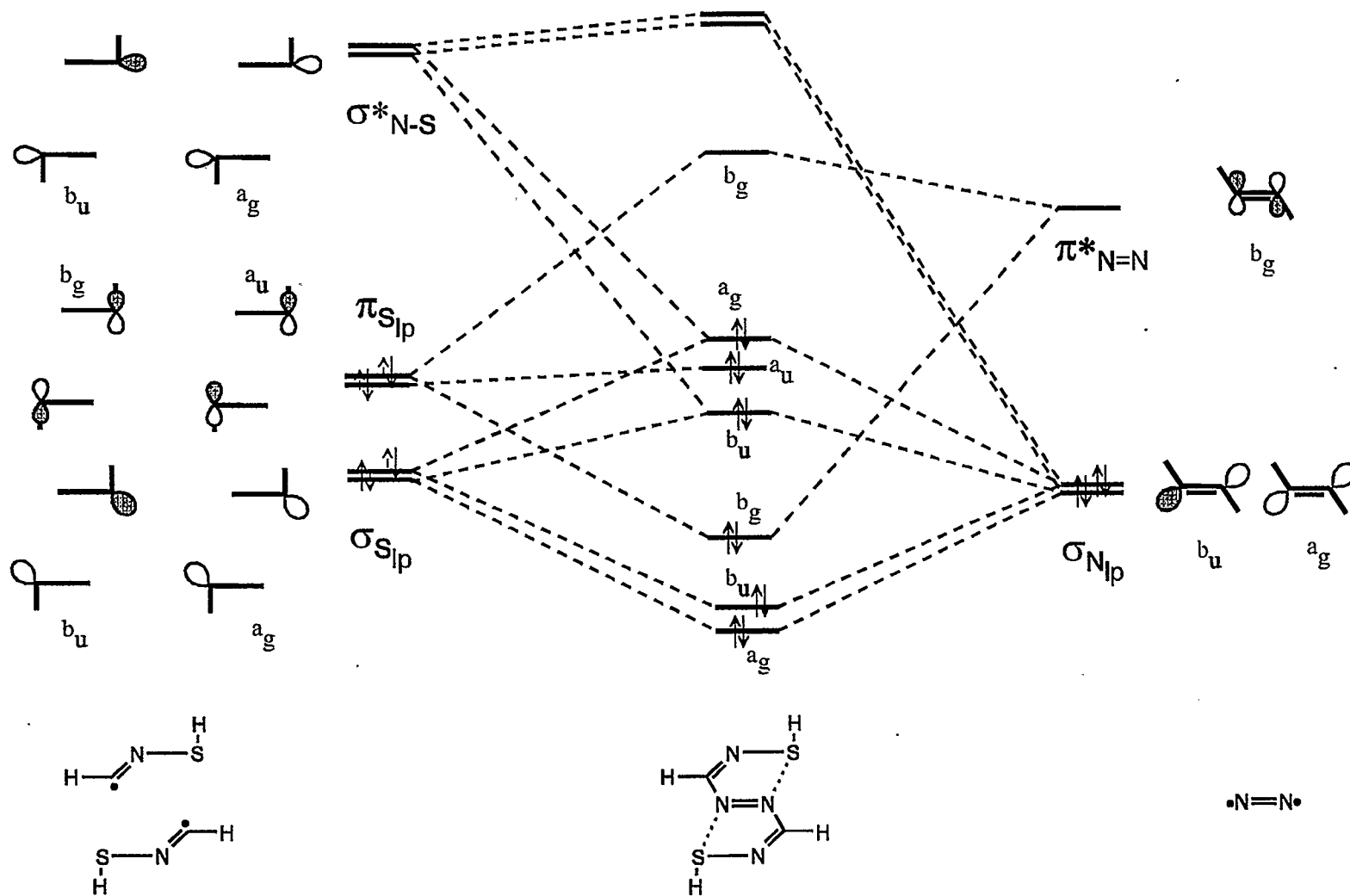
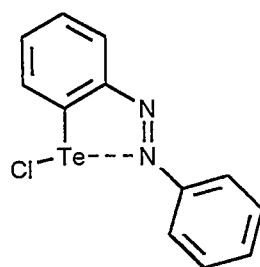


Figure 2.6. Orbital interactions for the fragments $(HS-N=C(H)\cdot)_2$ and $\cdot N=N \cdot$.

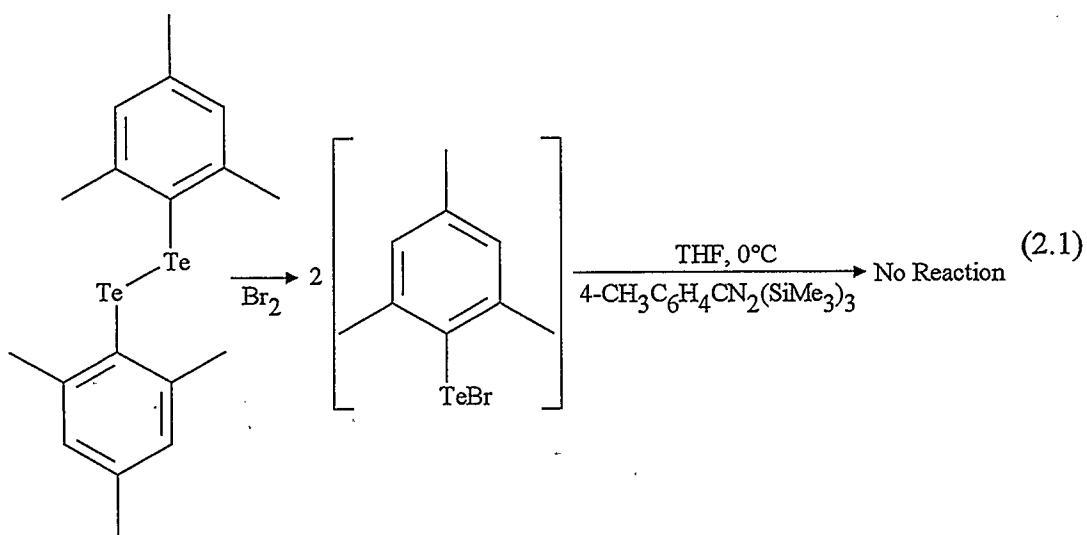
2.4. Considerations for the synthesis of $\text{RTeN}=\text{C}(\text{R}')\text{N}=\text{NC}(\text{R}')=\text{NTeR}$ (**28m**)

The donation into both the $\pi^*(\text{N}=\text{N})$ and $\sigma^*(\text{E}-\text{X})$ orbitals is more pronounced for the heavy chalcogen Te. Consequently, organotellurium compounds exhibit the greatest tendency towards “intramolecular coordination”. Intramolecular $\text{Te}\cdots\text{N}$ interactions are a common feature in organotellurium compounds, including *ortho*-tellurated azobenzenes [53]. Indeed such interactions stabilize tellurium(II) compounds of the type ArTeCl , e.g. **35b** [$d(\text{Te}-\text{N}) = 2.19(2)$ and $2.23(2)$ Å] [54].



35b

In view of these observations the preparation of a type-**28** tellurium-containing diazene was pursued by the same route that was successful for the S and Se compounds (eq. 1.10). ArTeX ($\text{X} = \text{Cl}, \text{Br}, \text{I}$) compounds are unstable. However, ArTeBr reagents can be prepared *in situ* by reaction of a ditelluride (Ar_2Te_2) with Br_2 at 0°C and they have been used as intermediates in the synthesis of vinylic tellurides, asymmetric tellurides and selenaditellurides [55]. The same approach was employed for the attempted synthesis of **28m**. However, the experiment was unsuccessful, owing to the low reactivity of MesTeBr (eq. 2.1).



2.5. Summary

Density functional theory calculations for the model diazenes $\text{HEN}=\text{C}(\text{H})\text{N}=\text{NC}(\text{H})=\text{NEH}$ ($\text{E} = \text{S}, \text{Se}, \text{Te}$) **28i,l,m** show that (a) Z,E,Z isomers with intramolecular $\text{E}\cdots\text{N}$ interactions are more stable than the E,E,E isomers, (b) the intramolecular interaction is stabilized by backdonation from a chalcogen lone pair into the $\pi^*(\text{N}=\text{N})$ orbital; donation from the $\sigma(\text{N})$ lone pairs into both the $\sigma^*(\text{S}-\text{H})$ and $\sigma^*(\text{S}-\text{N})$ orbitals alleviates the lone pair-lone pair repulsions, and (c) the intense visible absorption bands ($\lambda_{\text{max}} = 500\text{-}550 \text{ nm}$, $\epsilon \approx 104 \text{ M}^{-1} \text{ cm}^{-1}$) can be attributed to the HOMO-1 ($3a_u$) \rightarrow LUMO ($3b_g$) transition.

Examples of the three most stable isomers of the type-**28** sulfur diazenes are now structurally characterized. The diazene $\text{PhSN}=\text{C}(\text{H})-\text{N}=\text{N}-\text{C}(\text{H})=\text{NSPh}$ (**28f**) was shown by NMR to undergo complex exchange processes between the different isomers (I-V) in solution.

2.6. Computational Method and Calculations Details

All calculations were based on approximate Density Functional Theory (DFT) within the Local Density Approximation (LDA) [56], using the ADF program system developed by Baerends et al. [57, 58], and vectorized by Raveneck [59]. The numerical integration was based on a scheme developed by te Velde [60]. All molecular dimensions were fully optimized, by a procedure based on the method developed by Versluis and Ziegler [61]. All bonding energies were evaluated by the generalized transition state method due to Ziegler and Rauk [62]. A double Slater-Type-Orbital (STO) basis [63] was employed for the *ns* and *np* shells of the main group elements. This basis was augmented by a 3d STO function for sulfur, 4d STO for selenium, 5d STO for tellurium and for hydrogen a 2p STO was used as polarization. Electrons in lower shells were treated by the frozen core approximation [57]. A set of auxiliary [64] s, p, d, f, and g STO functions, centered on the different nuclei, was used in order to fit the molecular density and present Coulomb and exchange potentials accurately in each SCF cycle. Energy differences were calculated by LDA energy expression by Vosko et al. [65] with Becke's [66] exchange corrections and Perdew's nonlocal correlation correction [67].

2.7. Experimental Section

2.7.1. Reagents and General Procedures.

Solvents were dried by treatment with the appropriate drying agent and freshly distilled before use. All reactions and manipulation of moisture-sensitive products were carried out under an atmosphere of dry nitrogen by using Schlenk techniques or a Vacuum Atmospheres drybox. $\text{HCN}_2(\text{SiMe}_3)_3$ [68], PhSCl [69], and $4\text{-CH}_3\text{C}_6\text{H}_4\text{CN}_2(\text{SiMe}_3)_3$ [6] were prepared by literature methods.

2.7.2. Instrumentation

^1H and ^{77}Se NMR spectra were run on Bruker ACE-200 and Bruker AM-400 spectrometers, respectively, operating at 200.132 and 76.132 MHz. UV-visible spectra were determined by using a Cary 5E spectrophotometer. Infrared spectra were recorded as Nujol mulls (KBr plates) on a Mattson 4030 FTIR spectrometer. Elemental analyses were performed within the Chemistry Department at the University of Calgary. All X-ray diffraction studies described in this dissertation were performed by Dr. M. Parvez on a Rigaku AFC6S diffractometer using graphite monochromated Mo- $\text{K}\alpha$ radiation. Further details on the structure determinations are available from Dr. Parvez.

2.7.3. Preparation of PhSN=C(H)N=NC(H)=NSPh (28f)

A solution of PhSCl (2.96 g 20.5 mmol) in 20 mL of CH₂Cl₂ was slowly added to a solution of HCN₂(SiMe₃)₃ (1.82 g, 7.0 mmol) in 25 mL of the same solvent at 23°C. The mixture was refluxed for 18h, and then the solvent was evaporated. The residue was recrystallized from diethyl ether at -20°C; both the diazene and Ph₂S₂ are crystallized in this way, however the disulfide redissolves first by slowly warming the sample. (yield of **28f**: 0.21g, 0.67 mmol, 7%). Mp: 130°C. Anal. Calcd for C₁₄H₁₂N₄S₂: C, 55.98; H, 4.03; N, 18.65. Found C, 55.97; H, 3.77; N, 18.00. ¹H NMR (DMSO-d₆, 380K): δ 8.88 (s, C-H, ¹H), 7.60-7.20 (m, C₆H₅, 5H). IR (cm⁻¹, Nujol): 1299 m, 1156 m, 1088 m, 1079 m, 1022 m, 889 m, 800 m, 722 m, 705 m, 682 m. UV-vis (Toluene 95°C): λ_{max} = 470 nm, ε = 1.37×10⁴ M⁻¹cm⁻¹.

2.7.4. Attempted Preparation of MesTeN=C(4-CH₃C₆H₄)N=NC(4-CH₃C₆H₄)=NTeMes (28m) (Mes = 2,4,6-(CH₃C₆H₂))

A solution of Br₂ (0.192 g, 1.2 mmol) in 10 mL of THF was slowly added to a solution of Mes₂Te₂ (0.61g, 1.2 mmol) in 40 mL of the same solvent at 0°C, to produce *in situ* MesTeBr [55]. After 30 min, a solution of 4-CH₃C₆H₄CN₂(Si(CH₃)₃)₃ (0.29g, 0.4 mmol) in 10mL of THF was added. The mixture was stirred for 16h, after which the solvent was removed under vacuum. The ¹H NMR spectrum of the residue indicated the presence of only the starting reagents.

3. Molecular and Electronic Structures of $\text{RC}(\text{NH}_2)(\text{NEPh})$

($\text{R} = \text{H}, 4\text{-CH}_3\text{C}_6\text{H}_4$; $\text{E} = \text{S}, \text{Se}$) [70]

3.1. Preamble

After the structure of the selenium-containing diazene **28a** was established [33], several attempts were made in the Chivers' group to obtain the structures of other selenium derivatives and analogous sulfur-containing compounds. The preparation of new species of the type $\text{PhEN}=\text{C}(\text{R}')\text{N}=\text{NC}(\text{R}')=\text{NEPh}$ ($\text{E} = \text{S}, \text{Se}$) (**28**), with respect to the R' groups, was restricted by the availability of silylated amidines. Their synthesis by addition of $(\text{SiMe}_3)_2\text{N}^-$ to nitriles, and subsequent reaction with ClSiMe_3 was limited to benzonitrile and its substituted derivatives [6]. The reactions of these trisilylated benzamidines with PhSCl have resulted in the preparation of several new sulfur derivatives, the characterization of two new structures (**28g** and **28h**, Section 2.2.1.3), and the establishment of the conditions that optimize the yield of cyclic products [46].

The preparation of the trisilylated formamidine $\text{HCN}_2(\text{SiMe}_3)_3$ [68] offered the opportunity to investigate new diazene derivatives. Furthermore, it allowed a more detailed study of the reaction mechanism (Chapter 4), and an investigation of a sulfur-containing diazene which exhibits a new structure in the solid state (Section 2.2.1.2) and undergoes isomerization in solution (Section 2.2.4).

In the case of selenium the reaction of $\text{HCN}_2(\text{SiMe}_3)_3$ with PhSeCl produced a different coloured compound, which was not a diazene but a product from the decomposition of an intermediate. The accidental isolation of this product provided an explanation of an earlier observation by Dr. K. McGregor concerning the properties of $4\text{-CH}_3\text{C}_6\text{H}_4\text{C}[\text{N}(\text{SiMe}_3)_2](\text{NSePh})$ (**38b**). This species slowly decomposes at room temperature to a purple material, which had been tentatively identified as the diazene **28b**. It was, therefore, initially considered as a suitable starting material to study the mechanism of diazene formation. However, thermolysis of **38b** did not produce **28b** (*vide infra*). This chapter describes studies of the thermal decomposition of **38b** and the characterization of the chromophore responsible for the observed purple coloration. This study clarified one aspect of the diazene formation process and, therefore, it is presented before the mechanistic study in Chapter 4.

3.2. Properties of $4\text{-CH}_3\text{C}_6\text{H}_4\text{C}[\text{N}(\text{SiMe}_3)_2](\text{NEPh})$ (E = S, Se) (**38a,b**)

The monosubstituted compounds **38a** and **38b** were obtained by Dr. K. McGregor as moisture-sensitive, white crystals by the reaction of $\text{Li}[4\text{-CH}_3\text{C}_6\text{H}_4\text{C}(\text{NSiMe}_3)_2]$ (**39**) with PhSCl or PhSeCl , respectively. The use of the lithium derivative rather than $4\text{-CH}_3\text{C}_6\text{H}_4\text{C}(\text{NSiMe}_3)_3$ [34] yields a cleaner, more easily purified product, particularly in the case of the selenium derivative **38b**. The ^1H NMR spectrum of **38b** is almost identical to that of analytically pure **38a** and the ^{77}Se NMR spectrum exhibits a singlet at δ 779 ppm (c.f. δ (^{77}Se) 995 ppm for **28a**) [71]. Nevertheless satisfactory analytical data could not be

obtained for **38b** even on samples that appeared to be pure on the basis of ^1H and ^{77}Se NMR spectra.

Crystalline samples of **38b** develop a dark purple taint over a period of several weeks at 23°C even when stored under an argon atmosphere. The thermal decomposition of solid **38b** at 130°C for 12h produces $\text{PhSeN}(\text{SiMe}_3)_2$ (δ (^{77}Se) 682 ppm c.f. lit. δ 684 ppm [72]) and 4- $\text{CH}_3\text{C}_6\text{H}_4\text{CN}$, which was identified by IR and ^1H NMR spectroscopy. No evidence was obtained for the formation of the purple diazene **28b** in the solid state decomposition of **38b**. Thus it seems unlikely that the purple chromophore that is produced slowly in crystalline samples is **28b**. However, the diazene **28b** together with Ph_2Se_2 and $\text{PhSeN}(\text{SiMe}_3)_2$, were identified by ^{77}Se NMR spectroscopy as the decomposition products of **38b** in a purple THF solution.

3.3. Preparation and Characterization of $\text{HC}(\text{NH}_2)(\text{NSePh})$ (**40e**)

Although trithiolated benzamidines of the type $\text{PhCN}_2(\text{SPh})_3$ (**31a**) are thermally unstable at room temperature [34], the corresponding formamidine derivative $\text{HCN}_2(\text{SPh})_3$ can be isolated as colourless crystals (see Section 4.3). By contrast, the reaction of $\text{HCN}_2(\text{SiMe}_3)_3$ with three molar equivalents of PhSeCl produced the dark crystalline solid $\text{HC}(\text{NH}_2)(\text{NSePh})$, **40e**, presumably as a result of hydrolysis during the work-up procedure. Both the ^1H NMR and ^{77}Se NMR spectra of **40a**, which shows two resonances at δ 988 and

δ 912 ppm, suggest the existence of two tautomeric forms in solution. Compound **40e** exhibits an intense visible absorption band at 472 nm in CH_2Cl_2 solution.

3.3.1. X-ray Structure $\text{HC}(\text{NH}_2)(\text{NSePh})$ (**40e**)

The structure of **40e** was determined by X-ray crystallography. Pertinent crystallographic data are listed in Table 3.1. An ORTEP drawing with the atomic numbering scheme is displayed in Figure 3.1. Selected bond lengths and bond angles are summarized in Table 3.2. The molecule **40e** adopts a *syn* configuration with respect to the $\text{C}(1)=\text{N}(1)$ double bond as has been observed for **28a** [34]. The N-C-N-Se unit is nearly planar, with a dihedral angle of -7.5° , and the phenyl ring is twisted by 37.5° with respect to the N-C-N plane. As indicated in Figure 3.2, the molecules in the crystal lattice are connected by hydrogen bonds between nitrogen atoms of amino groups ($d(\text{N}\cdots\text{H}\cdots\text{N}) = 3.00 \text{ \AA}$). The C-N bond distances of 1.43(2) and 1.28(2) \AA are typical for single and double bonds, respectively [73]. The Se-N bond distance of 1.80(1) \AA is comparable to the value 1.817(3) \AA observed for the selenium-substituted diazene **28a** [34] and somewhat shorter than the single bond value of 1.87 \AA [74].

Table 3.1. Crystal data for HC(NH₂)(NSePh) (**40e**).

formula	C ₇ H ₈ N ₂ Se	Z	2
fw	199.11	T (°C)	23.0
space group	P2 ₁	λ (Å)	0.71069
a (Å)	7.514(1)	ρ _{calc} (g cm ⁻³)	1.800
b (Å)	5.575(1)	μ (cm ⁻¹)	50.28
c (Å)	8.925(1)	R	0.055
β (°)	100.71(1)	R _w	0.060
V (Å ³)	367.40(6)	dimensions (mm)	0.09×0.30×0.45

Table 3.2. Experimental and calculated values of selected bond distances (Å) and bond angles (°) for HC(NH₂)(NSePh) (**40e**).

	<u>Experimental</u>	<u>Calculated</u>
C(1)-N(2)	1.43(0.02)	1.38
C(1)-N(1)	1.28(0.02)	1.29
N(1)-Se(1)	1.80(0.01)	1.88
C(2)-Se(1)	1.90(0.01)	1.91
N(2)-C(1)-N(1)	121.9(1.6)	129.3
C(1)-N(1)-Se(1)	118.5(1.2)	116.0
C(2)-Se(1)-N(1)	106.2(0.5)	98.27

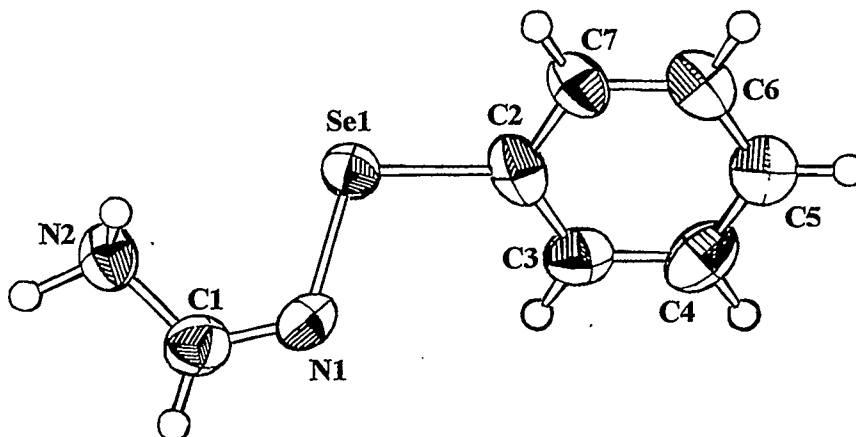


Figure 3.1. ORTEP diagram for HC(NH₂)(NSePh) (40e) showing atom labeling (50% probability ellipsoids are shown for non-hydrogen atoms).

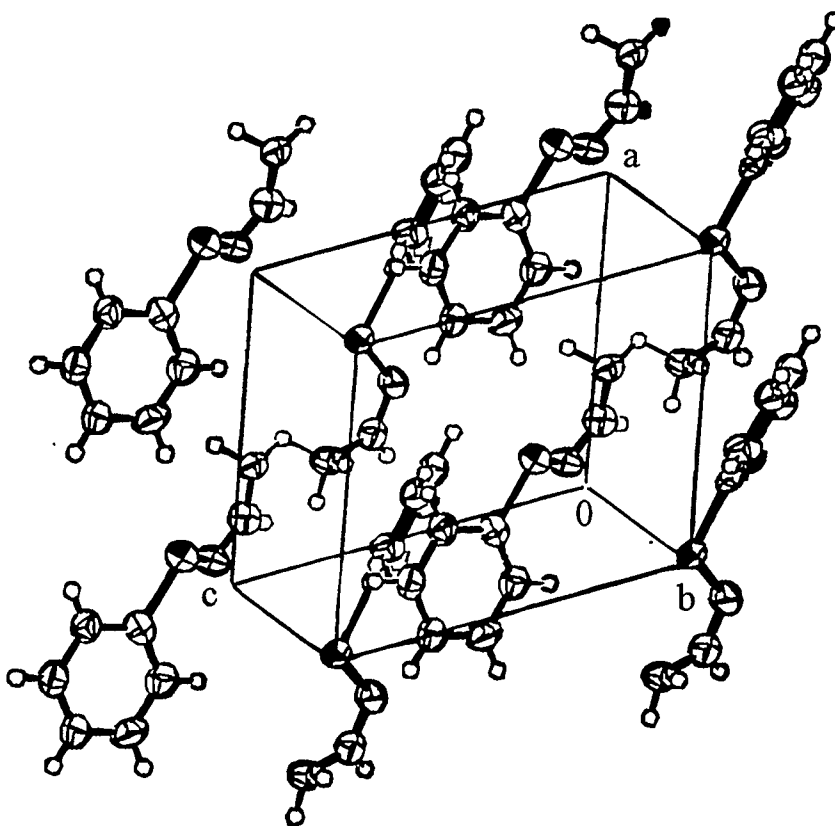
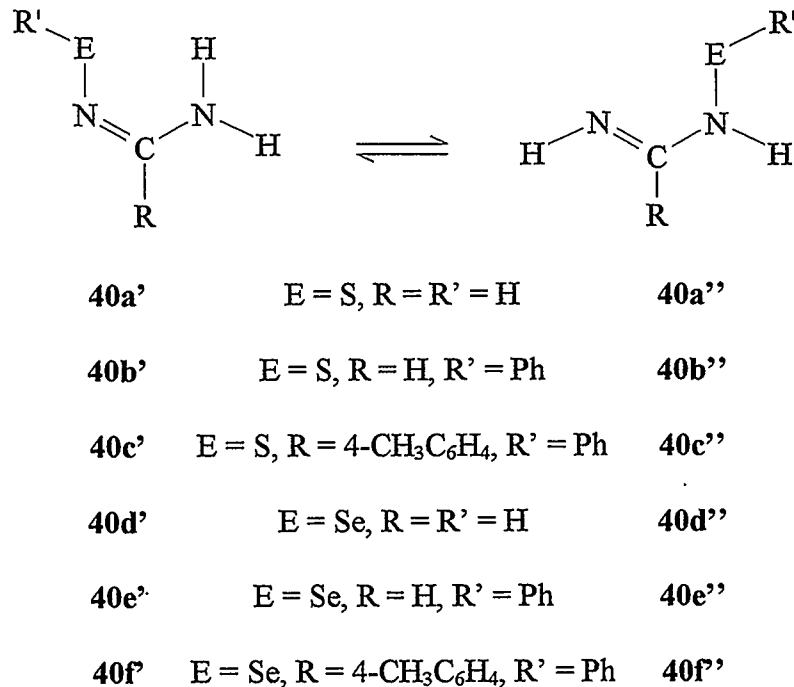


Figure 3.2. Packing diagram for HC(NH₂)(NSePh) (40e).

3.4. Hydrolysis of 4-CH₃C₆H₄C(NEPH)[N(SiMe₃)₂] (E = S, Se) (**38a**, **38b**).

The purple colour of HC(NH₂)(NSePh) suggested that hydrolysis might be an explanation for the purple colouration formed in solutions and crystalline samples of the monosubstituted compound **38b**. Consequently **38b** and, for comparison, **38a** were deliberately converted to the expected hydrolysis products 4-CH₃C₆H₄C(NH₂)(NEPh) (**40c**, E = S; **40f** E = Se) by the addition of methanol. The ¹H NMR spectrum of the pale yellow sulfur derivative, which remains unchanged down to -90°C, is consistent with the sole existence of the tautomer **40c'** in solution (see Scheme 3.1). By contrast, the ¹H NMR and ⁷⁷Se NMR spectra of 4-CH₃C₆H₄C(NH₂)(NSePh) (**40f**) suggest the existence of both tautomers **40f'** and **40f''** in approximately the same amounts in CD₂Cl₂ solutions at room temperature. Furthermore, the selenium derivative **40f** is dark purple and exhibits an intense visible absorption band at 551 nm. For comparison the diazene **28a** exhibits a visible absorption band at 553 nm with a shoulder at 580 nm [34].



Scheme 3.1

3.5. DFT Calculations for HC(NH₂)(NER) and HC(NH)[NH(ER)] (E = S, Se; R = H, Ph)

(40d-e', 40d-e'')

In order to compare the relative stabilities of the amino and imino tautomers **40'** and **40''**, respectively, and to provide an explanation of the purple colour of the selenium derivatives, approximate density functional theory (DFT) calculations were carried out on the model compounds HC(NH₂)(NER) and HC(NH)[NH(ER)] (E = S, Se; R = H, Ph) (**40d-e'**, **40d-e''**). The results are summarized in Table 3.3. The calculated structural parameters for the amino derivative HC(NH₂)(NSePh) **40e** are compared with the corresponding experimental values for **40e** in Table 3.2. Bond distances are reproduced

within 0.05 Å for the organic moiety and 0.10 Å for the bonds to the heavy element. Larger differences are observed between calculated and experimental values of the bond angles probably as a result of the intermolecular hydrogen bonding interactions in the solid state.

Table 3.3. Total atomization energies (TAE) and electronic transition energies (ΔE) for HC(NH₂)(NER) and HC(NH)[NH(ER)] (E = S, Se; R = H, Ph) (**40a'**,**b'**,**d'**,**e'**, **40a''**,**b''**,**d''**,**e''**).

	TAE ^a	ΔE^b	λ_{\max}^c
HC(NH ₂)(NSH) (40a')	-4062.99	4.34	286
HC(NH)[NH(SH)] (40a'')	-4033.77	3.74	332
HC(NH ₂)(NSPh) (40b')	-10553.07	3.44	360
HC(NH)[NH(SPh)] (40b'')	-10512.21	3.11	398
HC(NH ₂)(NSeH) (40d')	-3959.71	3.89	319
HC(NH)[NH(SeH)] (40d'')	-3942.22	3.34	371
HC(NH ₂)(NSePh) (40e')	-10484.45	3.30	376
HC(NH)[NH(SePh)] (40e'')	-10459.57	2.90	427

a in kJ mol⁻¹

b in eV

c in nm

The calculations show that the amino tautomers **40'** are more stable than the imino **40''** tautomers due to the larger π delocalization. Selenium forms a weaker π bond with nitrogen as compared to sulfur; as a consequence the energy barrier between the tautomers is smaller for the selenium structures. This is consistent with the NMR spectroscopic data which showed the existence of two tautomers in solution for the selenium derivatives **40e** and **40f**, whereas only the amino tautomer is evident in the ^1H NMR spectrum of **40c**. The lowest energy electronic transition for all the model compounds is the HOMO [n_{E}] \rightarrow LUMO [$\pi^*(\text{C}=\text{N})$] transition. In the amino tautomers mixing of the chalcogen lone pair with the $\pi^*(\text{C}=\text{N})$ orbital increases the HOMO-LUMO gap so that the electronic transitions are of higher energy than the corresponding transition for the imino tautomer (See Figure 3.3). The replacement of the H substituent on the chalcogen in the model compounds by an aryl group raises the energy of the lone pair so that the predicted value of the electronic transition for the imino tautomer $\text{HC}(\text{NH})=\text{NH}(\text{SePh})$ is 427 nm in reasonable agreement with the experimental value of 472 nm for **40e**. On the other hand, on the basis of NMR spectroscopic evidence, the sulfur derivative **40c** exists only as the amino tautomer and exhibits no absorption in the visible region consistent with the predicted trend of higher transition energies for the sulfur compounds compared to their selenium analogues (see Table 3.3).

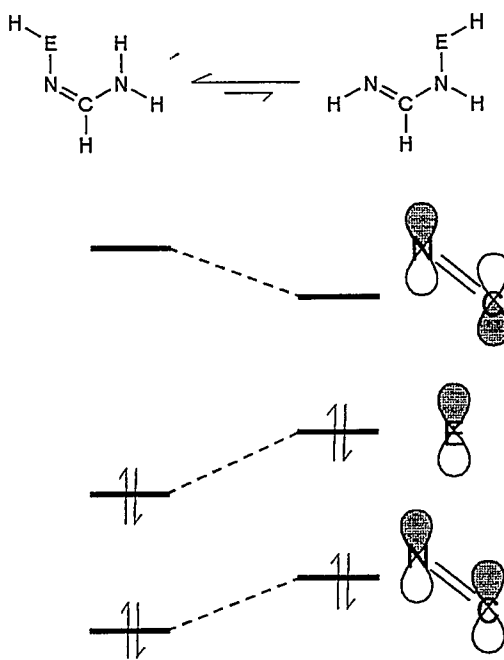


Figure 3.3. Correlation diagram for the π orbitals of $\text{HC}(\text{NH}_2)(\text{NEH})$ and $\text{HC}(\text{NH})[\text{NH}(\text{EH})]$ ($\text{E} = \text{S}, \text{Se}$) (**40a,d'**, **40a,d''**).

3.6. Summary.

The purple chromophore formed from $\text{RC}(\text{NSePh})[\text{N}(\text{SiMe}_3)_2]$ ($\text{R} = \text{H}, \text{aryl}$) in solution or, more slowly, in the solid state has been identified as the hydrolysis product $\text{RCN}_2\text{H}_2\text{SePh}$ which, for $\text{R} = \text{H}$, adopts a *syn* conformation in the solid state. In contrast to the corresponding sulfur derivatives, which form only the amino tautomer $\text{RC}(\text{NH}_2)(\text{NSPh})$ in solution, the selenium compounds exist as a mixture of amino and imino tautomers, $\text{RC}(\text{NH}_2)(\text{NSePh})$ and $\text{RC}(\text{NH})(\text{NHSePh})$, respectively. DFT calculations suggest relatively close values of the total bonding energies for the two tautomers in the case of the selenium

derivatives. The calculations also indicate that the purple colour of the Se compounds can be attributed to the HOMO [n_{E}] \rightarrow LUMO [$\pi^*(\text{C}=\text{N})$] transition of the imino tautomer.

3.7. Experimental Section

Details of the instrumental methods and synthetic procedures have been provided in 2.7. ^{77}Se NMR chemical shifts are reported relative to Me_2Se . The apparent molar extinction coefficients of **40e** and **40f** were calculated as the absorbance at the maximum divided by the total concentration and the optical path length (1 cm).

3.7.1. Preparation of 4- $\text{CH}_3\text{C}_6\text{H}_4\text{C}[\text{N}(\text{SiMe}_3)_2](\text{NSPh})$ (**38a**)

A solution of PhSCl (1.44 g, 10 mmol) in CH_2Cl_2 (20 mL) was added dropwise (20 min) to a solution of $\text{Li}[4\text{-CH}_3\text{C}_6\text{H}_4\text{C}(\text{NSiMe}_3)_2]$ (**39**) (10 mmol) in diethyl ether (60 mL) at -78°C . The yellow reaction mixture was allowed to warm slowly to 23°C to produce a white precipitate of LiCl . Solvent was removed under vacuum to give a yellow oil which was extracted with hexanes (2×50 mL). The hexanes were removed under vacuum to give an off-white solid, which was recrystallized from a minimum volume of pentane at -18°C yielding **38a** as an off-white solid (1.9 g, 5 mmol, 50%). Anal. calcd. for $\text{C}_{19}\text{H}_{30}\text{N}_2\text{SSi}_2$: C, 62.12; H, 7.82; N, 7.24; found: C, 62.15; H, 7.90; N, 7.88. ^1H NMR (CDCl_3) δ : 7.21-7.79 (m, 9H, $\text{CH}_3\text{C}_6\text{H}_4$ and SC_6H_5), 2.41 (s, 3H, $\text{CH}_3\text{C}_6\text{H}_4$), 0.27 (s, 18H, $\text{Si}(\text{CH}_3)_3$).

3.7.2. Preparation of 4-CH₃C₆H₄C[N(SiMe₃)₂](NSePh) (**38b**)

A solution of PhSeCl (1.91 g, 10 mmol) in CH₂Cl₂ (20 mL) was added dropwise (20 min) to a solution of **39** (10 mmol) in diethyl ether (60 mL) at -78°C. The yellow reaction mixture was allowed to warm slowly to 23°C to produce a white precipitate of LiCl. Solvent was removed under vacuum to give a yellow oil which was extracted with hexanes (2 × 50 mL). The hexanes were removed under vacuum to give a yellow solid, which was recrystallized from a *minimum* volume of pentane at -18°C yielding **38b** as an off-white solid (1.1 g, 2.5 mmol, 25%). ¹H NMR (CDCl₃) δ: 7.22-7.76 (m, 9H, CH₃C₆H₄ and SeC₆H₅), 2.40 (s, 3H, CH₃C₆H₄), 0.31 (s, 18H, Si(CH₃)₃). ⁷⁷Se NMR (THF) δ: 779 (s).

3.7.3. Preparation of 4-CH₃C₆H₄C(NH₂)(NSPh) (**40c**)

A stoichiometric amount of methanol was added to a solution of **3d** (0.36 g, 1.0 mmol) in THF (10 mL). The reaction mixture was heated gently during 10 min and then the volatile materials were removed under vacuum to give **40c** as a colourless solid (0.22 g, 0.90 mmol, 90%). Anal. calcd. for C₁₄H₁₄N₂S: C, 69.39; H, 5.82; N, 11.56; found: C, 70.26; H, 6.23; N, 11.62. ¹H NMR (CD₂Cl₂) δ: 7.75-7.50 (m, 4H, CH₃C₆H₄), 7.40-7.10 (m, 5H, SC₆H₅), 5.11 (s, 2H, NH₂), and 2.37 (s, 3H, CH₃C₆H₄). IR (cm⁻¹): 2723 m, 2674 m, 1627 m, 1304 m, 1153 m, 1086 m, 1022 m, 829 m, 769 m, 735 s, 688 m.

3.7.4. Reaction of $\text{HCN}_2(\text{SiMe}_3)_3$ with PhSeCl

A solution of PhSeCl (3.16 g, 17 mmol) in CH_2Cl_2 (20 mL) was added dropwise to a solution of $\text{HCN}_2(\text{SiMe}_3)_3$ (1.49 g, 5.7 mmol) in (20 mL) at -78°C . The reaction mixture was allowed to warm slowly to 23°C with stirring and the colour of the solution changed from yellow to orange-red and, finally, to dark purple. After 16h solvent was removed under vacuum to give a black solid which was extracted with hexanes (3×15 mL). Removal of hexanes under vacuum yielded PhSeSePh (2.28 g, 7.3 mmol) tainted with the purple product. The solid residue was recrystallized from CH_2Cl_2 to give dark-brown crystals of $\text{HC}(\text{NSePh})(\text{NH}_2)$ (**40e**) (0.55 g, 2.8 mmol, 48%). Anal. calcd. for $\text{C}_7\text{H}_8\text{N}_2\text{Se}$: C, 42.00; H, 4.03; N, 14.00; found: C, 42.16; H, 3.17; N, 13.95. ^1H NMR (CD_2Cl_2) δ : 9.79 (s, 1H, $\underline{\text{CH}}$), 7.90-7.80 and 7.60-7.30 (m, C_6H_5 and CH , ~10H). ^{77}Se NMR (CD_2Cl_2) δ : 988 (s), and 912 (s). IR (cm^{-1}): 2721 m, 2672 m, 1306 m, 1284 m, 1167 m, 1153 m, 1063 m, 1020 m, 893 m, 771 m, 685 m. UV-vis (CH_2Cl_2): $\lambda_{\text{max}} = 472$ nm, $\epsilon(\text{apparent}) = 3200 \text{ M}^{-1} \text{ cm}^{-1}$.

3.7.5. Preparation of $4\text{-CH}_3\text{C}_6\text{H}_4\text{C}(\text{NH}_2)(\text{NSePh})$ (**40f**)

$4\text{-CH}_3\text{C}_6\text{H}_4\text{C}(\text{NH}_2)(\text{NSePh})$ was obtained in 40% yield as dark purple crystals by the treatment of **3b** with methanol in a manner similar to that described above for the preparation of **4b**. Anal. calcd. for $\text{C}_{14}\text{H}_{14}\text{N}_2\text{Se}$: C, 58.14; H, 4.88; N, 9.69; found: C,

58.75; H, 4.56; N, 9.73. ^1H NMR (CD_2Cl_2) δ : 8.35-8.20 (m, 2H, $\text{CH}_3\text{C}_6\text{H}_4$), 7.90-7.75 (m, 2H, $\text{CH}_3\text{C}_6\text{H}_4$), 7.70-7.10 (m, 14H, $\text{CH}_3\text{C}_6\text{H}_4$ and C_6H_5), 5.12 (s, 4H, NH_2), 2.45 (s, 3H, $\text{CH}_3\text{C}_6\text{H}_4$), and 2.38 (s, 3H, $\text{CH}_3\text{C}_6\text{H}_4$). IR (cm^{-1}): 2721 m, 2671 m, 1306 m, 1261 m, 1018 m, 966 m, 822 m, 768 m, 733 s, 688 m, 669 m. UV-vis: λ_{max} 551 nm, $\epsilon(\text{apparent})$ 8000 $\text{M}^{-1} \text{cm}^{-1}$.

4. Mechanistic Studies of the Formation of the Diazenes of the Type



4.1. CSN Radicals

The formation of persistent free radicals is a pervasive and fascinating feature of sulfur-nitrogen chemistry [36]. A few of these species contain only nitrogen and sulfur, e.g. S_3N_2^+ , $\text{NS}\cdot$, $\text{NSN}\cdot$, $\text{S}_7\text{N}\cdot$. In most cases, however, an organic fragment is required to be part of the structure. Organo-sulfur-nitrogen (CSN) radicals can be classified into two major groups: cyclic and non-cyclic radicals.

4.1.1. Non-Cyclic CSN Radicals

A few families of non-cyclic radicals can be identified:

$\text{R}_2\text{N-S}\cdot$ (41) and $\text{R}_2\text{N-S(O)}\cdot$ (42). These may be regarded as the sulfur derivatives of organic radicals based on the amine-N-oxyl group. They are prepared by reaction of bis(dialkylamino)sulfides with photochemically-generated tert-butoxyl radicals. The average spectral parameters for 41 and 42 are $g = 2.0155$, $A_N = 10.7 \text{ G}$ and $g = 2.0060$, $A_N = 6.5 \text{ G}$, respectively [76].

$[(\text{RN})_2\text{S}]\cdot$ (43). These radical anions are obtained when alkali metals are used to reduce sulfur diimides, $\text{RN}=\text{S}=\text{NR}$ where R is an aryl or alkyl group other than methyl [77].

The average ESR parameters are $g = 2.0056$, $A_S = 9.2$ G, $A_N = 10.7$ G. Such species have been proposed to be involved in the skeletal scrambling of sulfur diimides in the presence of catalytic amounts of K or Na [78].

[RNSNRR']· (44). These are also derivatives of the sulfur diimides, obtained by reaction of $(t\text{BuN})_2\text{S}$ with $\text{R}'\cdot$ radicals, like $\text{F}_3\text{CS}\cdot$, $(\text{EtO})_2\text{P}(\text{O})\cdot$, $\text{CF}_3\cdot$ and $\text{Me}_3\text{Si}\cdot$. For these compounds $g = 2.0054\text{-}2.0064$, $A_{N\alpha} = 12.0\text{-}12.6$ G, $A_{N\gamma} \sim 1.0$ G [79].

[RSNR']· (45). These sulfur analogues of N-alkoxy-N-alkylaminyl radicals are prepared by hydrogen abstraction or photolysis of a suitable precursor. In solution they exhibit a bluish colour with $\lambda_{\text{max}} \sim 600$ nm. Some of these species are so stable that they show virtually no dimerization at all and can be isolated as monomeric radicals [80]. In one case the structure has been characterized by X-ray diffraction [81]. The nature of the R and R' groups has a definite effect on the spin delocalization and, as a consequence, on the spectroscopic parameters. For R, R' = alkyl $g = 2.0061\text{-}2.0075$, $A_S = 3.53$ G, $A_N = 12.13\text{-}12.91$ G [82]; R, R' = aryl $g = 2.0057\text{-}2.0061$, $A_S = 4.62$ G, $A_N = 9.52\text{-}9.64$ G [83]; R = aryl, R' = alkyl $g = 2.0061\text{-}2.0071$, $A_N = 9.32\text{-}9.93$ G [84]; R = alkyl, R' = aryl, $A_S = 5.8\text{-}6.7$ G, $A_N = 11.6\text{-}12.26$ G [85]; R = aryl, R' = H $g = 2.0075$, $A_N = 11.5$ G [86]; R = R''C(O), R', R'' = alkyl or aryl $g = 2.0091\text{-}2.0094$, $A_S = 10.5\text{-}10.8$ G, $A_N = 6.8\text{-}8.6$ G, $A_O = 2.7$ G [87]; R = 4-CH₃C₆H₄-S(O)₂, R' = aryl $g = 2.0074$, $A_S = 11.9\text{-}12.3$ G, $A_N = 7.4\text{-}8.9$ G [88].

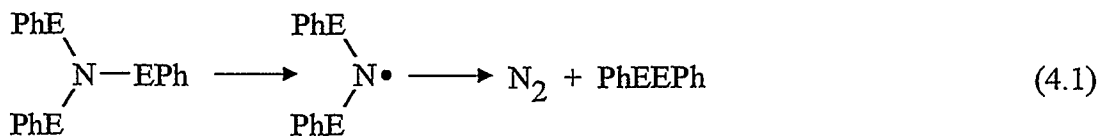
[(ArS)₂N]· (46a,b). The bisarylsulphenamidyl radicals have been known since 1925 [89]. Identified first by their purple colour, $\lambda_{\text{max}} \sim 500\text{-}570$ nm, they are prepared by oxidation of bisarylsulphenimides. There have been several reports of spectroscopic data for

these species [90, 91, 92]. In the most recent paper, Mayer [93] has reported $g = 2.0077$ and $A_N = 11.5$ G for $(\text{PhS})_2\text{N}\cdot$ in benzene at room temperature.

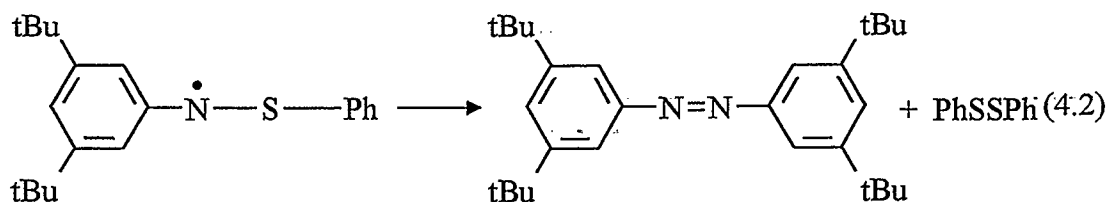
$[(\text{tBuN})_3\text{S}]^-$ (47). This radical anion is prepared by oxidation of the cage compound $[((\text{tBuN})_3\text{S})\text{Li}_2]_2$ (48). The solution ESR spectrum shows coupling to three equivalent nitrogen atoms with $A_N = 8$ G. Additional splitting has been interpreted in terms of interaction of the unpaired electron with two equivalent lithium nuclei, $A_{\text{Li}} = 0.8$ G [94].

4.2. The $\text{PhCN}_2(\text{ER})_2\cdot$ (E = S, Se) Radical (29)

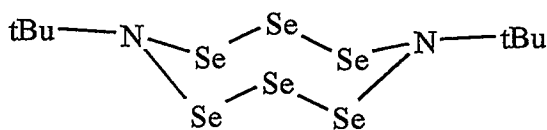
As discussed in Section 1.2.1, the reaction of trisilylated benzamidines (1) with 3 equivalents of PhECl produces intensely coloured diazenes. The ESR spectra of the reaction mixtures exhibit a 1:2:3:2:1 quintet for both S and Se (E = S: $g = 2.0071$, $A_N = 5.75$ G; E = Se: $g = 2.0201$, $A_N = 5.9$ G). This indicates the presence of a free radical in which the unpaired electron is coupled to two equivalent ^{14}N nuclei. The resonance-stabilized radical $\text{PhCN}_2(\text{EPh})_2\cdot$ (29) was proposed as the species providing the ESR signal and as an intermediate in the diazene formation [34]. It was also proposed that these radicals are formed from the tris(phenyl-chalcogen)-substituted benzamidines $\text{PhCN}_2(\text{EPh})_3$ (31a,e) in a process similar to decomposition of $(\text{PhE})_3\text{N}$ (49) (E = S, E = Se), which are thermally unstable species that decompose readily to N_2 and PhEPh , via the radicals $(\text{PhE})_2\text{N}\cdot$ (46a,b) (eq. 4.1) [95, 96].



Indeed some $[\text{RSNR}']\cdot$ (**45**) radicals decay to form a diazene and a disulfide (eq. 4.2), among other decomposition products [97].



Several other E-N (E = S, Se, Te) compounds decay to form E-E and N=N links. For instance the selenium diimides, $\text{RN}=\text{Se}=\text{NR}$ (R = *tert*-butyl, *tert*-octyl) (**14b**), are thermally unstable, decomposing to the eight-membered ring **50** and $\text{RN}=\text{NR}$ [98]. These products suggest that the mechanism may also involve free radicals.

**50**

4.3. Preparation of $\text{HCN}_2(\text{SPh})_3$

The benzamidine derivatives $\text{PhCN}_2(\text{EPh})_3$ (E = S, Se) (**31a,e**) are so unstable that they cannot be isolated. In contrast $\text{PhCN}_2(\text{SCCl}_3)_3$ (**31b**) and $\text{PhCN}_2(2,4\text{-}(\text{NO}_2)_2\text{C}_6\text{H}_3\text{S})_3$ (**31c**) are stable up to 140°C. In this project the tris(thiophenolato)formamidine, $\text{HCN}_2(\text{SPh})_3$ (**31d**), was isolated and it was shown to decompose under mild conditions to $\text{PhSN}=\text{C}(\text{H})-\text{N}=\text{N}-\text{C}(\text{H})=\text{NSPh}$ (**28f**). The derivative **31d** is readily prepared from the

reaction of $\text{HCN}_2(\text{SiMe}_3)_3$ (**1f**) with three molar equivalents of PhSCl at low temperature. The product is isolated as white crystals, usually slightly stained with the red diazene **28f**. It starts to decompose both in solution and in the solid state at room temperature. Consequently, it must be stored at low temperature (-20°C) to prevent any contamination.

4.3.1. X-ray Structure of $\text{HCN}_2(\text{SPh})_3$ (**31d**)

Single crystals of **31d** were obtained from a dilute hexanes solution at -20°C . Relevant crystallographic data are shown in Table 4.1. An ORTEP drawing of **31d** is displayed in Figure 4.1. Selected molecular dimensions are listed in Table 4.2. One of the S atoms was disordered over two sites S(3) and S(3)' with site occupancy factors of 0.67(1) and 0.33(1), respectively. The structure of **31d** is analogous to that of **31b**. The three-coordinate nitrogen adopts a planar geometry ($\Sigma\hat{N} = 359.9^\circ$), probably as a result of steric hindrance. The bond distances $d(\text{S}(1)-\text{N}(1)) = 1.691(3) \text{ \AA}$ and $d(\text{S}(2)-\text{N}(1)) = 1.709(3) \text{ \AA}$ are comparable to those of the $\text{PhCN}_2(\text{SCCl}_3)_3$ derivative (1.694(4) and 1.700(3) \AA) [34] and $(\text{PhS})_3\text{N}$ (average 1.699 \AA) [99]. From these metrical data there is no indication that the decomposition of **31b** is impeded by stronger S-N bonds.

Table 4.1. Crystallographic data for $\text{HCN}_2(\text{SPh})_3$ (**31d**).

formula	$\text{C}_{19}\text{H}_{16}\text{N}_2\text{S}_3$	Z	4
fw	368.53	T (°C)	-123
space group	$\text{P2}_1/\text{a}$	λ (Å)	0.71069
a (Å)	9.874(2)	ρ_{calc} (g cm ⁻³)	1.373
b (Å)	19.133(2)	μ (cm ⁻¹)	4.18
c (Å)	10.280(2)	R	0.042
β (°)	113.37(1)	R_w	0.049
V (Å ³)	1782.8(5)	dimensions (mm)	0.50×0.40×0.21

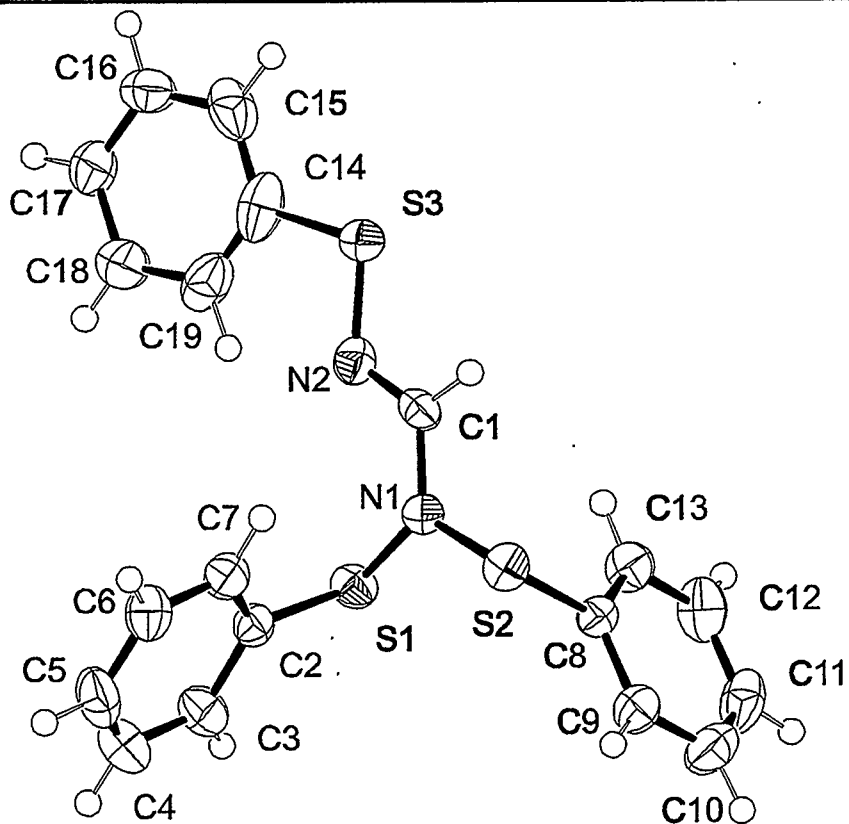
Figure 4.1. ORTEP diagram for $\text{HCN}_2(\text{SPh})_3$ (**31d**).

Table 4.2. Selected bond lengths (Å), bond angles and torsion angles (°) for HCN₂(SPh)₃ (**31d**).

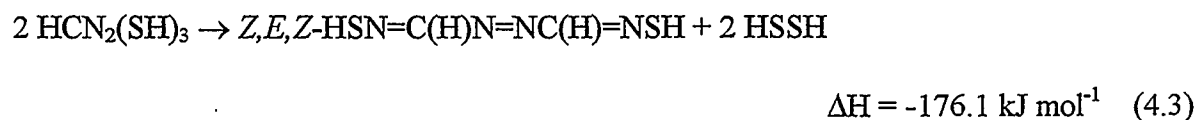
S(1)-N(1)	1.691(3)	S(1)-C(2)	1.772(4)
S(2)-N(1)	1.709(3)	S(2)-C(8)	1.773(4)
S(3)-N(2)	1.623(4)	S(3)-C(14)	1.786(5)
S(3')-N(2)	1.660(5)	S(3')-C(19)	1.669(6)
N(1)-C(1)	1.401(5)	N(2)-C(1)	1.261(5)
N(1)-S(1)-C(2)	103.1(2)	N(1)-S(2)-C(8)	101.7(2)
N(2)-S(3)-C(14)	103.4(3)	N(2)-S(3')-C(19)	112.8(3)
S(1)-N(1)-S(2)	120.5(2)	S(1)-N(1)-C(1)	121.7(3)
S(2)-N(1)-C(1)	117.7(3)	S(3)-N(2)-S(3')	102.2(2)
S(3)-N(2)-C(1)	119.6(3)	S(3')-N(2)-C(1)	138.2(3)
N(1)-C(1)-N(2)	124.1(4)	S(1)-N(1)-S(2)-C(8)	67.9(2)
S(1)-N(1)-C(1)-N(2)	12.3(5)	S(2)-N(1)-S(1)-C(2)	81.4(2)
S(2)-N(1)-C(1)-N(2)	-171.1(3)	S(3)-N(2)-S(3')-C(19)	4.6(3)
S(3)-N(2)-C(1)-N(1)	-176.3(3)	S(3')-N(2)-S(3)-C(14)	-2.3(3)
S(3')-N(2)-C(1)-N(1)	1.7(7)	N(1)-S(1)-C(2)-C(3)	-158.6(3)
N(1)-S(1)-C(2)-C(7)	19.6(4)	N(1)-S(2)-C(8)-C(9)	-140.9(3)
N(1)-S(2)-C(8)-C(13)	40.1(4)	N(2)-S(3)-C(14)-C(15)	175.0(4)
N(2)-S(3)-C(14)-C(19)	-0.9(5)	N(2)-S(3')-C(19)-C(14)	-5.3(5)
N(2)-S(3')-C(19)-C(18)	-175.1(5)	C(1)-N(1)-S(1)-C(2)	-102.0(3)
C(1)-N(1)-S(2)-C(8)	-108.8(3)	C(1)-N(2)-S(3)-C(14)	176.3(3)
C(1)-N(2)-S(3')-C(19)	-173.6(4)		

4.4. Mechanism and Thermodynamics of the Formation of $\text{RSN}=\text{C}(\text{R}')\text{N}=\text{NC}(\text{R}')=\text{NSR}$ (28)

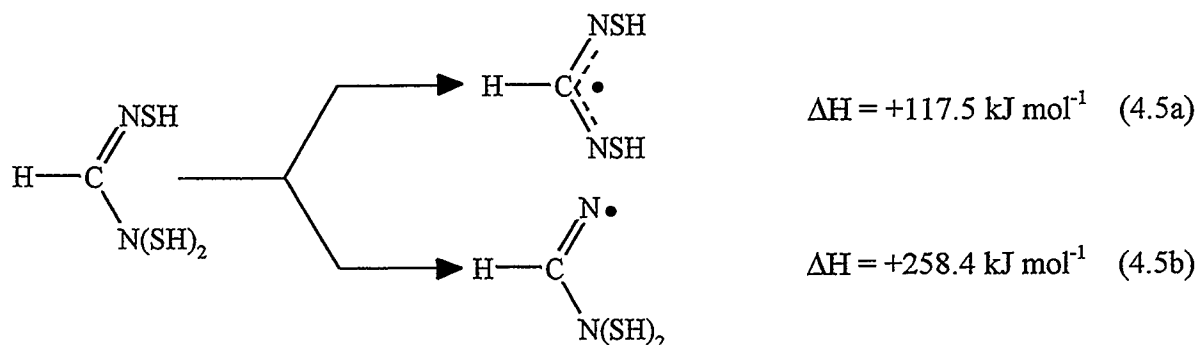
4.4.1. Mechanism of the Thermolysis of $\text{HCN}_2(\text{SH})_3$ (31f)

Theoretical calculations have become an important tool in the study of reaction mechanisms, including those involving chalcogen-containing molecules [100]. The main steps of a reaction mechanism for the thermolysis of $\text{RCN}_2(\text{SR}')_3$ (31) were outlined in the original work [34]. Here it has been attempted to provide a more detailed description of each step, including the enthalpy changes, by using DFT calculations based on the model compounds $\text{HCN}_2(\text{SH})_3$ (31f), $\text{HSN}=\text{C}(\text{H})\text{N}=\text{NC}(\text{H})=\text{NSH}$ (28i) in geometry II, and related intermediates. Total atomization energies (TAE) were calculated for the molecules in their most stable geometries; the reaction enthalpies have been evaluated as the difference of TAE between products and reactants.

The formation of both the *Z,E,Z*-diazene and the eight-membered ring are exothermic (equations 4.3 and 4.4). However, since two S-N bonds are weaker than the N=N bond, diazene formation is favored.



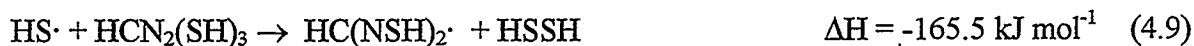
The generation of the radical $\text{HC(NSH)}_2\cdot$ requires an exothermic step, i.e. homolytic cleavage of an S-N bond. Homolysis should be preferred at the amino nitrogen (eq 4.5a), since it is less endothermic than at the imino nitrogen (eq 4.5b).



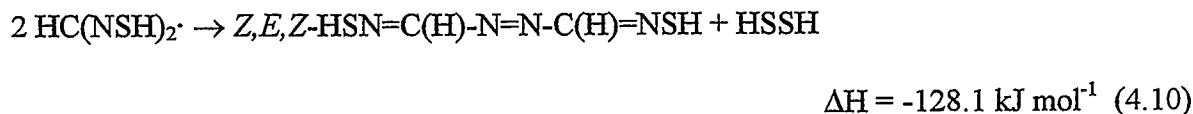
The imino radical must be very unstable and it may fragment into HCN and $(\text{HS})_2\text{N}\cdot$ (eq 4.6).



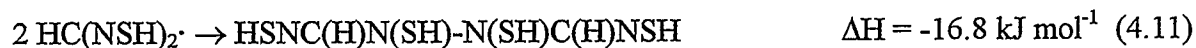
The formation of HSSH is a strong driving force (eq 4.7) (c.f. $\Delta H = -285 \pm 11 \text{ kJ/mol}$ for the dimerization of $\text{RS}\cdot$ ($\text{R} = \text{alkyl}$), and -262 kJ/mol in the case of $\text{HS}\cdot$) [101], which makes the process shown in equation 4.8 exothermic. It can be regarded as dissociation (eq 4.5a) followed by abstraction (eq 4.9).



Diazene formation from the intermediate radical is still a very exothermic process (eq 4.10).



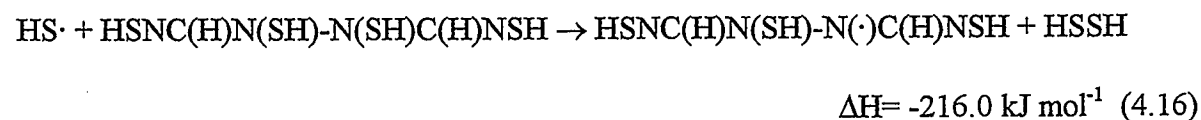
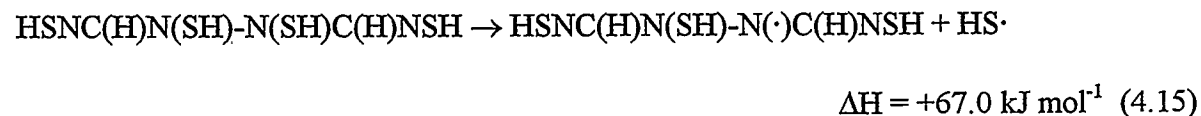
Dimerization of the intermediate radical should occur by N-N bond formation to give a hydrazine derivative (eq 4.11).



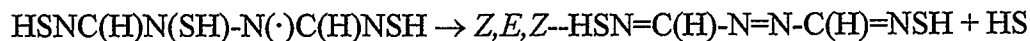
This dimer is closely related to those formed from the $[\text{R}\dot{\text{S}}\text{NR}']\cdot$ radicals (45) [81, 102]. Although the diazene formation (eq 4.12) is exothermic, it cannot occur in a concerted step, because such a four-center process is symmetry forbidden. Consequently, a two step sequence (eq. 4.13, 4.14) must be involved.



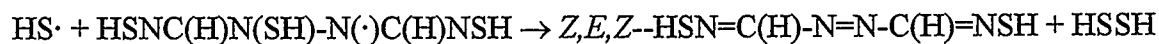
Therefore it is proposed that the formation of the diazene occurs through a hydrazinyl radical (eq 4.15 and 4.16) in a sequence analogous to that shown in eq 4.5a and 4.9 (*i.e.* dissociation followed by abstraction).



The loss of $\text{HS}\cdot$ from this radical (eq 4.17) would account for the formation of a diazene in a process that is well known in carbon chemistry [103]. Alternatively, the diazene could be formed by an abstraction process (eq 4.18).



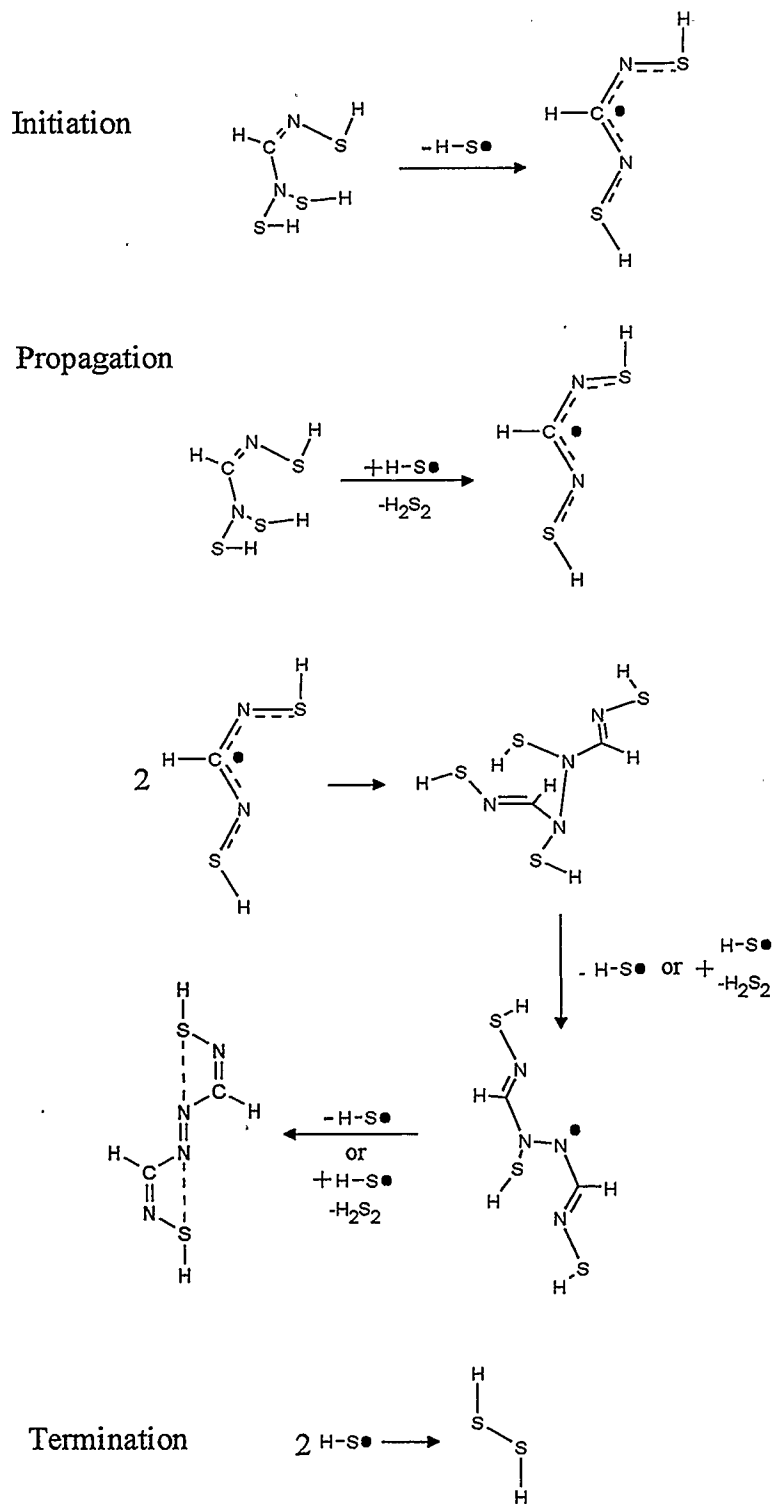
$$\Delta H = +104.7 \text{ kJ mol}^{-1} \quad (4.17)$$



$$\Delta H = -178.3 \text{ mol}^{-1} \quad (4.18)$$

4.4.2. Thermodynamics: N-S Homolysis versus HS· Abstraction

Consideration of the various processes involved in eq 4.3-4.18 leads to the general conclusion that while most of the steps are exothermic, those that involve homolysis of the S-N bond are strongly endothermic. The endothermic steps must be facilitated in some way and HS· seems to be the most likely catalytic species. In fact this mechanism would be a radical chain process (Scheme 4.1) if the availability of the chain propagator were not drastically reduced by the dimerization reaction 4.7.



4.5. Thermolysis of $\text{HCN}_2(\text{SPh})_3$ (**31d**)

4.5.1. Preliminary Visible and ^1H NMR Spectroscopy Studies

The noticeable colour changes observed in the decomposition of **31d** to the red diazene **28f** allowed a study of the initial stages of the process by UV-vis spectroscopy. The thermolysis of **31d** at 95°C in toluene solution revealed complicated kinetics. Formation of **28f** can be monitored by the continuous increase of absorbance between 450 and 500 nm; absorption by a transient species was observed at 820 nm. No other absorption maxima were detected (Figure 4.2).

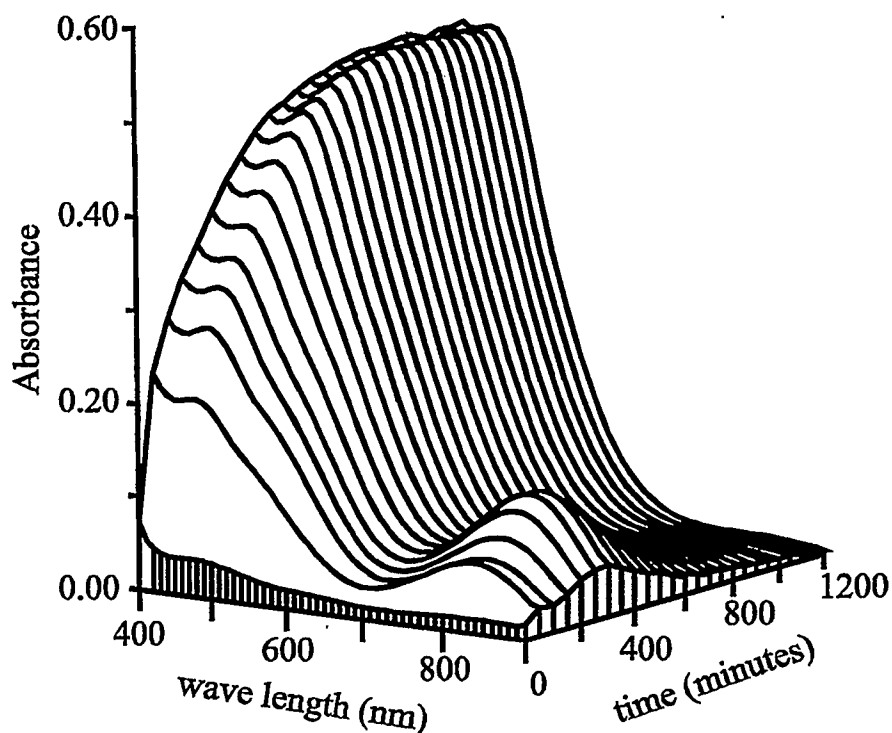


Figure 4.2. Evolution of the absorption spectrum during the decomposition of $\text{HCN}_2(\text{SPh})_3$ in toluene solution.

4.5.2. Kinetic Study

The reaction is slow; less than 5% conversion is achieved in 20h and then the reaction becomes even slower. Small increases of the absorbance attributable to **28d** continued during the following 8h. The limited solubility of **31d** in toluene precluded using higher concentrations to increase the reaction rate. We note, however, that the decomposition of **31d** is much faster if PhSCl is present in the reaction mixture (*vide infra*). Both absorptions at 470 and 820 nm showed a complex dependence on time (Figure 4.3), which prevented a more detailed kinetic study. The slope of the absorbance at 470 nm ($\Delta\text{Abs}_{470\text{nm}} = [\text{Abs}_{470\text{nm},t} - \text{Abs}_{470\text{nm},t-1200\text{s}}] / 1200\text{s}$) is correlated with the square of the absorbance at 820 nm (Figure 4.4). This suggests that the transient species is an intermediate that yields **28f** with second order kinetics. The negative y-intercept may indicate some reversible character for that step.

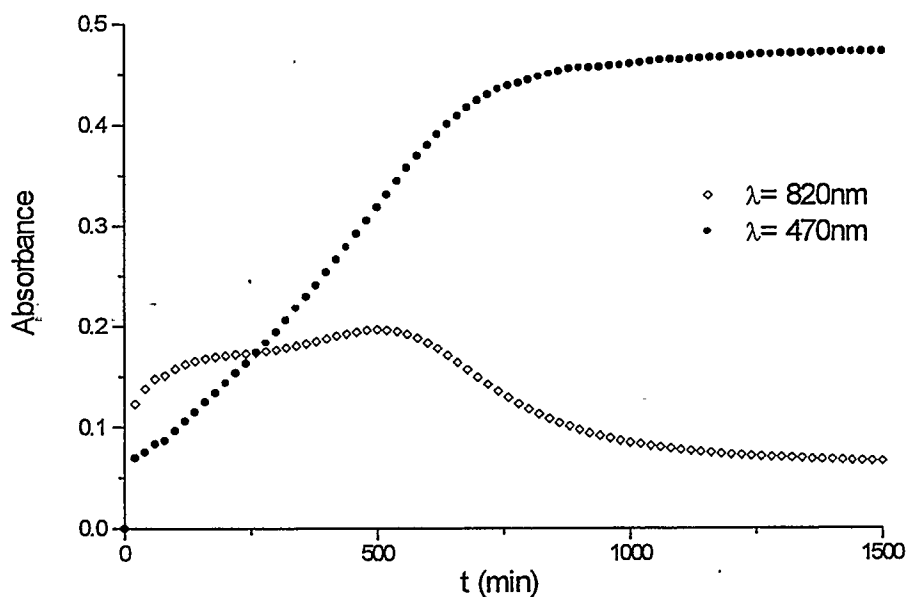


Figure 4.3. Time dependence of the absorbances at 820 and 450 nm during the decomposition of $\text{HCN}_2(\text{SPh})_3$ (**31d**) $1.4 \times 10^{-4} \text{ M}$ in toluene solution, at 95°C .

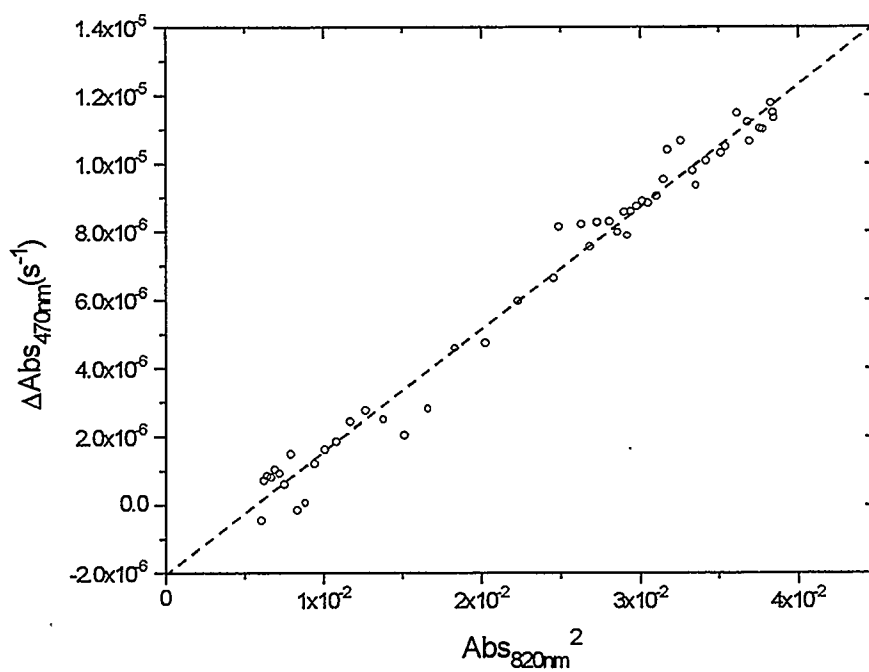


Figure 4.4. Dependence of the slope of $\Delta\text{Abs}_{450\text{nm}}$ on $\text{Abs}_{820\text{nm}}^2$ during the decomposition of $\text{HCN}_2(\text{SPh})_3$ (**31d**) $1.4 \times 10^{-4} \text{ M}$ in toluene solution, at 95°C . $r = 0.991$, slope: $3.6 \pm 0.1 \times 10^{-4} \text{ s}^{-1}$, y-intercept: $-2.1 \pm 0.4 \times 10^{-6} \text{ s}^{-1}$.

4.5.3. NMR Study

Although more concentrated solutions of **31d** (~ 0.1M) quickly acquire an intense red colour, the ^1H NMR spectra demonstrated that the process is still slow. Decomposition of **31d** in CD_2Cl_2 solution at 40°C was monitored by ^1H NMR. After eleven days, the apparent intensity ratio of the HC singlet (δ 8.18 ppm) to the aromatic multiplet at δ 7.1-7.6 decreases from 1:15 to 1:120.

4.5.4. ESR Study

In order to characterize any radical species formed in the decomposition of **31d** in hot toluene, ESR spectra were recorded at various time intervals. Initially the solution had a pale red tinge and gave a weak ESR spectrum. After heating the solution the intensity of the signal increased by an order of magnitude. The strongest signal was obtained at 55 min. This spectrum was integrated to give the absorption spectrum shown in Figure 4.5a. A three line spectrum was calculated (Figure 4.5c) and subtracted from the experimental spectrum to give a difference spectrum consisting of a quintet of doublets (Figure 4.5b). The ESR spectrum recorded on the next day was very weak. The three line species corresponds to a species with a single ^{14}N coupling ($g = 2.0074$, $A_{\text{N}} = 11.45$ G) and no proton splitting. The A_{N} factor is comparable to those of the $(\text{ArS})_2\text{N}\cdot$ radicals, described in Section 4.1. Thus this spectrum is tentatively attributed to $(\text{PhS})_2\text{N}\cdot$ generated via imino homolysis and

fragmentation. The changes of solvent, temperature and the fact that this spectrum is hidden by the five line species may account for the observed small difference in ESR parameters.

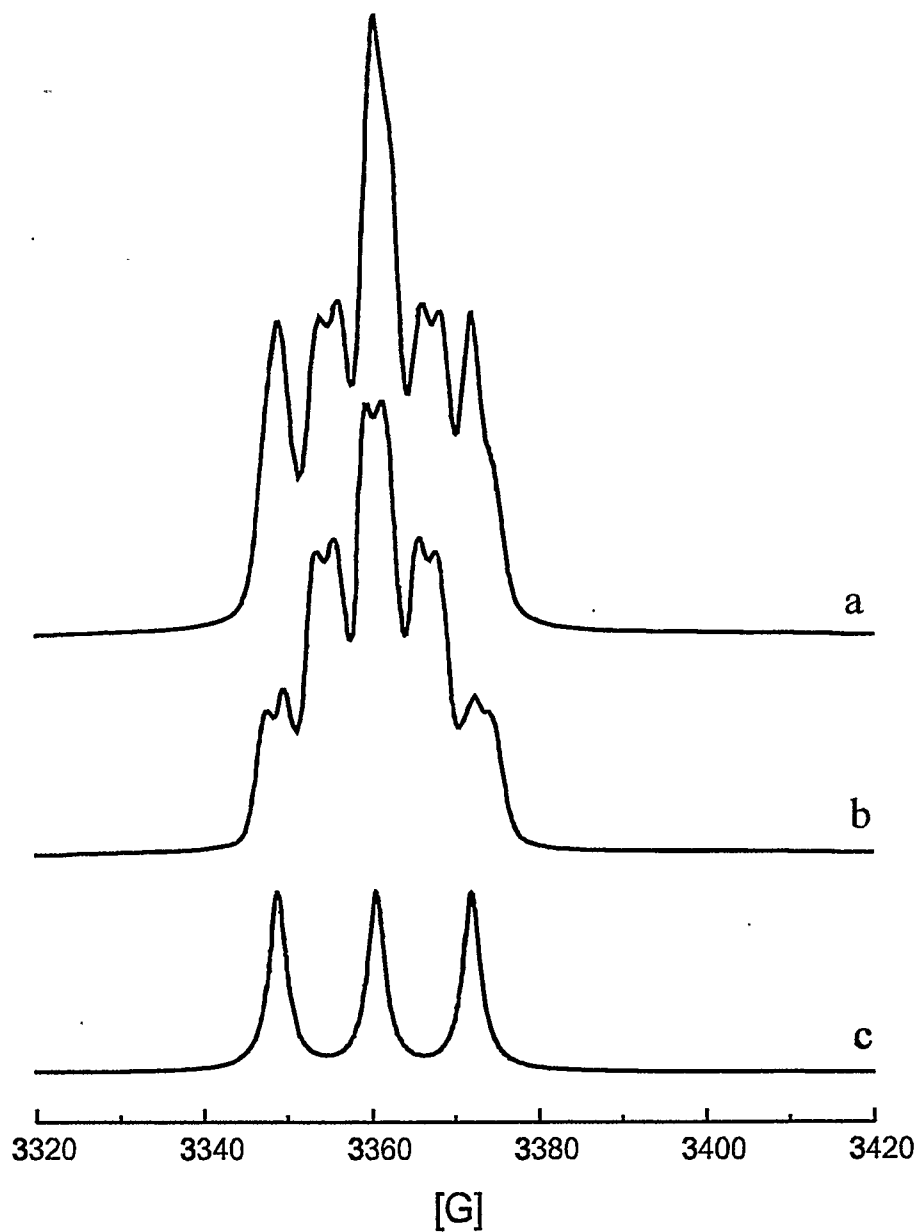


Figure 4.5. a) Integrated (absorption) ESR spectrum for the decomposition of $\text{HCN}_2(\text{SPh})_3$ (**31d**) in toluene solution. b) difference spectrum. c) calculated three line spectrum.

The five line spectrum belongs to a free radical with two ^{14}N splitting plus a small doublet splitting from coupling to one proton ($g = 2.0070$, $A_{\text{N}} = 6.14\text{G}$, $A_{\text{H}} = 2.1\text{G}$). There have been extensive ESR studies of hydrazinyl radicals, which produce a five-line spectrum despite the nonequivalence of the two nitrogen atoms [104]. A hydrazinyl radical analogous to that proposed as an intermediate in the decomposition of **31f** (eq 4.15 and 4.16) should also exhibit coupling to two nonequivalent protons. The observed five line spectrum is therefore attributed to the radical $\text{HC}(\text{NSPh})_2\cdot$ (**29c**).

4.6. Molecular Modeling of the Free Radical $\text{HC}(\text{NSH})_2\cdot$ (**29e**)

The ESR studies of the formation of the diazenes have consistently provided evidence for the presence of the radicals $\text{RC}(\text{NSPh})_2\cdot$ (**29**), but no examples of such species have been isolated and characterized. DFT optimized structures of the model **29e** were employed to provide an understanding of their properties.

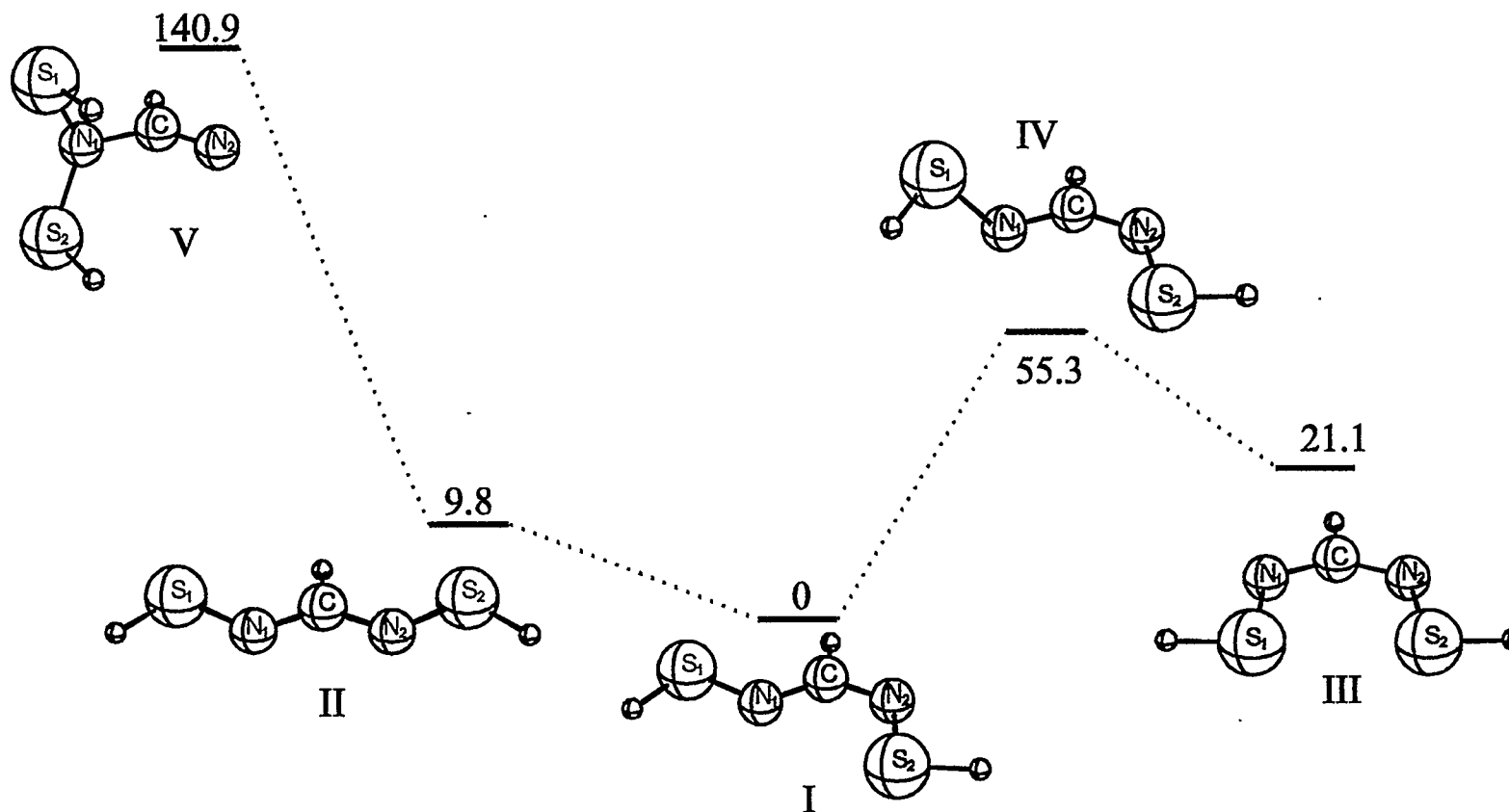


Figure 4.6. Potential energy diagram for the isomers of HC(NSH)_2 . Relative energy differences are given in kJ/mol. Dimensions: **I**: C-N₁ 1.310 Å, C-N₂ 1.319 Å, N₁-S₁ 1.665 Å, N₂-S₂ 1.665 Å, N₁-C-N₂ 123.5°, S₁-N₁-C 117.2°, S₂-N₂-C 117.2°; **II**: C-N₁ 1.317 Å, N₁-S₁ 1.663 Å, N₁-C-N₂ 119.6°, S₁-N₁-C 114.6°; **III**: C-N₁ 1.321 Å, N₁-S₁ 1.667 Å, N₁-C-N₂ 135.0°, S₁-N₁-C 119.4°; **IV**: C-N₁ 1.364 Å, C-N₂ 1.283 Å, N₁-S₁ 1.630 Å, N₂-S₂ 1.711 Å, N₁-C-N₂ 124.3°, S₁-N₁-C 120.0°, S₂-N₂-C 115.4°; **V**: C-N₁ 1.450 Å, C-N₂ 1.235 Å, N₁-S₁ 1.709 Å, N₁-C-N₂ 120.9°, S₁-N₁-C 115.5°, S₁-N₁-S₂ 123.4°.

4.6.1. Structure

The relative energies of the five structural isomers considered for **29e** are depicted in Figure 4.6. The three planar, π -delocalized structures **I** (C_s), **II** (C_{2v}), and **III** (C_{2v}) are more stable than the imido isomer **V**. The most stable free radical (**I**) has an *E,Z* geometry.

4.6.2. Rotational Barrier and Interconversion

The relative small energy differences suggest that an equilibrium between **I**, **II** and **III** is feasible. Structural interconversion involves rotation of the S-N bond; the transition state (**IV**) between **I** and **III** was optimized in order to evaluate the barrier, which is indeed small enough to permit dynamic equilibrium. The results are reminiscent of the well established behavior of sulfur diimides, $RN=S=NR$ (**14a**), for which the *E,Z*-isomer is usually the most stable structural entity [105].

4.6.3. Electronic Structure, ESR and Visible Spectra

The isomers **I**, **II** and **III** have a SOMO which is a π^*_{N-S} orbital (Figure 4.7). The coefficients of the p_z orbitals of the nitrogen atoms are nearly constant from one geometry to another. Thus the A_N coefficients are expected to have the same value and the isomer **I** would provide an almost symmetrical five-line ESR spectrum despite the geometric inequivalence of the N atoms. The SOMO possesses a nodal plane on carbon, therefore the

coupling to the proton observed for the radical $\text{HC(NSPh)}_2\cdot$ (**29c**) must be due to spin polarization through the C-N and C-H bonds.

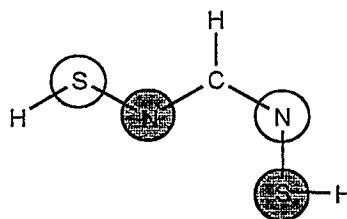
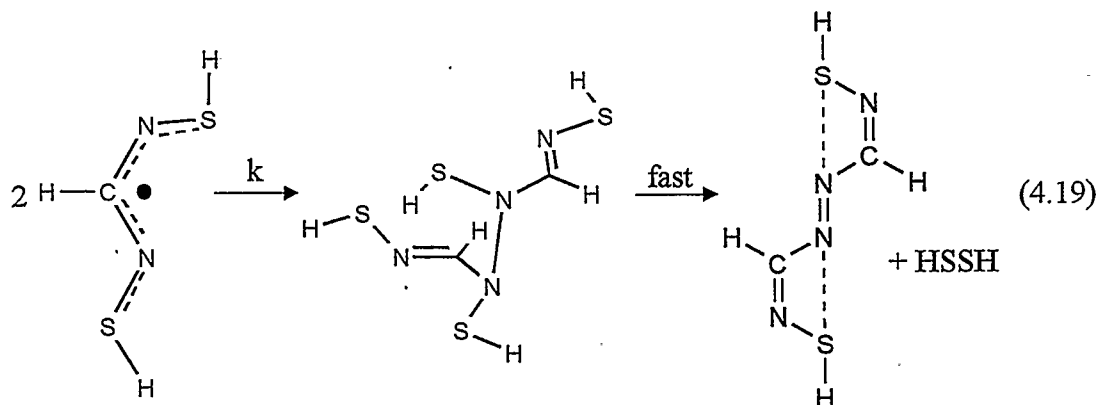


Figure 4.7. SOMO for $\text{HCN}_2(\text{SH})_2\cdot$ I.

The calculated energy for the first electronic transition, HOMO ($3a''$) \rightarrow SOMO ($4a''$), for structure I is 1.78 eV (702 nm), close to the observed absorbance in the UV-vis spectra, 1.51 eV (820 nm), for the transient species. The difference of 0.27 eV is within the limits of DFT calculations. The transient species is, therefore, identified as $\text{HCN}(\text{SPh})_2\cdot$ (**29c**).

4.7. Decay of $\text{HCN}(\text{SPh})_2\cdot$ (**29c**)

The second order rate law for the decay of **29c** indicates that the dimerization equilibrium is negligible. It is a slow process possibly due to steric hindrance, but the diazene is formed quickly once the dimer is formed (eq. 4.19).



The rate law, according to the experimental data, can be written as:

$$\frac{dC_p}{dt} = kC_i^2 - c \quad (4.20)$$

where C_p is the concentration of the diazene **28l** and C_i the concentration of **29c**. In terms of absorbance:

$$\frac{dAbs_{470nm}}{dt} = \frac{\varepsilon_p k}{\varepsilon_i \ell} Abs_{820nm} - c' \quad (4.21)$$

where ε_p and ε_i represent the molar absorptivities of **28l** and **29c**, respectively. The value of ε_i cannot be measured directly because of the transient nature of the intermediate radical **29c**, however it can be estimated as $\approx 10^4 \text{ L mol}^{-1} \text{ cm}^{-1}$. This affords $k \approx 1.0 \text{ L mol}^{-1} \text{ S}^{-1}$. The result is remarkably similar to the decay of $[(\text{ArS})_2\text{N}]^\bullet$ (**46a**), which decomposes with a second order rate law and a $k = 1.1 \text{ L mol}^{-1} \text{ S}^{-1}$ [106].

4.8. Effect of PhS· Radicals on the Thermolysis of $\text{HCN}_2(\text{SPh})_3$ (**31d**)

Up to this point, the slow thermolysis of **31d** does not explain by itself why the diazenes **28** are easily formed from the mixture of $\text{RCN}_2(\text{SiMe}_3)_3$ and ArSCl even at low

temperatures. The thermodynamic study suggests that the process is slow due to the strongly endothermic nature of the steps that involve homolysis of the S-N bond. The key factor appears to be the availability of $\text{PhS}\cdot$, which may catalyze the decomposition of **31**. In any case the amounts of phenylthiyl radical present in the reaction medium must be very small. A sample of **31d** was refluxed in toluene for 20 h; after removal of the solvent, a GCMS of the residue showed the presence of small amounts of $4\text{-CH}_3\text{C}_6\text{H}_4\text{SPh}$, presumably formed by reaction of the solvent with $\text{PhS}\cdot$. The effect of this radical could be inferred by studying the influence of species that may supply or scavenge it in the reaction mixture.

4.8.1.1. Effect of PhSSPh

It was observed that the beginning of the thermolysis process is slower in the presence of an excess of PhSSPh (Figure 4.8). Disulfides effectively reduce the amount of $\text{RS}\cdot$ by formation of the adduct $\text{R}_3\text{S}_3\cdot$ [107]. The structures of these radicals are unknown, but the corresponding cations R_3S_3^+ have been characterized [108].

4.8.1.2. Effect of PhSCl

An excess of PhSCl (2.6:1) accelerates the decomposition of **31d** in CDCl_3 (0.14M) remarkably. At room temperature the ^1H NMR spectrum shows that the decomposition is complete in 30 min. PhSCl can be regarded as a source of $\text{PhS}\cdot$ radicals that catalyze the reaction [109].

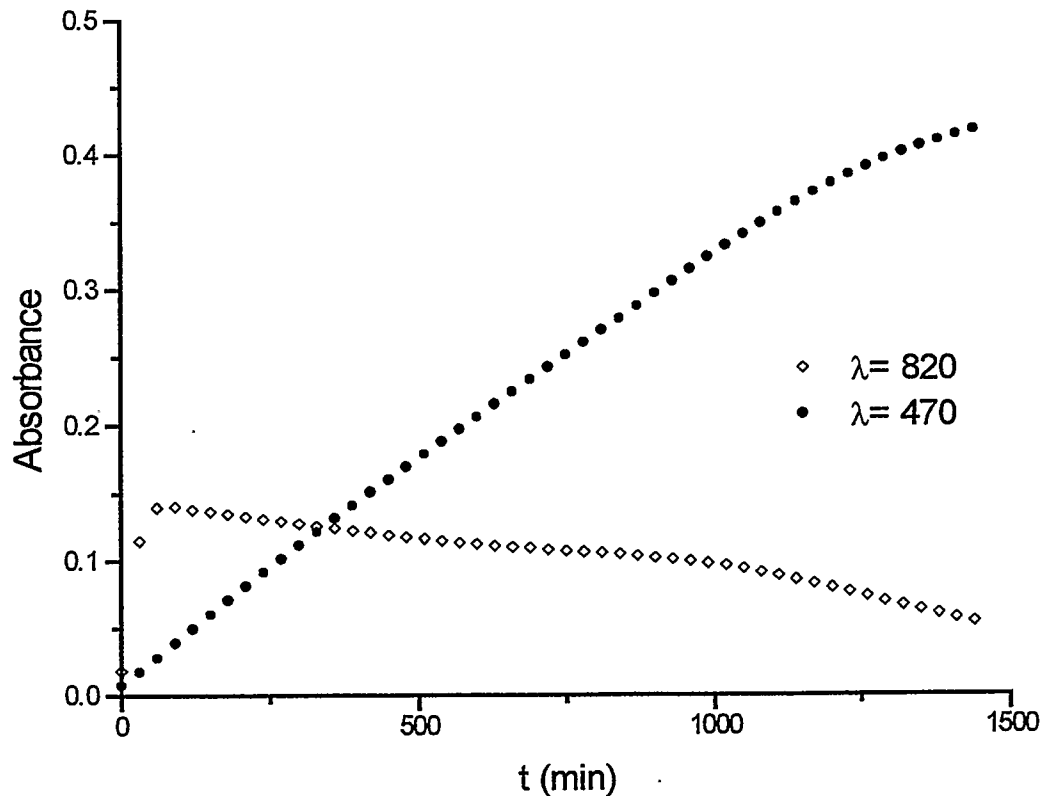


Figure 4.8. Time dependence of the absorbances at 820 and 450 nm of the mixture $\text{HCN}_2(\text{SPh})_3$ 1.4×10^{-4} M, PhSSPh 1.3×10^{-3} M in toluene solution, at 95°C .

4.8.1.3. Attempted Reaction of $\text{PhCN}_2(\text{SCCl}_3)_3$ (**31b**) with $4\text{-CH}_3\text{C}_6\text{H}_4\text{SCl}$

Since PhSCl accelerates the decomposition of **31d**, it was decided to study the effect of an arenesulfonyl chloride on the stable derivative **31b**. A 1:1 mixture of $4\text{-CH}_3\text{C}_6\text{H}_4\text{SCl}$ and **31b** in toluene remained unchanged after 16h of reflux. This indicates that Cl_3CS units cannot be abstracted by $\text{ArS}\cdot$ radicals.

4.9. Summary

Spectroscopic investigations and thermochemical calculations of the decomposition of trithiolated formamidines, $\text{HCN}_2(\text{SR})_3$ ($\text{R} = \text{Ph}, \text{H}$), indicate that the formation of the diazenes $\text{RSN}=\text{C}(\text{H})-\text{N}=\text{N}-\text{C}(\text{H})=\text{NSR}$ occurs via a radical process. The initiation step involves the production of the radicals $\text{HCN}_2(\text{SR})_2^\cdot$, which dimerize slowly and then quickly form the corresponding diazenes. The properties of the model radical $\text{HCN}_2(\text{SH})_2^\cdot$ have been studied by DFT calculations. The most stable geometry of the radical was found to be an *E-Z* structure. The composition of the calculated SOMO and the estimated ΔE for the first electronic transition for the model radical are in agreement with the spectroscopic measurements. Inhibition and catalysis by PhSSPh and PhSCl , respectively, are consistent with the role of the radical PhS^\cdot as a catalyst. The radical $\text{HCN}_2(\text{SR})_2^\cdot$ was identified by ESR and UV-vis spectra.

4.10. Details of Calculations

The following model structures were fully optimized: $\text{HCN}_2(\text{SH})_3$, $\text{HSNC}(\text{H})\text{N}(\text{SH})-\text{N}(\text{SH})\text{C}(\text{H})\text{NSH}$, $\text{HSNC}(\text{H})\text{N}(\cdot)-\text{N}(\text{SH})\text{C}(\text{H})\text{NSH}$, *Z,E,Z*- $\text{HS}-\text{N}=\text{C}(\text{H})-\text{N}=\text{N}-\text{C}(\text{H})=\text{N}-\text{SH}$, *E*- $\text{HN}=\text{NH}$, HSSH , $\text{HN}(\cdot)\text{SH}$, $\text{HS}(\text{H})\text{N}-\text{N}(\text{H})\text{SH}$, $(\text{HS})_2\text{N}^\cdot$, HCN and HS^\cdot . The disulfide HSSH and $(\text{HS})_2\text{N}^\cdot$ were assumed to have C_2 geometry; a C_{2h} symmetry was used for *Z,E,Z*- $\text{HS}-\text{N}=\text{C}(\text{H})-\text{N}=\text{N}-\text{C}(\text{H})=\text{N}-\text{SH}$ and *E*- $\text{HN}=\text{NH}$. Details of the structure optimization of $(\text{HC})_2\text{N}_4(\text{SH})_2$ are provided in Section 5.6. A thorough study of the structure of

$\text{HCN}_2(\text{SH})_2$ was carried out as well (*vide supra*) and the most stable geometry was considered for the thermodynamic analysis. All other structures were calculated assuming no symmetry constraints. Open shell species were optimized at the unrestricted level.

4.11. Experimental Section

Details of the synthetic and instrumental methods have been provided in Section 2.7. $4\text{-CH}_3\text{C}_6\text{H}_4\text{SCl}$ [69] and $\text{PhCN}_2(\text{SCCl}_3)_3$ [34] were prepared according to literature methods. ESR spectra were recorded, by Dr. B. McGarvey, at the University of Windsor, on a Bruker ESP-300e spectrometer equipped with a NMR magnetometer, a microwave counter, and a variable temperature accessory.

4.11.1. Preparation of $\text{HCN}_2(\text{SPh})_3$

A solution of PhSCl (2.45 g, 16.94 mmol) in 25 mL of hexanes was slowly added to a solution of $\text{HCN}_2(\text{SiMe}_3)_3$ (1.47 g, 5.65 mmol) in 25 mL of the same solvent at -100°C . The yellow mixture was stored at -20°C for 60 h. The product $\text{HCN}_2(\text{SPh})_3$ was isolated as an off white powder, which was washed with hexanes and recrystallized from $\text{CH}_2\text{Cl}_2/\text{hexanes}$. The colourless crystals were finally rinsed with diethyl ether (yield: 1.01g, 2.97 mmol, 53%). Mp: 100°C dec. Anal. Calcd. for $\text{C}_{19}\text{H}_{16}\text{N}_2\text{S}_3$: C, 61.92; H, 4.38; N, 7.60. Found C, 61.43; H, 4.46; N, 7.74. ^1H NMR (CD_2Cl_2): δ 8.18 (s, C-H, 1H), 7.60-7.10 (m, C_6H_5 , 15H). EI-MS (m/Z): 368 (M^+), 218 (Ph_2S_2), 109 (PhS). IR (cm^{-1} , Nujol): 1606 m, 1578 m, 1303 m, 1169 m, 1115 m, 1082 m, 1023 m, 736 s, 688 m.

4.11.2. Visible Spectroscopy Studies of the Thermolysis of $\text{HCN}_2(\text{SPh})_3$

In a typical experiment a $\sim 10^{-3}\text{M}$ solution of **31d** in toluene was heated at 95°C under nitrogen. The UV-vis spectrum was recorded at constant intervals. Raw experimental data and the calculated $\Delta\text{Abs}_{470\text{nm}}$ and $\text{Abs}_{820\text{nm}}^2$ are given in Table 4.3.

Table 4.3. Absorbances at 820 and 450 nm during the decomposition of $\text{HCN}_2(\text{SPh})_3$ (**31d**) $1.4 \times 10^{-4}\text{ M}$ in toluene solution, at 95°C ; $\text{Abs}_{820\text{nm}}^2$, and $\Delta\text{Abs}_{470\text{nm}} = [\text{Abs}_{470\text{nm},t} - \text{Abs}_{470\text{nm},t-1200\text{s}}]/1200\text{s}$.

t (min)	$\text{Abs}_{820\text{nm}}$	$\text{Abs}_{470\text{nm}}$	$\text{Abs}_{820\text{nm}}^2$	$\Delta\text{Abs}_{470\text{nm}} (\text{s}^{-1})$
20	0.123187	0.069139		
40	0.137728	0.075148	0.018969	5.01×10^{-6}
60	0.147768	0.083209	0.021835	6.72×10^{-6}
80	0.151148	0.087063	0.022846	3.21×10^{-6}
100	0.157786	0.096816	0.024897	8.13×10^{-6}
120	0.162202	0.106660	0.02631	8.2×10^{-6}
140	0.165183	0.116581	0.027285	8.27×10^{-6}
160	0.167478	0.126519	0.028049	8.28×10^{-6}
180	0.169057	0.136082	0.02858	7.97×10^{-6}
200	0.170343	0.146346	0.029017	8.55×10^{-6}
220	0.171515	0.156644	0.029417	8.58×10^{-6}
240	0.172570	0.167106	0.02978	8.72×10^{-6}
260	0.173636	0.177765	0.030149	8.88×10^{-6}
280	0.174745	0.188346	0.030536	8.82×10^{-6}
300	0.176173	0.199185	0.031037	9.03×10^{-6}

320	0.178174	0.211653	0.031746	1.04×10^{-05}
340	0.180542	0.224425	0.032595	1.06×10^{-05}
360	0.182573	0.236159	0.033333	9.78×10^{-06}
380	0.184982	0.248229	0.034218	1.01×10^{-05}
400	0.187454	0.260583	0.035139	1.03×10^{-05}
420	0.190148	0.274330	0.036156	1.15×10^{-05}
440	0.192253	0.287092	0.036961	1.06×10^{-05}
460	0.193911	0.300310	0.037602	1.1×10^{-05}
480	0.195735	0.314431	0.038312	1.18×10^{-05}
500	0.196239	0.328018	0.03851	1.13×10^{-05}
520	0.196022	0.341804	0.038425	1.15×10^{-05}
540	0.194396	0.354995	0.03779	1.1×10^{-05}
560	0.191980	0.368434	0.036856	1.12×10^{-05}
580	0.188194	0.381005	0.035417	1.05×10^{-05}
600	0.183196	0.392224	0.033561	9.35×10^{-06}
620	0.177543	0.403642	0.031522	9.52×10^{-06}
640	0.170911	0.413085	0.02921	7.87×10^{-06}
660	0.163921	0.422132	0.02687	7.54×10^{-06}
680	0.156771	0.430066	0.024577	6.61×10^{-06}
700	0.149374	0.437210	0.022312	5.95×10^{-06}
720	0.142377	0.442868	0.020271	4.72×10^{-06}
740	0.135437	0.448357	0.018343	4.57×10^{-06}
760	0.128930	0.451710	0.016623	2.79×10^{-06}
780	0.122960	0.454135	0.015119	2.02×10^{-06}
800	0.117540	0.457139	0.013816	2.5×10^{-06}
820	0.112601	0.460425	0.012679	2.74×10^{-06}
840	0.108189	0.463340	0.011705	2.43×10^{-06}

860	0.104142	0.465543	0.010846	1.84×10^{-06}
880	0.100582	0.467482	0.010117	1.62×10^{-06}
900	0.097302	0.468917	0.009468	1.2×10^{-06}
920	0.094189	0.469006	0.008871	7.35×10^{-08}
940	0.091419	0.468816	0.008357	-1.6×10^{-07}
960	0.089089	0.470586	0.007937	1.48×10^{-06}
980	0.086763	0.471291	0.007528	5.88×10^{-07}
1000	0.084897	0.472373	0.007208	9.01×10^{-07}
1020	0.083243	0.473600	0.006929	1.02×10^{-06}
1040	0.081682	0.474566	0.006672	8.05×10^{-07}
1060	0.080293	0.475560	0.006447	8.28×10^{-07}
1080	0.078997	0.476395	0.006241	6.96×10^{-07}
1100	0.077775	0.475843	0.006049	-4.6×10^{-07}
1120	0.076796	0.477128	0.005898	1.07×10^{-06}
1140	0.075686	0.477857	0.005728	6.08×10^{-07}
1160	0.074816	0.477938	0.005597	6.76×10^{-08}
1180	0.073981	0.478479	0.005473	4.51×10^{-07}
1200	0.072996	0.479292	0.005328	6.78×10^{-07}

4.11.3. ^1H NMR Spectroscopy Studies of the Thermolysis of $\text{HCN}_2(\text{SPh})_3$

A 0.1M solution of **31d** in deuterated dichloromethane was kept at constant 40°C. The ^1H NMR spectrum was monitored during 14 days until the reaction was apparently complete.

4.11.4. ESR Spectroscopy Studies of the Thermolysis of $\text{HCN}_2(\text{SPh})_3$

A 10^{-3}M solution of **31d** in deoxygenated toluene was prepared and stored at 0°C before the measurements started. The ESR spectrum was acquired at 5, 10, 55 and 85 min. while the sample was heated at 92°C . The solution was stored at room temperature and an additional spectrum was obtained the next day.

4.11.5. Visible Spectroscopy Studies of the Effect of PhSSPh on the Thermolysis of $\text{HCN}_2(\text{SPh})_3$

Table 4.4. Absorbance at 820 and 470 nm of the mixture $\text{HCN}_2(\text{SPh})_3$ $1.4 \times 10^{-4}\text{ M}$, PhSSPh $1.3 \times 10^{-3}\text{ M}$ in toluene solution, at 95°C .

t (min)	Abs _{820nm}	Abs _{470nm}	t (min)	Abs _{820nm}	Abs _{470nm}
30	0.017400	0.114500	630	0.215720	0.111210
60	0.027730	0.139540	660	0.224760	0.110000
90	0.038730	0.140210	690	0.233630	0.109220
120	0.049440	0.138230	720	0.242690	0.108180
150	0.059980	0.136320	750	0.251960	0.107200
180	0.070660	0.134500	780	0.260990	0.106270
210	0.081080	0.132560	810	0.270040	0.105610
240	0.091430	0.130920	840	0.279030	0.104520
270	0.101430	0.129380	870	0.288040	0.103280
300	0.111740	0.127450	900	0.297400	0.102070
330	0.121800	0.125940	930	0.306400	0.100840
360	0.131560	0.124230	960	0.315370	0.099510
390	0.141370	0.122370	990	0.324220	0.097750

420	0.150980	0.121000	1020	0.332860	0.096140
450	0.160160	0.119060	1050	0.341390	0.093700
480	0.169650	0.117580	1080	0.349550	0.091090
510	0.179070	0.116290	1110	0.357460	0.088420
540	0.188230	0.114680	1140	0.364940	0.085510
570	0.197290	0.113390	1170	0.372290	0.082430
600	0.206370	0.112170	1200	0.378920	0.079470

$\text{HCN}_2(\text{SPh})_3$ and PhSSPh were dissolved in toluene to give concentrations of $1.4 \times 10^{-4} \text{ M}$ and $1.3 \times 10^{-3} \text{ M}$, respectively. The mixture was kept at -20°C before the measurements. The mixture was then heated to 95°C and the visible absorption spectrum was monitored frequently. The experimental data are given in Table 4.4.

4.11.6. ^1H NMR Spectroscopy Studies of the Effect of PhSCl on the Thermolysis of $\text{HCN}_2(\text{SPh})_3$

PhSCl and **31d** were mixed in CDCl_3 to give total concentrations of 0.14 M and 0.36 M , respectively. The mixture was kept at -78°C , then quickly warmed up to room temperature and the ^1H NMR spectrum was monitored at 5 min intervals, during a total period of 1h.

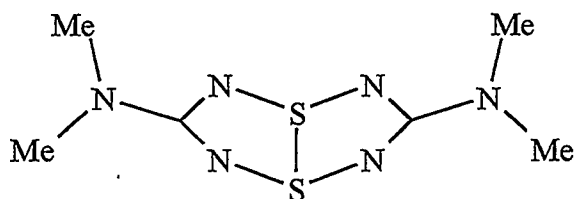
4.11.7. Attempted Reaction of PhCN₂(SCCl₃)₃ (**31b**) with 4-CH₃C₆H₄SCl

4-CH₃C₆H₄SCl (0.07g, 0.4 mmol) and **31b** (0.25g, 0.4 mmol) were mixed in 30mL of toluene. The mixture was refluxed for 16h. The solvent was removed under vacuum and the residue was extracted with acetonitrile. The ¹H-NMR spectrum of the solid residue in CD₂Cl₂ corresponded only to that of **31b**.

5. Theoretical Study of the $(R'C)_2N_4(SR)_2$ Ring

5.1. The Electronic Structure of Dithiatetrazocines

1,5-Dithiatetrazocines (**20**) have attracted attention due to their 10 π -electron aromatic character. Several investigations of their properties have been published, including synthetic, spectroscopic, structural, theoretical and electrochemical studies [110,26]. In derivatives where the R group is aryl, *tert*-butyl, furyl or thienyl the ring is planar. As a contrast the dimethylamino substituent produces a folded structure (**20g**) with a short S \cdots S contact (2.428 Å) [111]. Similar geometric distortions forming transannular S-S bonds are common in S-N systems involving two-coordinate sulfur, *e.g.* S_4N_4 [112], 1,5- $(Ph_3PN)_2S_4N_4$ [113], and 1,5- $R_4P_2N_4S_2$ [114].



20g

This geometry is rationalized in terms of perturbation theory. The HOMO (b_{1u} under D_{2h} symmetry) is destabilized by an amino-N lone-pair orbital, which allows for interaction with the LUMO (b_{3g}) in a second order Jahn-Teller distortion [115]. The result is the observed C_{2v} geometry; the S-S link is stabilized by mixing of the HOMO (b_{1u}) with the former LUMO+2 (a_{1g}) (Figure 5.1) [110]. As a consequence of these electronic changes,

some characteristic properties of these structural isomers allow one to distinguish easily one geometry from the other. For instance, the UV-vis spectra of the D_{2h} rings exhibit maxima at ~ 410 nm and a series of bands around 300 nm, while the folded compounds show a maximum at 229 nm [115a]; also **20g** has a more negative reduction potential than the planar molecules [26].

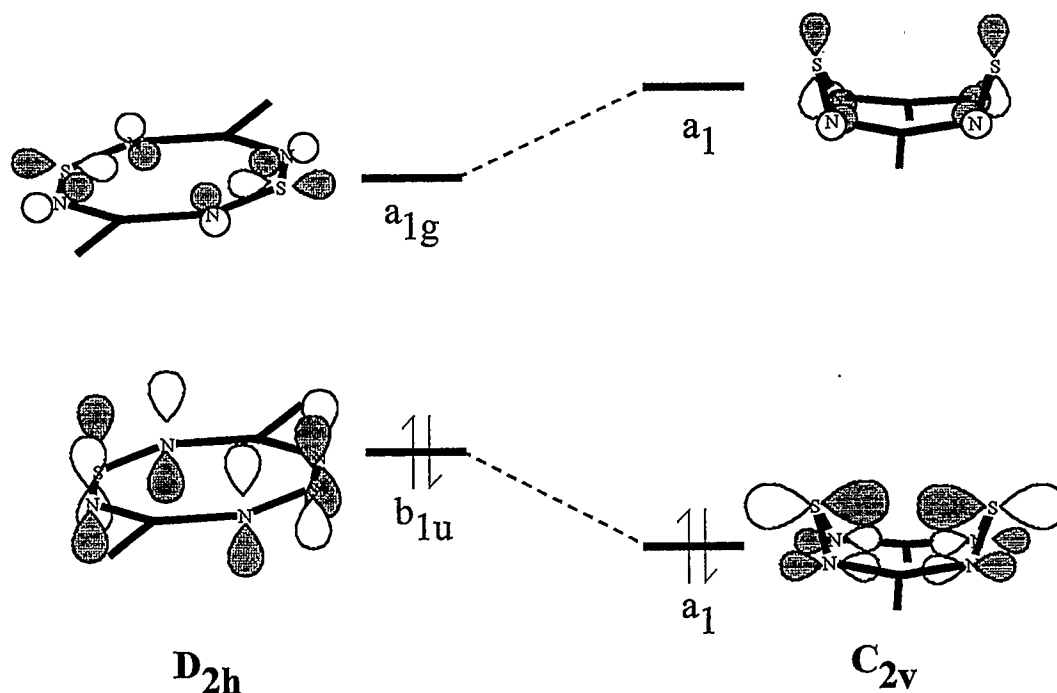


Figure 5.1. Mixing of molecular orbitals of dithiatetrazocines in D_{2h} and C_{2v} geometries.

While C-N-S heterocycles containing three-coordinate sulfur are readily accessible, investigations of their properties have received comparatively little attention. No theoretical studies are available on the S,S' diorgano-substituted dithiatetrazocines (**27**). As a part of this investigation a brief DFT study of these systems was included with the main purpose of

comparing the energy and electronic structures of **27** with those of the isomeric diazenes (**28**).

5.2. Molecular Structure of $(\text{HC})_2\text{N}_4(\text{SH})_2$ (**27h**)

The structure of the model ring **27h** was optimized, using the data from a preliminary crystallographic study. The structural characterization of two derivatives of the type **27** was accomplished later (46). The ring adopts a folded geometry. This C_{2v} arrangement resembles that of **20g** (Figure 5.2), but the S-S distance is larger. Structural parameters of the model are compared with the average values found for $(4\text{-CF}_3\text{C}_6\text{H}_4\text{C})_2\text{N}_4(\text{SPh})_2$ (**27d**) and $(4\text{-BrC}_6\text{H}_4\text{C})_2\text{N}_4(\text{SPh})_2$ (**27g**) in Table 5.1. The calculated structure provides a fair estimate of the actual geometry; the largest deviations are for the parameters which involve the sulfur atoms.

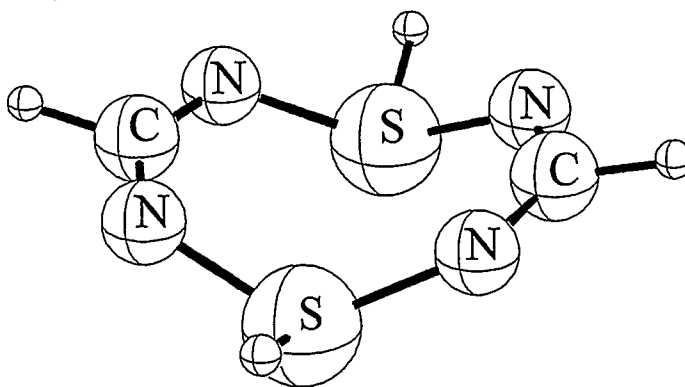


Figure 5.2. Optimized structure of the model ring $(\text{HC})_2\text{N}_4(\text{SH})_2$ (**27h**).

Table 5.1. Comparison of molecular dimensions calculated for the model ring $(\text{HC})_2\text{N}_4(\text{SH})_2$ (**27h**), experimental data, and the calculated anion $(\text{HC})_2\text{N}_4(\text{SH})_2^{2-}$ (**51**).

	C_{2v} 27h	Exp. Av. ^a	D_{2h} 27h	C_{2h} 27h	C_{2v} 51
Bond Distances (Å)					
C-N	1.327	1.329	1.320	1.331	1.341
N-S	1.710	1.645	1.757	1.705	1.877
S...S	3.260	2.85	3.249	3.247	2.537
Bond Angles (°)					
N-C-N	139.4	133.9	139.6	135.2	134.4
C-N-S	122.6	120.5	122.9	118.6	113.8
N-S-N	124.9	112.5	154.6	130.1	156.3
R-S-N	92.9	98.8	102.7	92.8	85.2
Torsion Angles (°)					
N-C-N-S	16.8	9.8	0	26.8	3.6
N-S-N-C	69.6	82.6	0	81.7	86.6

a. Average values calculated from the crystallographic study of the structures of $(4\text{-CF}_3\text{C}_6\text{H}_4\text{C})_2\text{N}_4(\text{SPh})_2$ (**27d**) and $(4\text{-BrC}_6\text{H}_4\text{C})_2\text{N}_4(\text{SPh})_2$ (**27g**) [46].

The observed geometry can be explained by considering a hypothetical planar (D_{2h}) structure (See Figure 5.3). In this optimized structure, a 12 π -electron system, the HOMO ($2b_{3g}$) lies just 0.12 eV below the LUMO ($5b_{2u}$). It is therefore predicted that a second order Jahn-Teller distortion will occur in the direction of the axis perpendicular to the plane ($B_{3g} \times B_{2u} = B_{1u}$; $\Gamma_Z \subset \Gamma_{B_{1u}}$) so that the S atoms are lifted from the plane. Indeed the structure is the result of the same effect that leads to folding in **20g**. The relationship between **27h** and **20g** becomes apparent by considering that the attachment of two substituents on the S atoms moves two electrons into the S-S antibonding orbital, breaking the bond and forming two lone pairs. There are two important consequences of the geometric change: (a) electrons occupying the high lying π^* frontier orbitals in the planar structure are localized on S lone pairs in the folded structure, this affords a stabilization energy of 267.8 kJ mol⁻¹; (b) there is mixing of the σ and π orbitals.

The relatively short S-S separation of 2.8-2.9 Å observed in the X-ray structures of the rings **27d** and **27g** [46] may suggest a transannular bond. However, the optimized S-S distance for the model heterocycle **27h** corresponds to a van der Waals contact and none of the occupied molecular orbitals indicate a bonding interaction between the sulfur atoms.

Although the most stable geometry of **27h** is the boat conformer (C_{2v}), there is also the possibility of observing a chair conformer (C_{2h}) which is only 9.5 kJ mol⁻¹ higher in energy.

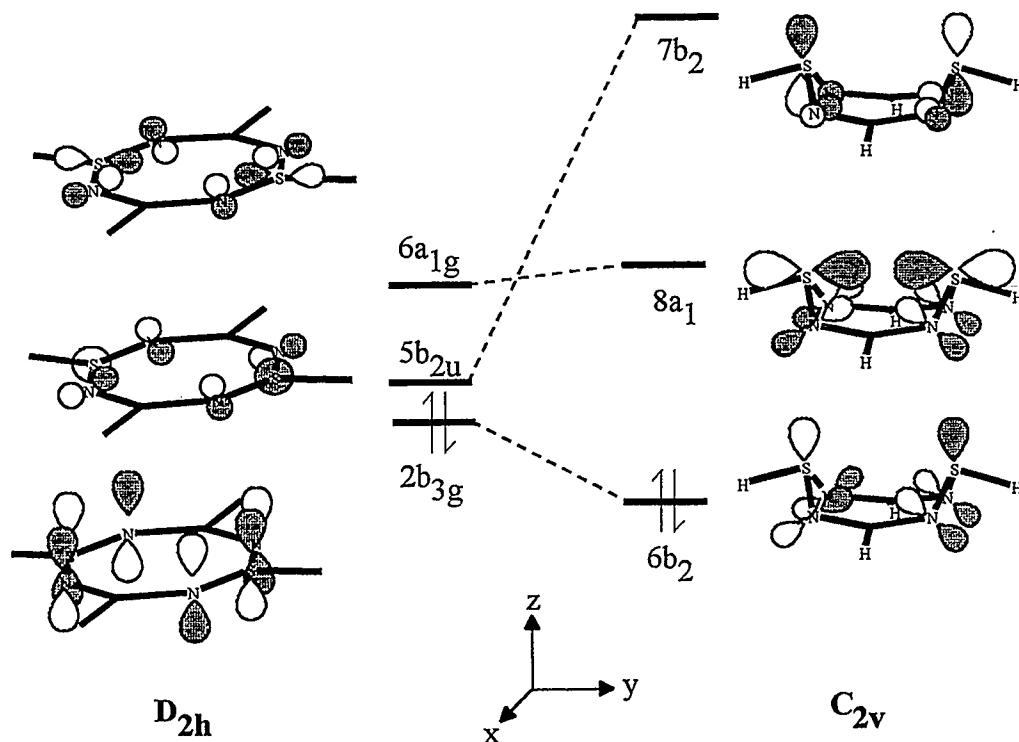
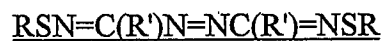


Figure 5.3. Qualitative correlation diagram for $(HC)_2N_4(SH)_2$ in D_{2h} and C_{2v} geometries.

5.3. Relative Thermodynamic Stabilities of $(R'C)_2N_4(SR)_2$ and the Diazene Isomers



The total energy of the optimized C_{2v} model was used to estimate the enthalpy of formation of the ring from $HCN_2(SH)_3$ (**31f**) and $HC(NSH)_2$ (**29d**). While the first reaction (eq 5.1) is exothermic, the second alternative (eq 5.2) is endothermic.





These thermochemical calculations indicate that the formation of eight-membered $\text{C}_2\text{N}_4\text{S}_2$ rings (or larger ring systems) from the decomposition of benzenethiolato substituted carbamidines may not proceed by a pathway involving the dimerization of the $\text{HCN}_2(\text{SR})_2 \cdot$ radical (29).

5.4. Electronic Structure of $(\text{HC})_2\text{N}_4(\text{SH})_2$

5.4.1. Frontier Orbitals

In the C_{2v} geometry, the HOMO ($6b_2$) of the model compound $(\text{HC})_2\text{N}_4(\text{SH})_2$ (27h) can be identified with a lone pair delocalized on all four nitrogen atoms with some sulfur contribution. The LUMO ($8a_1$) has N-S antibonding character (See Figure 5.3). As discussed in the next Section, the composition of these frontier orbitals has interesting implications for the chemistry of these systems.

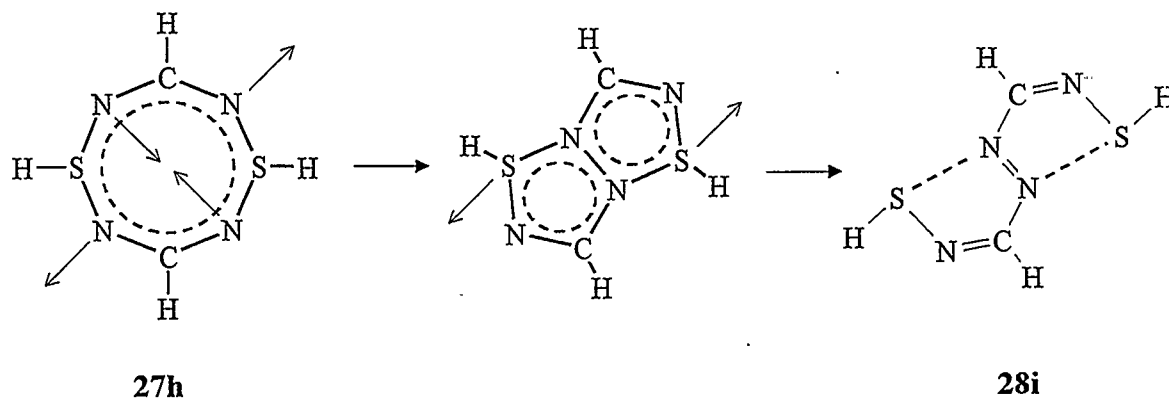
5.4.2. Calculated Structure of the Anion $(\text{HC})_2\text{N}_4(\text{SH})_2^{2-}$ (51)

The composition of the LUMO of the neutral ring system 27h is similar to that of the a_1 orbital which stabilizes the C_{2v} geometry of the 3,7-diamino-1,5-dithiatetrazocines. This implies that a dianionic derivative would display the same type of transannular S-S contact. In view of this suggestion, the geometry of the model ring $(\text{HC})_2\text{N}_4(\text{SH})_2^{2-}$ (51) was optimized. The structural parameters of this dianion are given in Table 5.1. The calculated

structure does predict a S-S distance of about 2.5 Å. The N-S-N bond angles increase making the ring flatter. The S-N links are elongated, as expected from the S-N antibonding character of the LUMO. The calculated S-N distance of 1.88 Å seems to indicate very weak bonds. However, it must be noted that the optimized structure of $(\text{HC})_2\text{N}_4(\text{SH})_2$ (C_{2v}) overestimates the S-N bond length by more than 0.1 Å and similar errors were obtained by *ab initio* (STO-3G) optimization of 1,5 dithiatetrazocines [115a]. Therefore it is expected that the actual S-N bond length of the S-N bond in a dianion of the type **51** would be < 1.77 Å (c.f. 1.73-1.76 Å for a single S-N bond in H_3NSO_3) [9].

5.4.3. Theoretical Basis for the Photochemical Isomerization of $(\text{R}'\text{C})_2\text{N}_4(\text{SR})_2$ Ring Systems [116]

Photochemical investigations of the rings **27d** and **27g** have demonstrated that ultraviolet light causes isomerization to the corresponding diazenes **28** [46]. DFT calculations were used in order to understand this photochemical process. In this study the total reaction enthalpy was calculated to be $-154.7 \text{ kJ mol}^{-1}$. The driving force is the formation of a very stable N=N bond at the expense of elongation of two S-N bonds.



Scheme 5.1.

A unimolecular transformation of $(\text{HC})_2\text{N}_4(\text{SH})_2$ (**27h**) into $\text{HSN}=\text{C}(\text{H})-\text{N}=\text{N}-\text{C}(\text{H})=\text{NSH}$ (**28i**) would occur with conservation of the only common symmetry element (the C_2 axis) (Scheme 5.1). The process starts with an a_2 normal vibrational mode of the ring. Along the C_2 pathway there is a bicyclic transition state from which the two S-N bonds are elongated while the N=N bond is formed. There is an a-b HOMO-LUMO crossing according to the calculated molecular orbitals. For **27h** the HOMO (11b) and LUMO (12a) energies are -5.54 eV and -3.06 eV, respectively; the corresponding values for **28i** are -5.66 eV for the HOMO (12a) and -4.29 eV for the LUMO (11b). Consequently, despite the strongly exothermic character of the isomerization, it will not occur spontaneously because it is thermally a symmetry forbidden process. However, UV light can provide the energy necessary to overcome the activation barrier, since the process is photochemically allowed.

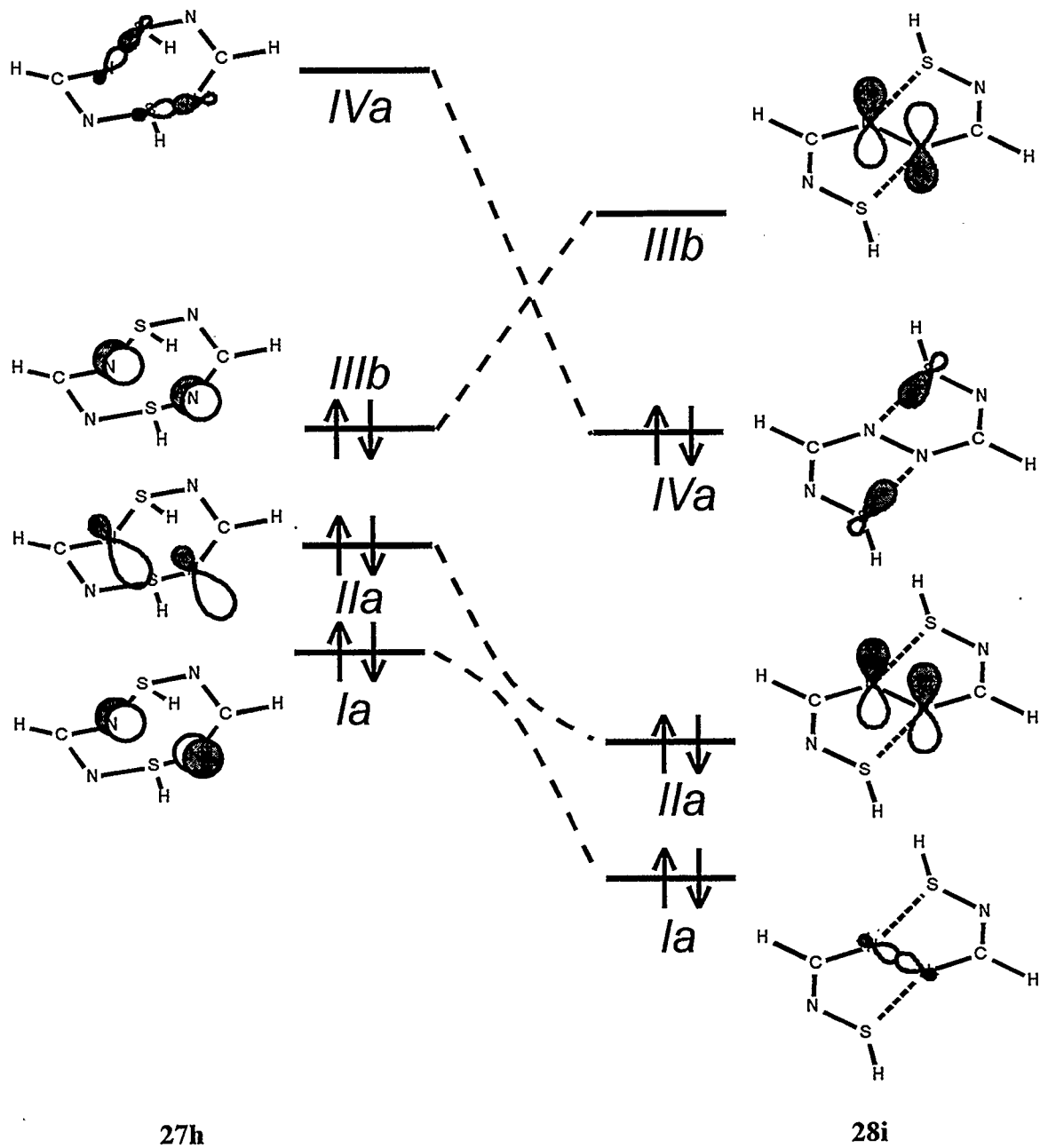


Figure 5.4 Qualitative correlation diagram for the isomerization of $(\text{HC})_2\text{N}_4(\text{SH})_2$ (**27h**) into $\text{HSN}=\text{C}(\text{H})-\text{N}=\text{N}-\text{C}(\text{H})=\text{NSH}$ (**28i**) based on the calculated energies of MOs I-IV.

A qualitative explanation of the photochemical process can be provided in terms of the crucial MOs involving the reactive S-N centers. Only the relevant contributions to those functions are shown in Figure 5.4. As the antipodal N atoms of the $C_2N_4S_2$ ring approach each other, two in-phase combinations of p orbitals (I and II, a symmetry) will lead to the formation of the σ and π bonding orbitals, respectively, driving the system towards the transition state. Simultaneously, an out-of-phase combination of p orbitals (III, b symmetry) will rise in energy to form the π^* orbital. This implies a HOMO-LUMO crossing along the reaction coordinate. The transformation in the ground state is, therefore, symmetry forbidden. Ultraviolet irradiation can promote one electron into the N-S antibonding LUMO (IV) making the process allowed.

5.5. Summary

The first theoretical models for S,S' disubstituted 1,5-dithiatetrazocines were developed by using the model system $(HC)_2N_4(SH)_2$. It is predicted that these rings cannot adopt a planar geometry, D_{2h} , because a small HOMO-LUMO gap promotes a second order Jahn-Teller distortion which imposes a C_{2v} (boat) geometry. An alternative C_{2h} (chair) conformation may be accessible since it is only 9.5 kJ mol^{-1} above the most stable structure. The optimized structure of the model system was employed for thermochemical calculations which indicate that the formation of eight-membered $C_2N_4S_2$ rings from the decomposition of benzenethiolato substituted carbamidines may not proceed by a pathway involving the dimerization of two $HCN_2(SR)_2$ radicals. Consideration of the electronic structures of the

model dianionic derivative $(\text{HC})_2\text{N}_4(\text{SH})_2^{2-}$ leads to the prediction of a transannular contact between the three coordinate sulfur atoms. MO calculations for the model system successfully explain the experimentally observed photochemical transformation of the $\text{C}_2\text{N}_4\text{S}_2$ ring into the isomeric diazene.

5.6. Details of Calculations

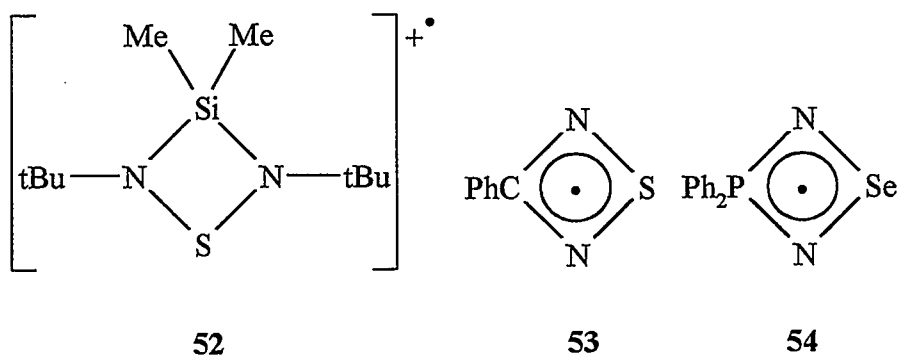
Details of the method used for the calculations of the model diazene **28i** are provided in Section 2.5. The optimum C_{2v} structure of the eight-membered ring, $(\text{HC})_2\text{N}_4(\text{SH})_2$, was calculated based on the geometry obtained from a preliminary structure determination of $(4\text{-BrC}_6\text{H}_4\text{C})_2\text{N}_4(\text{SPh})_2$. The initial estimates for the D_{2h} and C_{2h} geometries were derived from average bond distances and angles.

6. Studies on 1,4,5,7-Dithiadiazepinyl Radicals

6.1. Cyclic CSN Radicals

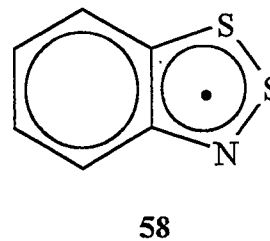
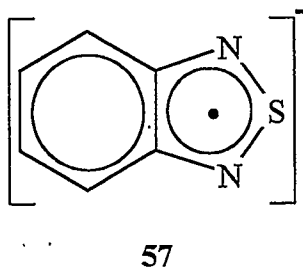
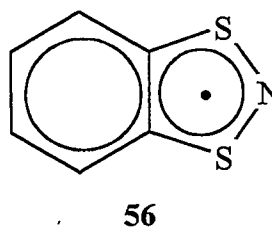
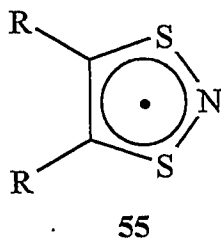
6.1.1. Four-Membered Rings

Only a few examples of radicals involving four-membered rings are known, probably due to the limited stability of such strained rings. The radical cation **52** is nitrogen-centered, with $g = 2.0059$, $A_N = 4.50$ G and $A_{Si} = 6.00$ G [117]. The radical **53** has been implicated in the reaction of 1,2,3,5-dithiadiazolyl radicals (**61**) with \dot{O}_2 [26], which is an efficient method to produce dithiatetrazocines (**20**). This claim was based on the previous observation of the radical **54**, which exists in equilibrium with the diphosphadiselenatetrazocine **12d** [28], but no ESR evidence for **53** was provided.

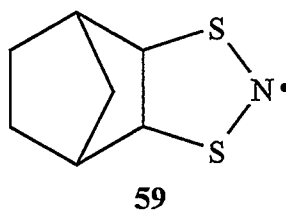


6.1.2. Five-Membered Rings

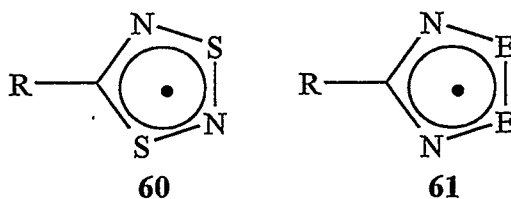
An extensive family of radicals is based on the 1,3,2-dithiazolyl ring (**55**) [36]. These radicals can be prepared by reaction of S_4N_2 with alkynes, or by reduction of the corresponding cation. The R substituents may be part of a benzene ring (**56**) or other aromatic systems. Such polycyclic radicals are in general more stable than their monocyclic counterparts. Typical spectroscopic parameters are $g = 2.0065$, $A_N = 11.0$ G, and $A_S = 4.0$ G [118]. The benzothiadiazole anion (**57**) displays $g = 2.0043$, $A_N = 5.26$ [119]. This type of CSN radicals is able to delocalize the unpaired electron into the adjacent ring. In spite of its instability, the 1,2,3-dithiazolyl ring (**58**) has been characterized, $g = 2.0081$, $A_N = 8.20$ G and $A_S = 3.51$ G [118].



The substituted derivatives of the *cis-exo*-2,3-norbornyl-1',3',2'-dithiazolidin-2'-yl radical (**59**) have *g* values similar to those of **55**. The magnitudes of $A_N = 12.9\text{--}13.2$ G and $A_S = 2.98$ G indicate that the spin is localized more on nitrogen and less on sulfur in **59** compared to **55**.

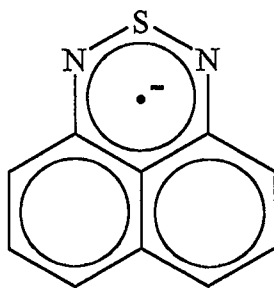


Other large families of radicals are represented by the 1,3,2,4-dithiadiazolyl (**60**) and 1,2,3,5-dithiadiazolyl (**61**) rings [120]. Both are usually prepared by reduction of the corresponding cations. Radicals of the type **61** produce a 1:2:3:2:1 quintet while those of the type **60** produce a 1:1:1 triplet. The value of *g* is about 2.01 in both cases; $A_N \sim 5$ G, $A_S \sim 6$ G for **61** and $A_N \sim 11$ G for **60**. The 1,3,2,4 rings are photochemically isomerized to the 1,2,3,5 systems [121].



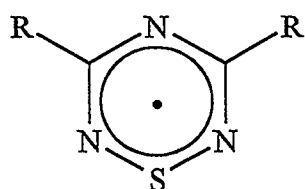
6.1.3. Larger Rings

As compared to the five-membered systems, fewer radicals have been prepared based on six-membered rings. The radical anion **62** has ESR parameters very similar to those of **57**, and should be considered as part of that family [36].

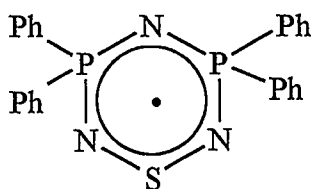


62

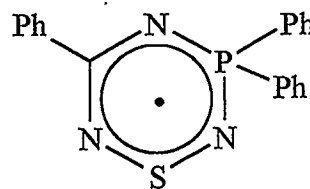
Two families of triazinyl radicals, **63** and **64**, have been characterized. For **63** the g values range from 2.0055 to 2.0065, $A_{N_{2,6}} = 3.4\text{--}4.0$ G, and $A_{N_4} = 3.7\text{--}4.6$ G. As a contrast, the unpaired electron in **64** is not delocalized over N_4 ; the ESR parameters are $g = 2.0058$, $A_{N_{2,6}} = 4.02$ G and $A_P = 0.67$ G [122]. The hybrid system **65** shows significant spin density on sulfur [123].



63

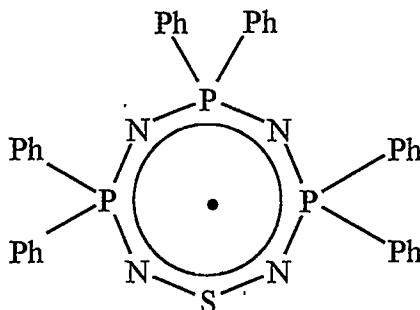


64



65

No cyclic CSN radicals larger than six-membered rings have been reported. In fact, the only larger cyclic S-N radical known is the 1,3,5,7,2,4,6,8-thiatriphosphatetrazocinyl ring **66** [124].



66

6.2. Singly Occupied Molecular Orbitals (SOMOs)

Due to the electron-richness of these rings, the unpaired electron usually resides in a π orbital with N-S antibonding character. Figure 6.1 represents the composition of the SOMOs of some of the radicals discussed in the previous section. Solid state measurements of their ESR spectra are consistent with these MO descriptions [36].

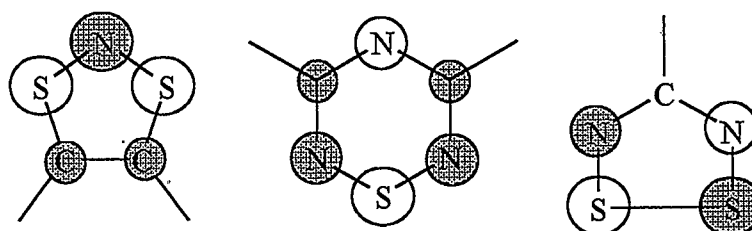


Figure 6.1. SOMOs of some common CSN cyclic free radicals.

6.3. Molecular Conductors Based on CSN radicals

Stable radicals may have useful electrical properties in solid state. A large number of materials that exhibit the electrical properties of metals, while not containing any metallic element, has been characterized during the last 30 years. Synthetic metals (synmetals), organic metals, organic conductors, one dimensional conductors, and molecular conductors are terms frequently applied to these materials [125].

If a series of radical molecules is arranged in such a way that the singly occupied molecular orbitals (SOMOs) overlap with each other, the resulting material will exhibit metallic conductivity. A "simple" approach is to build a uniform stack of planar π -radicals. However, a uniform arrangement is unstable with respect to the formation of discrete

dimers, as a result of the Peierls distortion; moreover, these dimers may easily adopt a solid state arrangement that disrupts the columns and the electric conductivity (Figure 6.2). Consequently, in order to enhance conductivity it is desirable that these materials involve interdimer interactions. Extensive synthetic work has been carried out in attempts to control these effects.

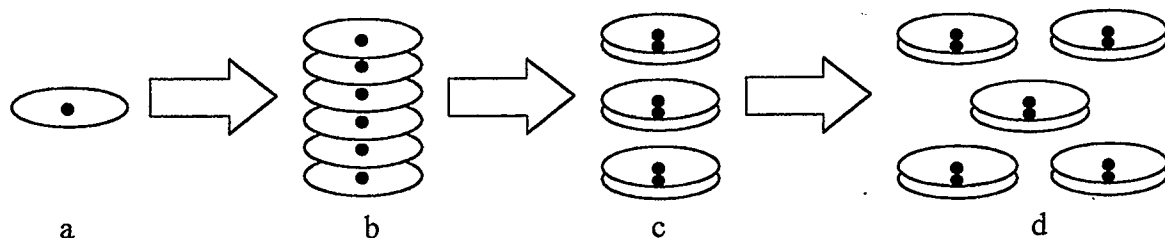
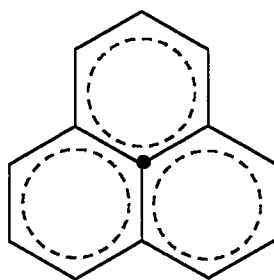


Figure 6.2. a) Radical plate. b) Uniform stack. c) dimer formation. d) crystal packing (Adapted from Figure 5 in reference 127c and Figure 1 in reference 128a).

Most of the effort has been dedicated to materials that are made up of ion radicals in the form of charge transfer salts, such as tetrathiofulvalene-tetracyanoquinodimethane (TTF·TCNQ). The interest in these substances resides in the superconductivity that some of them display at low temperature [126]. The need for either counterions or the combination of two different kinds of molecules complicates the design of the solid-state structures. An appealing alternative is the use of neutral stable radicals as the building blocks of molecular conductors. The first proposal was based on odd alternant hydrocarbons like the phenalenyl radical (67) [127], which has never been actually prepared.

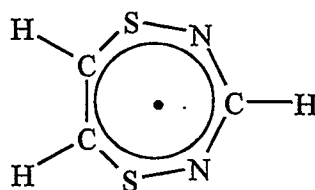


67

The preparation of conducting materials from CSN cyclic free radicals has been actively pursued in recent years. The most promising materials are based on the 1,2,3,5-dithiadiazolyl radicals (**61**) [128]. The salt $[S_2N_2C-CN_2S_2]I$ is the first of these materials to exhibit metallic conductivity at ambient temperature, 460 S cm^{-1} [129].

6.4. 1,4,5,7-Dithiadiazepinyl Radicals

It has been shown in Chapter 4 that $RCN(ER)_2\cdot$ (**29**) radicals are persistent; their instability with respect to dimerization and the formation of diazenes may be due to their open chain structure. Such radicals could perhaps be stabilized in a cyclic system, especially if there is full delocalization in the ring. With that idea in mind, this project included the theoretical study of the 1,4,5,7-dithiadiazepinyl radical (**68a**) and its selenium analog, as well as the exploration of synthetic procedures for the preparation of these novel $C_2S_2N_2C$ 9 π -electron heterocycles.



68a

6.4.1. Molecular Structures of the Neutral Radicals $(\text{HC})_2\text{E}_2\text{N}_2\text{CH}\cdot$ (E = S, Se)

The structures of the model cyclic radical $(\text{HC})_2\text{S}_2\text{N}_2(\text{CH})\cdot$ (**68a**) and the selenium analog **68b** were fully optimized assuming a C_{2v} geometry. Relevant molecular dimensions of the optimal structures are given in Table 6.1.

Table 6.1. Calculated bond distances (Å) and bond angles (°) of $(\text{HC})_2\text{E}_2\text{N}_2(\text{CH})$ (E = S, Se).

	E = S (68a)	E = Se (68b)
C-N	1.325	1.324
N-E	1.630	1.782
E-C	1.783	1.928
C-C	1.334	1.331
N-C-N	134.7	137.8
C-N-E	134.3	133.6
N-E-C	118.0	116.6
E-C-C	130.4	130.5

6.4.2. Electronic Structures of the Radicals $(\text{HC})_2\text{E}_2\text{N}_2\text{CH}\cdot$ ($\text{E} = \text{S}, \text{Se}$)

The singly occupied molecular orbital of **68a** is depicted in Figure 6.3. This orbital resembles the SOMO of the 1,2,3,5-dithiadiazolyl radical **61**; it is N-S and C-C antibonding but bonding with respect to S-C. A nodal plane passes through the unique C atom.

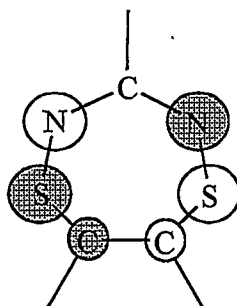


Figure 6.3. Calculated SOMO of the model ring $(\text{HC})_2\text{S}_2\text{N}_2(\text{CH})\cdot$ (**68a**).

6.4.3. The $[(\text{HC})_2\text{E}_2\text{N}_2\text{CH}]^+$ Cation and $[(\text{HC})_2\text{E}_2\text{N}_2\text{CH}]^-$ Anion ($\text{E} = \text{S}, \text{Se}$):

Disproportionation Enthalpies

The original proposition of using **67** as a building block for molecular conductors was based on its small disproportionation energy, *i.e.* the energy of the process in which two neutral radicals ($\text{N}\cdot$) generate the corresponding cation (C^+) and anion (A^-) (eq. 6.1). This is qualitatively identified with the electron-electron repulsion in the conduction band (ionic fluctuation energy) [127b]; small repulsions favor electrical conduction.



In order to evaluate the potential application of radicals of the type $C_2S_2N_2C\cdot$ for the preparation of molecular conductors, it was considered of interest to calculate the disproportionation energy, and other related parameters, and to compare these values with those of the 1,2,3-dithiazolyl (**55**) and 1,2,3,5-dithiadiazolyl (**61**) radicals.

To evaluate both the vertical ionization potential and electron affinity (ΔSCF), the optimized structure of the neutral heterocyclic radical was used in the calculation of the energy of the cation and the anion. The ionic structures were also optimized to calculate the corresponding adiabatic parameters. The disproportionation energy is calculated as the energy of the optimized anion and cation minus the energy of two neutral radical molecules. In addition, for a given ion, the energy difference between the optimized and non-optimized structures is called the "relaxation energy"; it is a measure of the degree of structural reorganization upon electron transfer and it should be small to facilitate electron conduction.

Previously published theoretical studies on heterocycles of the types **61** are based on *ab initio* calculations. The results are sensitive to the inclusion of electron correlation and the order of perturbation which is employed [130]. The Local Density Approximation (LDA) employed in the DFT calculations included in this dissertation already considers electron correlation effects. In order to make a valid comparison, all the calculations were also carried out on models of **55** and **61**. The selenium analogs were also considered in this study. The reliability of this study may be assessed by comparison of the calculated ionization potentials for the 1,2,3,5-(HC)N₂E₂· (E = S, Se) radicals (**61**) with the experimental values (See Table 6.2).

Table 6.2. Calculated (DFT) and experimental Vertical Ionization Potentials (ΔSCF) of 1,2,3,5-(HC)N₂E₂· (E = S, Se) radicals (eV).

	1,2,3,5-(HC)N ₂ S ₂	1,2,3,5-(HC)N ₂ Se ₂
Calculated (DFT)	7.87	7.70
Experimental [130]	7.87 ± 0.03	7.71 ± 0.03

Although there is good agreement between calculated and experimental values, the results are employed mainly for a qualitative analysis. The results of all calculations are summarized in Table 6.3. Electron-electron repulsions were found to be smaller for the 7-membered rings than for the 5-membered cycles, as it is expected from the size of the rings. The Se systems offer smaller disproportionation energies than the sulfur analogous structures. On the other hand the "relaxation enthalpies" are considerably larger for the seven-membered ring cations.

6.4.4. Dimers: Structures and Dimerization Energies

The structure of the dimers of the radicals was optimized, assuming a face-to-face orientation since this arrangement provides the best SOMO-SOMO overlap, although it is known that this may not be the arrangement observed in some solid structures [131]. The dimerization energy was calculated as the difference between two isolated radicals and the dimer. The results are given in Table 6.3.

Table 6.3. Comparison of calculated properties of cyclic CSN and CSeN radicals (in kJ mol⁻¹).

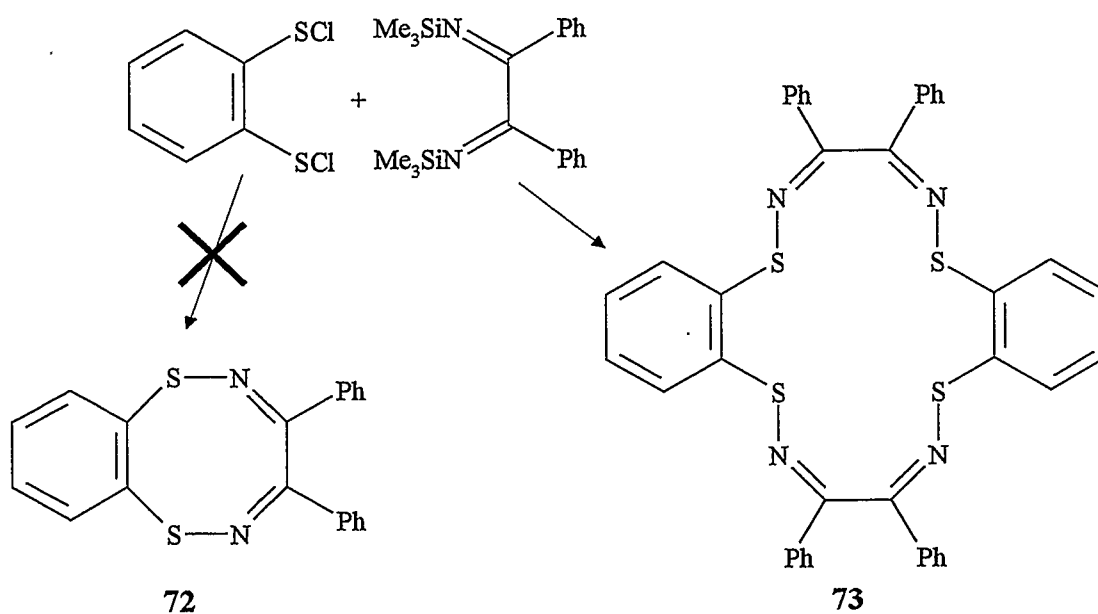
	(HC) ₂ N ₂ S ₂ (CH)	(HC) ₂ N ₂ Se ₂ (CH)	(HC)N ₂ S ₂	(HC)N ₂ Se ₂	(HC) ₂ S ₂ N	(HC) ₂ Se ₂ N
Vertical IP	850.94	827.00	758.93	742.65	669.89	664.26
Vertical EA	280.45	285.07	106.41	132.01	6.09	33.02
Adiabatic IP	797.38	736.52	755.88	742.68	664.29	662.97
Adiabatic EA	291.33	296.73	132.42	157.33	24.07	50.27
Relaxation Enthalpy +	-53.56	-90.48	-3.05	0.02	-5.60	-1.29
Relaxation Enthalpy -	-10.88	-11.66	-26.01	-25.32	-17.98	-17.25
Disprop. Enthalpy	506.06	439.79	623.46	585.35	640.22	612.70
Dimerization Energy	-14.09	-11.31	-21.71	-23.44	-12.46	-11.07

The dimerization energy calculated for the dithiadiazolyl radicals **61** is of the same order of magnitude as the values obtained from MP3 calculations and experimental observations [130]. However, these dimerization energies are taken as a qualitative estimate of the dimerization tendency, since no zero point energy correction was applied. The calculations indicate that the dichalcogenadiazepinyl radicals have a smaller tendency to dimerization than the 1,2,3,5-dichalcogenadiazolyl radicals.

6.5. Attempted Synthesis of Cyclic $C_2S_2N_2C\cdot$ Radicals: Reaction of 1,2- $C_6H_4(SCl)_2$ with $PhCN_2(SiMe_3)_3$ and $PhSeCl$

The preparation of a radical of the type **68a** would require the use of the dithiol $HS-C(H)=C(H)-SH$, which is not stable. A common approach for the preparation of the related heterocycles **56** is the use of a phenylene ring instead of the alkene. The first attempts to synthesize the radical **71b** were carried out by Dr. Chandrasekar (Scheme 6.1) [132]. The proposed synthesis relies on the cyclocondensation of a benzene-1,2-bis(sulfurchloride) with the trisilylated benzamidine (**1**). The seven-membered ring precursor (**69b**), obtained in this way, has an N-bonded trimethylsilyl group which may be replaced by PhSe. Given the known tendency of the Se-N bond to undergo homolysis, the intermediate **70b** should be unstable and readily decompose to the radical **71b**. A dark, impure material was indeed isolated and it displayed a slightly asymmetric ESR spectrum. The value of $g = 2.0070$ is similar to that observed for the radicals $RC(NSPh)_2\cdot$ (**29**) (Sections 4.2 and 4.5.4). The value of

mixtures had been obtained. The product was very soluble in polar solvents making purification by recrystallization difficult. Preliminary TLC experiments indicated no separation of components ruling out the use of column chromatography. The complexity of the products may be due to the formation of oligomers larger than the seven-membered ring. In a similar reaction the sixteen-membered ring **73** was isolated instead of the target molecule **72** (Scheme 6.1) [134].

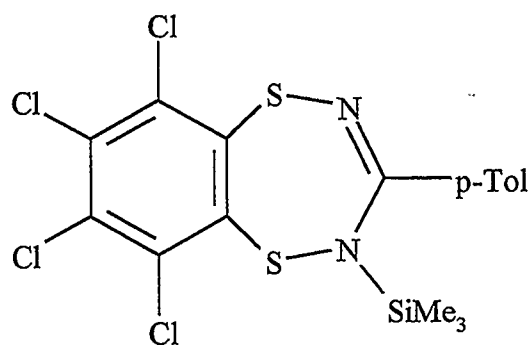


Scheme 6.2

6.6. Isolation of $S(C_6Cl_4)S(NSiMe_3)(4-CH_3C_6H_4C)=N$ (**74**)

In the light of the preliminary experiments described in the previous section, the isolation of a pure sample of a precursor of the type **69** was necessary. Different conditions for the reaction of $4-RC_6H_3-1,2(SCl)_2$ ($R = H, Me$) with $RCN_2(SiMe_3)_3$ ($R = H, Ar$) were tested without success. Both $C_6H_4-1,2(SCl)_2$ and $4-MeC_6H_3-1,2(SCl)_2$ are liquids miscible

with most organic solvents. In contrast $C_6Cl_4-5,6-(SH)_2$ is a poorly soluble solid. This dithiol was employed in the hope that the derivatives would be easier to isolate and purify. In the initial attempts the dithiol was chlorinated and used immediately for the reaction with 4- $CH_3C_6H_4CN_2(SiMe_3)_3$ (**1b**) in Et_2O . This method was successful in producing the precursor **74**, as pale yellow crystals, among other products that were separated by fractional crystallization.



74

6.6.1. X-ray Structure of $S(C_6Cl_4)S(NSiMe_3)(4-CH_3C_6H_4C)=N$ (**74**)

The heterocycle **74** was structurally characterized by X-ray diffraction. An ORTEP diagram of the structure, showing the numbering scheme, is shown in Figure 6.4. Relevant crystallographic data and molecular dimensions are provided in Tables 6.3 and 6.4, respectively. The heterocyclic molecule shows a puckered geometry. The structure displays localized single and double bonds.

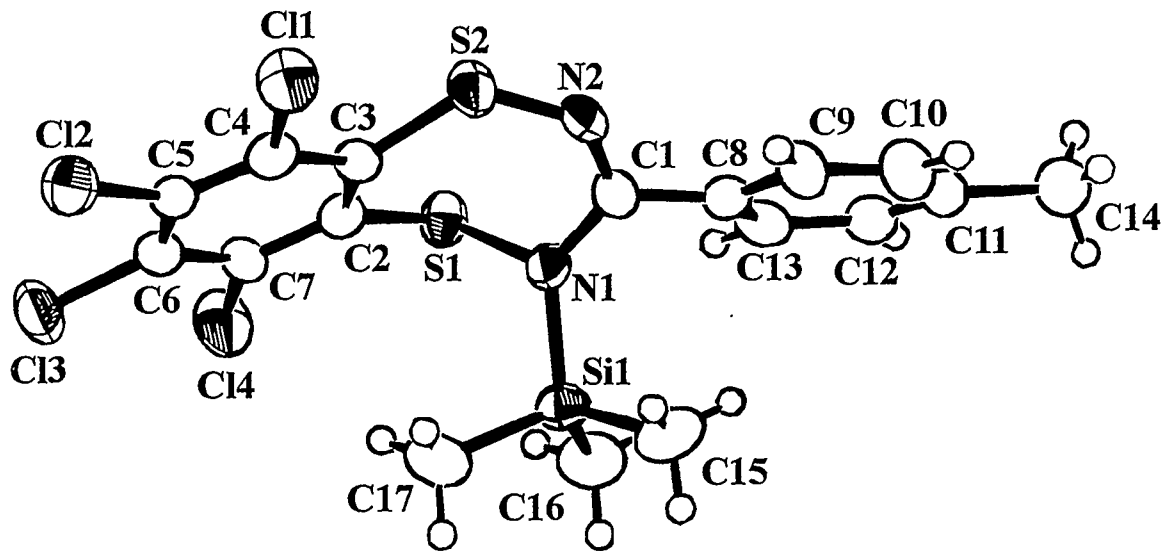


Figure 6.4. ORTEP diagram for $S(C_6Cl_4)S(NSiMe_3)(4-CH_3C_6H_4C)=N$ (74).

Table 6.4. Crystallographic data for $S(C_6Cl_4)S(NSiMe_3)(4-CH_3C_6H_4C)=N$ (74).

formula	$C_{17}H_{16}N_2S_2SiCl_4$	Z	4
fw	482.34	T(°C)	23
space group	$P2_1/a$	λ (Å)	0.71069
a (Å)	12.585(3)	ρ_{calc} (g cm ⁻³)	1.521
b (Å)	12.211(2)	μ (cm ⁻¹)	8.22
c (Å)	14.003(2)	R	0.042
β (°)	101.86(2)	R_w	0.049
V (Å ³)	2106.0(7)	dimensions (mm)	0.32×0.20×0.23

Table 6.5: Bond lengths (Å), bond angles and torsion angles (°) for

$$\overline{\text{S}(\text{C}_6\text{Cl}_4)\text{S}(\text{NSiMe}_3)(4\text{-CH}_3\text{C}_6\text{H}_4\text{C})=\text{N}} \text{ (74)}.$$

S(1)-N(1)	1.688(7)	S(1)-C(2)	1.763(8)
S(2)-N(2)	1.626(7)	S(2)-C(3)	1.774(8)
Si(1)-N(1)	1.800(7)	N(2)-C(1)	1.31(1)
N(1)-C(1)	1.40(1)	C(2)-C(3)	1.42(1)
N(1)-S(1)-C(2)	104.3(4)	N(2)-S(2)-C(3)	119.1(4)
S(1)-N(1)-Si(1)	117.3(4)	S(1)-N(1)-C(1)	117.9(6)
Si(1)-N(1)-C(1)	124.7(6)	S(2)-N(2)-C(1)	134.3(6)
N(1)-C(1)-N(2)	123.5(8)	S(1)-C(2)-C(3)	120.4(6)
S(2)-C(3)-C(2)	126.3(6)		
S(1)-N(1)-C(1)-N(2)	51.1(1)	C(1)-N(1)-S(1)-C(2)	-91.0(7)
S(1)-C(2)-C(3)-S(2)	1(1)	C(1)-N(2)-S(2)-C(3)	-5(1)
Si(1)-N(1)-C(1)-N(2)	-126.4(8)	S(2)-N(2)-C(1)-N(1)	6(1)
N(1)-S(1)-C(2)-C(3)	54.7(7)	Si(1)-N(1)-S(1)-C(2)	86.7(5)
N(2)-S(2)-C(3)-C(2)	-25.7(9)		

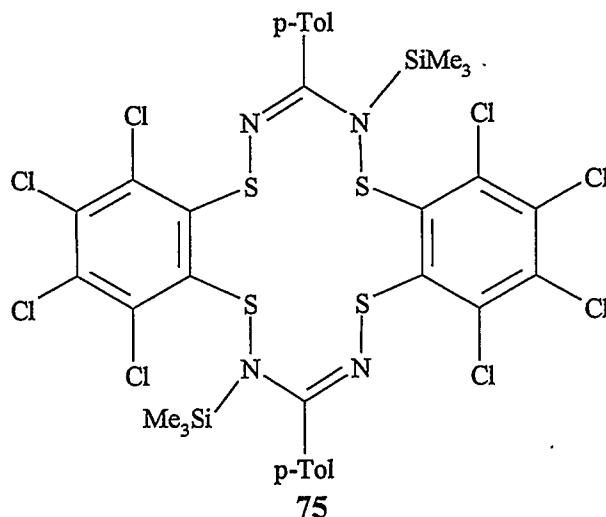
The -S-N< , -S-N= and C-N bond distances, 1.688, 1.626 and 1.40 Å, respectively, are comparable to those observed for HCN₂(SPh)₃ (**31d**) (see Table 4.2). The C=N distance, 1.31Å, is slightly longer than the value of 1.26 Å found for **31d**. The N-C-N bond angle measured for **74** is equivalent to that for **31d**, within the standard deviation ranges. The geometries at both C(1) and N(1) are planar (sum of bond angles ~ 360°). The S-C-C-S and N-C=N-S units are also planar. All these data indicate that there is no steric strain on the amidine moiety.

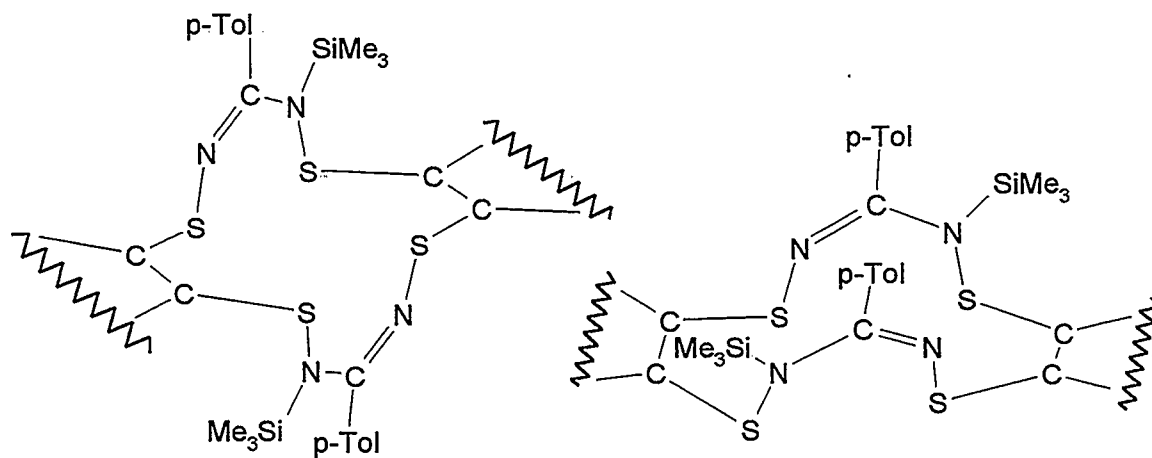
The C-S distances are comparable to the average 1.763 Å observed for **73** [134]. The S-C-C bond angles in **73** are in the range 116-123.2°, in a similar way two different values are observed for **74**, 120.4° and 126.3°. The S-C-C-S torsion angles of **73** are 5.2° and 12.0°; in **74** the corresponding torsion angle is only of 1°. The >N-S-C angle of 104.3° in **74** is comparable to those observed for **73** and **31d**, 99.5-100.9° and 101.7-103.1°, respectively. Larger differences are apparent for S(2) and N(2): the =N-S-C and S-N=C bond angles, 119.1° and 134.3, are larger than those of **73** and **31d**, 113.9-117.8° and 119.6°, respectively.

6.6.2. By-products of the Synthesis of $\text{S}(\text{C}_6\text{Cl}_4)\text{S}(\text{NSiMe}_3)(4\text{-CH}_3\text{C}_6\text{H}_4\text{C})=\text{N}$

The ¹H NMR spectrum of the crude product of the reaction of C₆Cl₄-5,6-(SCl)₂ with 4-CH₃C₆H₄CN₂(SiMe₃)₃ displayed at least six signals, of comparable intensities, which can be attributed to SiMe₃ groups: δ 0.27, 0.26, 0.17, 0.15, 0.03, -0.02 ppm. The resonances for aromatic and methyl protons were also complicated, but less well resolved. The highest field

SiMe₃ peak corresponds to 74. A second fraction was isolated and purified. It was shown to exhibit the peak at $\delta = 0.15$ ppm (Figure 6.5). The rest of the spectrum for this product consisted of the signals of two different 4-CH₃C₆H₄ groups with equal integrations, as well as the resonances of Et₂O, persistent after two recrystallizations. The integrations suggest that there is one Et₂O molecule for two *para*-tolyl groups and two SiMe₃ groups. The elemental analysis for this material is consistent with the formula C₃₄H₃₂N₄S₄Cl₈Si₂·C₄H₁₀O. The FABMS spectrum does not show the molecular ion, but it does show an ion larger than 74, identified as [C₆Cl₄(SNC(4-CH₃C₆H₄)N(SiMe₃))₂]⁺ on the basis of the M/Z = 686 and the isotopic distribution pattern. Based on these data it is proposed that this second fraction is at least double the molecular weight of 74, i.e. a fourteen-membered ring 75. It is expected that such ring will have a puckered structure; as a consequence the ¹H NMR pattern for two different *para*-tolyl groups may arise from two conformers, e.g. chair and boat structures (see Scheme 6.3.). While this species crystallizes from Et₂O as thin flakes, other solvents afford only amorphous powders, which has precluded structural characterization.





Scheme 6.3.

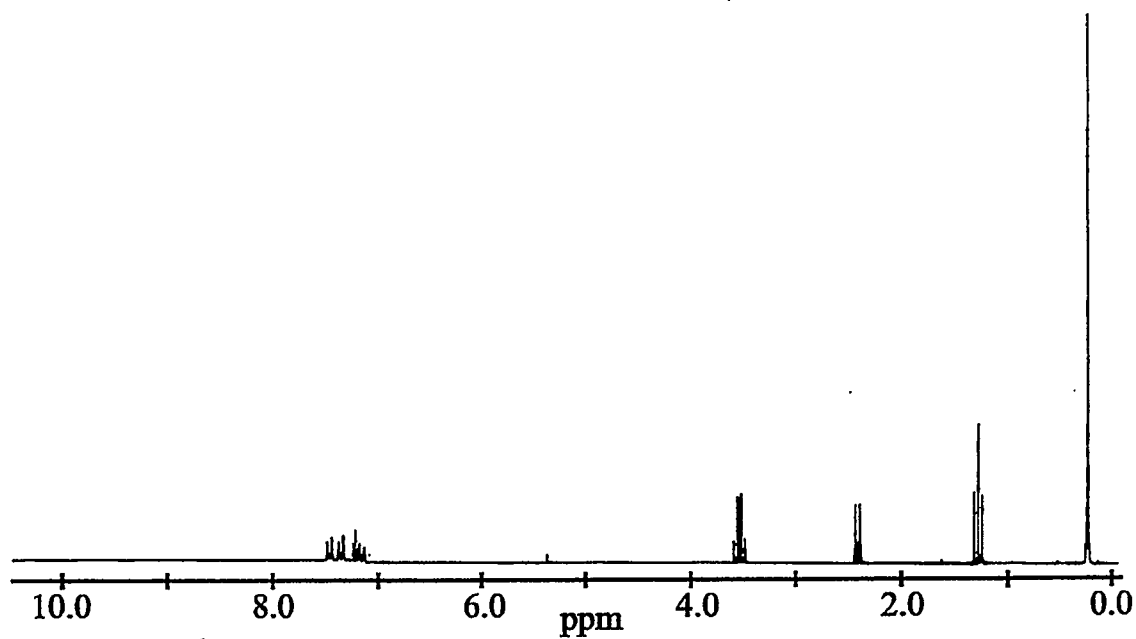
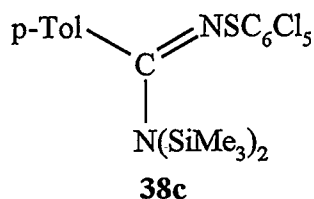


Figure 6.5. ¹H NMR spectrum for the second fraction of the product from the reaction of C₆Cl₄-5,6(SCl)₂ with 4-CH₃C₆H₄CN₂(SiMe₃)₃.

The monosubstituted derivative 4-CH₃C₆H₄C(N(SiMe₃)₂)(NSC₆Cl₅) (**38c**) was isolated as a third impure fraction in small amounts. Its identity was corroborated by comparison with an authentic sample, obtained by reaction of 4-CH₃C₆H₄CN₂(SiMe₃)₃ with C₆Cl₅SH. The SiMe₃ signal at $\delta = 0.26$ ppm was identified as due to this species. No other fractions could be purified.



The formation of **38c** is undoubtedly due to the presence of C₆Cl₅SH as an impurity in C₆Cl₄-5,6-(SH)₂. This dithiol was prepared by a modification [135] of the original procedure [136], which produces "erratic and poor" yields [137]. It was found that the preparation actually affords a mixture of C₆Cl₄-5,6-(SH)₂ and C₆Cl₅SH, the relative amounts of which were usually variable. The best results for the synthesis of **74** were obtained with those samples containing the dithiol as the major component.

The yield of **74** is also optimized when the reaction is carried out under high dilution conditions keeping a 1:1 stoichiometry of reagents to minimize polycondensation. With this approach the crude product consisted mainly of **74** and **38c**.

6.7. Reactions of $S(C_6Cl_4)S(NSiMe_3)(4-CH_3C_6H_4C)=N$ (74)

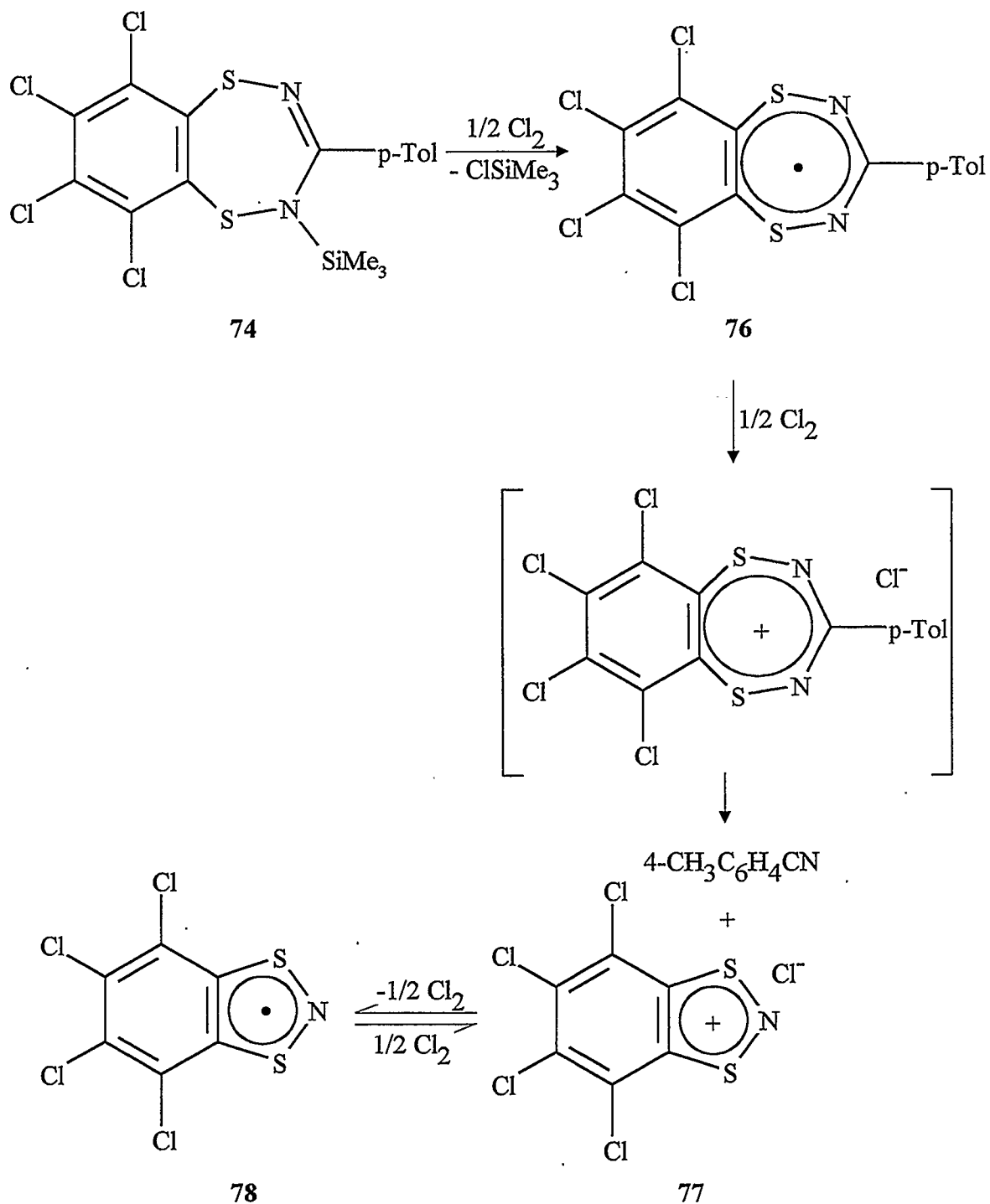
6.7.1. Attempted Reactions with $ArECl$ ($E = S, Se$)

It was attempted to transform the precursor **74** into the corresponding radical (**76**) by substitution of the trimethylsilyl group with PhSe. However, **74** was surprisingly unreactive towards PhSeCl and even towards 4- $CH_3C_6H_4SCl$.

6.7.2. Oxidation with Cl_2

As an alternative route to the radical **76**, the removal of the trimethylsilyl group by oxidation with Cl_2 leaving the heterocyclic ring as a cation, was considered (Scheme 6.4). The cation generated in this way could be reduced to the radical with Ph_3Sb , in the same way that the radicals **61** are synthesized.

The reaction of **74** with Cl_2 , either pure gas or as SO_2Cl_2 , was observed to occur in stages. Initially a dark purple species was generated. This was subsequently oxidized by Cl_2 to form orange crystals, which are stable only when there is an excess of Cl_2 present in the reaction medium. When the Cl_2 was removed a dark brown species was formed. These changes were reversed by adding Cl_2 to the reaction mixture. The process was monitored by 1H NMR and the spectrum displayed only the resonances of $ClSiMe_3$ and 4- $CH_3C_6H_4CN$. The EI-mass spectrum of the brown species showed $Cl_4C_6S_2N$ as the heaviest fragment ($M/Z = 292$).



Scheme 6.4

It is proposed that Cl_2 oxidizes **74** to the radical **76** (the purple species), which is then oxidized to the cation. Subsequently a ring contraction to form the nitrile and the 1,3,2-

dithiazolium cation (77) (orange crystals) occurs. Two interpretations can be offered to the reversible formation of the final brown species: a) The cation 77 may have a high oxidation potential due to the perchlorinated benzene ring, and could be spontaneously reduced by the chloride anion to the brown free radical 78. The radical-cation equilibrium would be controlled by the amount of Cl_2 present in the medium (Scheme 6.4). b) Under an excess of Cl_2 , the Cl^- ion forms reversibly the Cl_3^- anion as counterion of 77. The orange crystals correspond to the trichloride salt and the brown solid to the chloride compound.

6.7.3. Thermodynamics of the Ring Contraction

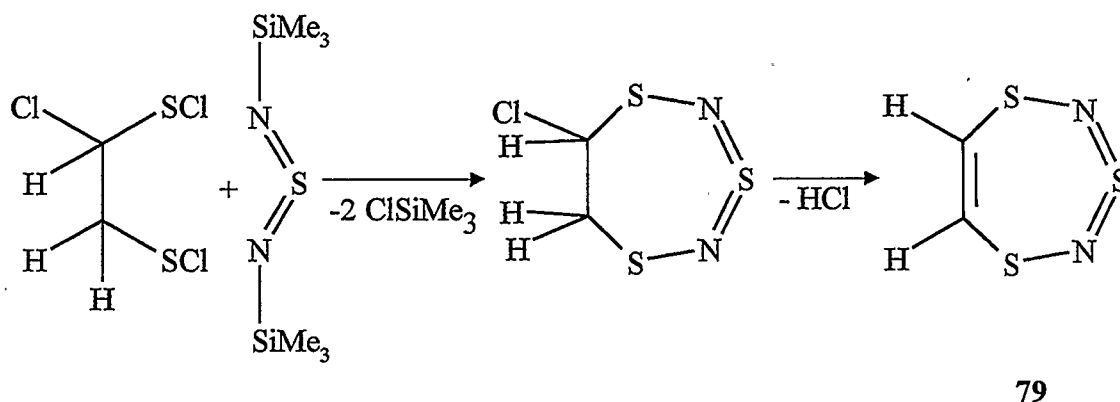
Although many main group heterocycles are unstable with respect to ring contraction or expansion, some of them can be stabilized by high kinetic barriers. In this case it is evident that no such barrier exists to prevent the decomposition of the seven-membered cation. The reaction enthalpy for this ring contraction (eq 6.2) was calculated from the total energies of the model rings 1,4,5,7-(HC)₂S₂N₂(CH) 68a, (HC)₂S₂N (55) and HC≡N. The calculations were repeated for the corresponding neutral radicals (eq. 6.3) and anions (eq. 6.4). Contraction of the cation is a strongly exothermic process. This can be understood by considering that the 8 π -electron antiaromatic ring breaks apart into a very stable 6 π -electron system and a strong C≡N bond. On the other hand the analogous process for the anion is strongly endothermic. In this case a 10 π -electron aromatic system would generate an 8 π -electron antiaromatic ring. For the radicals it is predicted that the reaction would be approximately thermoneutral, suggesting that such a radical would be stable only under mild

conditions. The materials prepared by Chandrasekhar's method are readily decomposed by heating.



6.7.4. Attempts to Prepare the Anion $[\text{C}_6\text{Cl}_4\text{S}_2\text{N}_2\text{C}(4\text{-CH}_3\text{C}_6\text{H}_4)]^-$: Reaction of $\text{S}(\text{C}_6\text{Cl}_4)\text{S}(\text{NSiMe}_3)(4\text{-CH}_3\text{C}_6\text{H}_4)=\text{N}$ with CsF

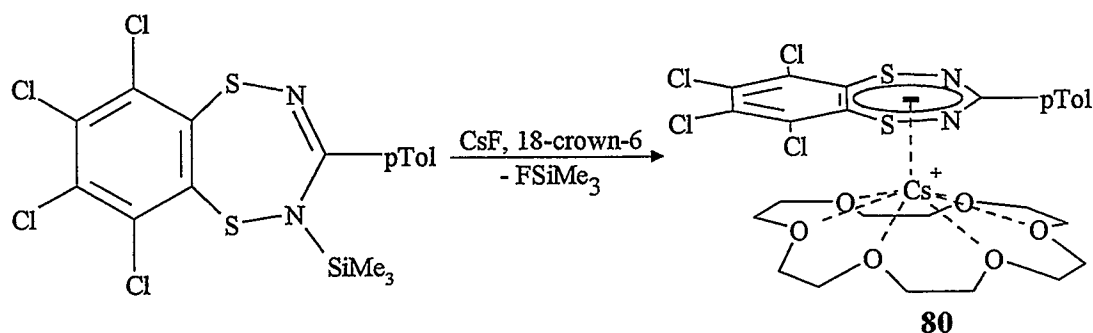
In view of these calculations, the thermodynamically most favorable process to remove the SiMe_3 group from the precursor 74 would be the formation of the anion. It is known, for example, that the 10 π -electron system 79 is formed by spontaneous HCl elimination from a saturated C-C precursor (Scheme 6.5) [138].



Scheme 6.5

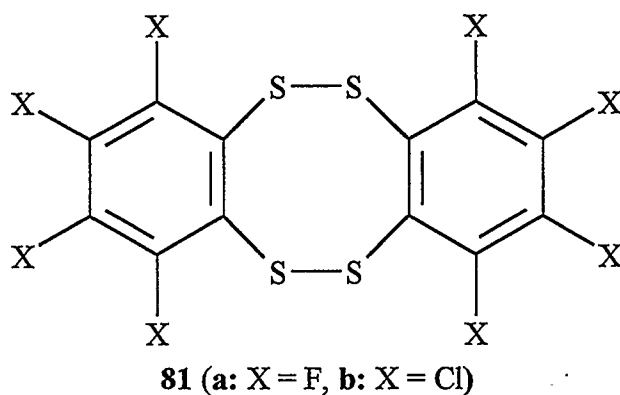
Preliminary studies were carried out to show the feasibility of removing the SiMe_3 group from 74 by nucleophilic attack with CsF. It was found that F^- does react with 74.

However, attempts to purify the product, from an intensely brown coloured solution, were frustrated by the very high solubility in polar solvents. The presence of a crown ether (18-crown-6) in the medium facilitated the purification of a pale microcrystalline solid whose ^1H NMR spectrum is consistent with the composition $[(\text{Cl}_4\text{C}_6)_2\text{S}_2\text{N}_2(4\text{-CH}_3\text{C}_6\text{H}_4\text{C})][\text{Cs}(\text{C}_{12}\text{H}_{24}\text{O}_6)]$ (**80**). Due to its ionic radius, Cs^+ prefers to coordinate two 18-crown-6 molecules [139, 140]. Coordination to only one crown ether molecule is possible only when other species are available to bind to the cation. Therefore it is proposed that the anionic seven-membered ring interacts with Cs^+ in solid state (Scheme 6.6).



Scheme 6.6

6.8. X-ray Structures of $(\text{C}_6\text{X}_4\text{S}_2)_2$ ($\text{X} = \text{F}, \text{Cl}$) (**81a,b**)



Given the composition of the SOMO of $(\text{HC})_2\text{S}_2\text{N}_2(\text{CH})$ (**68a**) (Figure 6.3), the radicals of the types **71** and **76** are expected to exhibit spin delocalization onto the aromatic rings. Spin coupling to the chlorine atoms in **76** would be difficult to evaluate from an ESR spectrum. In consideration of this, it was attempted to prepare the fluorinated analog of the precursor **74**. However, attempts to prepare $\text{C}_6\text{F}_4\text{-1,2-(SCl)}_2$ by chlorination of $\text{C}_6\text{F}_4\text{-1,2-(SH)}_2$ were unsuccessful. Instead the dimer $(\text{C}_6\text{F}_4\text{S}_2)_2$ (**81a**) was obtained quantitatively. Single crystals of **81a** were grown from a diethyl ether solution and the structure was obtained by X-ray diffraction. The structure of $(\text{C}_6\text{F}_4\text{S}_2)_2$ represents the first characterized chair (C_{2h}) conformer for the 1,2,5,6-tetrathiocine ring (Figure 6.6). It has been proposed that 1,2,5,6-tetrathiocines should exhibit several conformers in the same way as cyclooctadiene [141]. Theoretical calculations (*ab initio*) indicated that these rings are more stable in a conformation of D_2 symmetry, and two examples with this geometry have been structurally characterized. The alternative C_{2h} chair conformation is only 5.3 kJ/mol less stable, but no examples are known [141]. Therefore, it is of interest to compare the structure of $(\text{C}_6\text{F}_4\text{S}_2)_2$ (**81a**) with that of $(\text{C}_6\text{Cl}_4\text{S}_2)_2$ (**81b**), which also displays the D_2 geometry (Figure 6.7). Single crystals of **81b** were obtained by the slow decomposition of a THF solution of the proposed fourteen-membered ring **75**.

Crystallographic data for **81a** and **81b** are given in Table 6.6. Relevant molecular dimensions are included in Table 6.7 and Table 6.8. The bond distances in these two heterocycles have very similar values (averages: 1.40 Å for C-C, 1.77 Å for C-S and 2.05 Å for S-S). The bond angles C-C-S and C-S-S (averages 124.3° and 103.8°, respectively) are also comparable between **81a** and **81b**. The benzene-dithiolato units are nearly planar, with

S-C-C-S and S-C-C-C torsion angles close to 0 and 180°, respectively. The C-S-S-C torsion angles are in the range 110-120° in both molecules. The major difference between the two structures is in the S-S-C-C torsion angles: 79.9° for **81a** and 42.3-52.2° for **81b**.

The ¹⁹F NMR spectrum of **81a** displays four resonances. These can be separated in two groups, on the basis of their relative intensity (ratio 1:4). The less intense set of AA'XX' multiplets is centered at δ -131.0 ppm and -153.2 ppm; the second group appears at δ -135.8 ppm and -148.2 ppm. This suggests that **81a** actually exists as a mixture of the two conformers in solution. The possible interconversion of isomers could be investigated by a variable temperature NMR study.

Table 6.6. Crystallographic data for (C₆X₄S₂)₂ (X = F, Cl) (**81a,b**).

	81a	81b
formula	C ₁₂ F ₈ S ₄	C ₁₂ Cl ₈ S ₄
fw	424.36	556
space group	P2 ₁ /c	C2/c
a (Å)	4.825(2)	15.243(3)
b (Å)	11.302(2)	8.703(2)
c (Å)	12.453(2)	27.010(14)
β (°)	91.45(3)	92.81(4)
V (Å ³)	678.8(3)	3578(1)
Z	2	8
T (°C)	-123.0	-103.0
λ (Å)	0.71069	0.71069
ρ _{calcd} (g cm ⁻³)	2.076	2.064
μ (cm ⁻¹)	7.89	17.17
R	0.025	0.047
R _w	0.024	0.045
dimensions (mm)	0.50×0.27×0.24	0.30×0.27×0.10

Table 6.7 Selected bond distances (Å) bond angles and torsion angles (°) for $(C_6F_4S_2)_2$ (**81a**).

S(1)-S(2)*	2.064(1)	C(1)-C(2)	1.409(4)
S(1)-C(1)	1.771(3)	S(2)-C(2)	1.772(3)
S(2)*-S(1)-C(1)	102.73(9)	S(1)*-S(2)-C(2)	102.97(9)
S(1)-C(1)-C(2)	123.1	S(2)-C(2)-C(1)	123.6(2)
S(1)*-S(2)-C(2)-C(1)	79.9(2)	S(1)-C(1)-C(2)-S(2)	-1.8(3)
S(1)-C(1)-C(2)-C(3)	176.1(2)	S(2)-C(2)-C(1)-C(6)	-179.6(2)
C(1)-S(1)-S(2)-C(2)	-111.3(1)		

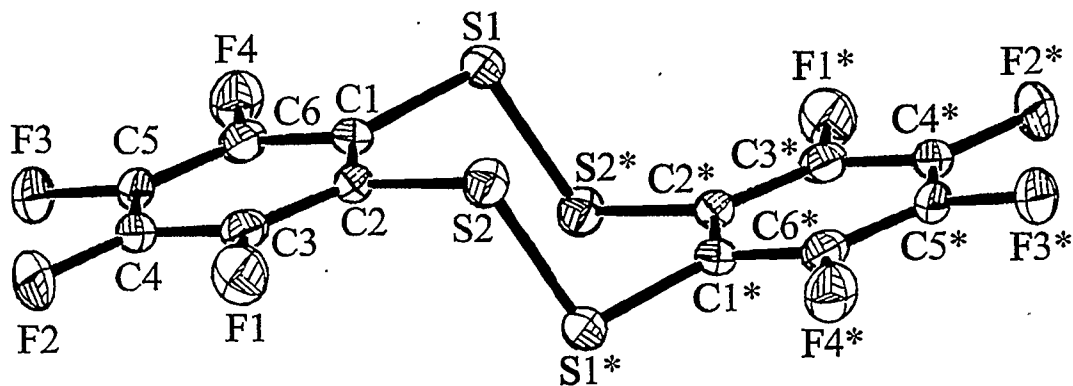


Figure 6.6. ORTEP diagram for $(C_6F_4S_2)_2$ (**81a**).

Table 6.8. Selected bond distances (Å) bond angles and torsion angles (°) for $(C_6Cl_4S_2)_2$ (**81b**).

S(1)-S(4)	2.033(3)	S(2)-S(3)	2.042(3)
S(1)-C(1)	1.782(8)	S(2)-C(6)	1.783(9)
S(3)-C(7)	1.799(8)	S(4)-C(12)	1.772(8)
C(1)-C(6)	1.40(1)	C(7)-C(12)	1.40(1)
S(1)-C(1)-C(6)	125.2(7)	S(2)-C(6)-C(1)	124.8(6)
S(3)-C(7)-C(12)	123.5(7)	S(4)-C(12)-S(7)	127.3(6)
S(4)-S(1)-C(1)	104.7(3)	S(3)-S(2)-C(6)	102.7(3)
S(1)-S(4)-C(12)	104.5(3)	S(2)-S(3)-C(7)	104.4(3)
S(4)-S(1)-C(1)-C(6)	-48.7(9)	S(3)-S(2)-C(6)-C(1)	-52.2(8)
S(2)-S(3)-C(7)-C(12)	-42.3(8)	S(1)-S(4)-C(12)-C(7)	-42.4(9)
S(1)-C(1)-C(6)-S(2)	3(1)	S(3)-C(7)-C(12)-S(4)	-7(1)
S(1)-C(1)-C(6)-C(5)	-178.1(7)	S(2)-C(6)-C(1)-C(2)	-178.8(7)
S(3)-C(7)-C(12)-C(11)	171.9(7)	S(4)-C(12)-C(7)-C(8)	171.9(7)
C(1)-S(1)-S(4)-C(12)	115.3(4)	C(6)-S(2)-S(3)-C(7)	118.2(4)

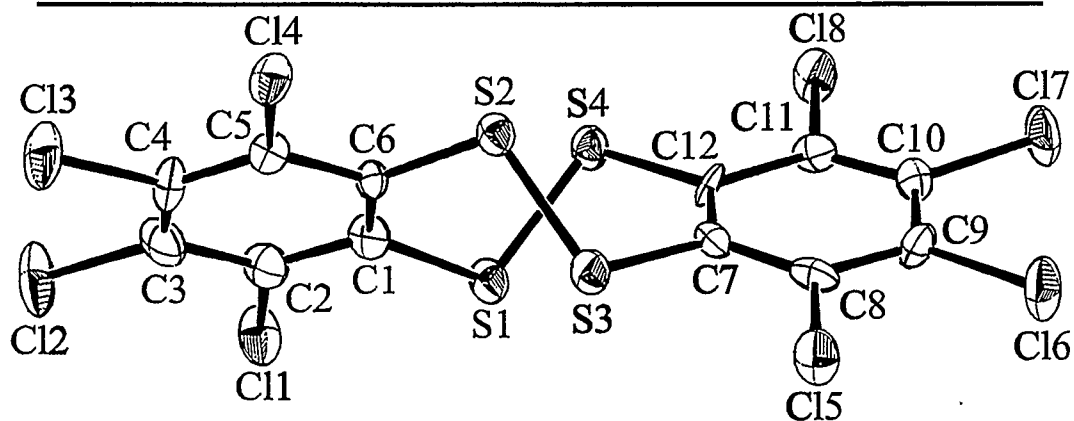


Figure 6.7. ORTEP diagram for $(C_6Cl_4S_2)_2$ (**81b**).

6.9. Summary.

A novel family of 9 π -electron $C_3S_2N_2$ cyclic radicals has been investigated. Their properties have been calculated by DFT, and compared to those of other well known radicals. Although synthetic and spectroscopic experiments are consistent with the preparation of such species, contamination with by-products and thermal instability precluded a full characterization of these systems. The trimethylsilyl derivative, $\overline{S(C_6Cl_4)S(NSiMe_3)(4-CH_3C_6H_4C)=N}$, a precursor to the radical $[C_6Cl_4S_2N_2C(4-CH_3C_6H_4)]\cdot$, has been prepared and structurally characterized. Thermochemical calculations indicate that the most promising route to the radicals involves formation of the corresponding anion as an intermediate, followed by oxidation of the anion. Preliminary evidence for the formation of the anion $C_6Cl_4S_2N_2C(4-CH_3C_6H_4)^-$ was obtained.

During this investigation, $(C_6F_4S_2)_2$ and $(C_6Cl_4S_2)_2$ were shown to possess solid state structures which correspond to two different conformers of the tetrathiocine ring.

6.10. Details of Calculations

Details of the computational method have been provided in Section 2.6; the calculation of $HC\equiv N$ is described in Section 4.10. Full geometry optimization was carried out on the model rings $(HC)_2E_2N$, HCN_2E_2 , $(HC)_2E_2N_2(CH)$ ($E = S, Se$), and their neutral dimers assuming C_{2v} symmetry. In order to calculate vertical ionization potentials and

electron affinities, the total atomization energy of the cations and anions was calculated using the optimized structure of the neutral radicals.

6.11. Experimental Part

Details of the experimental procedures and instrumentation have been provided in Section 2.7. The following commercial reagents were used as received: C₆H₄-1,2-(HS)₂ and 4-CH₃C₆H₃-1,2-(HS)₂, C₆Cl₆, Na₂S·9H₂O, NaOH, Fe powder, ZnO, H₂SO₄, (4-CH₃C₆H₄S)₂, Br₂, TASF, 18-crown-6, 1,2,3,4-F₄C₆H₂, n-BuLi (2.5 M solution in hexane). SO₂Cl₂ was distilled under N₂. CsF was baked at 400°C during 40 h and stored under N₂. Cl₂ was dried by passage through H₂SO₄. Elemental sulfur was recrystallized from CS₂. ¹⁹F NMR were recorded on a Bruker AM-400 spectrometer; the chemical shifts are reported with respect to CFCl₃ and were measured with a secondary external standard of C₆F₆ (δ -162.9 ppm).

6.11.1. Reaction of 1,2-C₆H₄(SCl)₂ with PhCN₂(SiMe₃)₃ and PhSeCl

A solution of C₆H₄-1,2-(HS)₂ (0.39 g, 2.7 mmol) in 40 mL of CH₂Cl₂ was treated with Cl₂ for 1h at 0°C. The solvent was evaporated to leave an orange viscous oil. This was redissolved in CH₂Cl₂ (200 mL) and the solution was slowly (40 min) added to a solution of PhCN₂(SiMe₃)₃ (0.903 g, 2.6 mmol) in 200 mL of CH₂Cl₂ at -30°C. After 18h of stirring, a solution of PhSeCl (0.50 g, 2.6 mmol) in 100 mL of CH₂Cl₂ was added to the mixture. The solution colour changed from orange to dark purple. After 3h the solvent was evaporated

and the dark residue was repeatedly extracted with hexanes to remove PhSeSePh. However, appreciable amounts of diselenide and the product were detected by ^1H NMR in both the extract and the residue. Recrystallization attempts failed to purify the product. Sublimation at 125°C under vacuum ($50\ \mu\text{mHg}$) was attempted. After 4h small drops of a liquid were observed on the wall of the vessel. GCMS identified this liquid as Ph-CN.

6.11.2. Reaction of 4- RC_6H_3 -1,2(SCl) $_2$ ($\text{R} = \text{H, Me}$) with 4- $\text{CH}_3\text{C}_6\text{H}_4\text{CN}_2(\text{SiMe}_3)_3$

In a typical experiment 1.5 mmol of dithiol were dissolved in 50 mL of CCl_4 . Dry Cl_2 gas was bubbled into the solution for 40 min. The solvent was removed under vacuum to leave an orange oil, which was recrystallized from the least amount of pentane. The orange solid was redissolved in 100 mL of hexanes and slowly (2h) added to a solution of 4- $\text{CH}_3\text{C}_6\text{H}_4\text{CN}_2\text{CN}_2(\text{SiMe}_3)_3$. After the addition was complete a white powder began to precipitate. Stirring was continued for 16h. The solid was allowed to settle down and the solvent was decanted by cannula. The crude product was rinsed with hexanes (2 x 10 mL). The material yielded dark red solutions in CH_2Cl_2 and CHCl_3 . In both cases, the ^1H NMR spectrum in CD_2Cl_2 indicated the presence of a very complex mixture.

6.11.3. Reaction of C_6Cl_6 with Na_2S and Fe: Preparation of C_6Cl_4 -1,2-(SH) $_2$

In a typical preparation C_6Cl_6 (32.66 g, 0.11 mol), Fe (6.2 g, 0.11 mol), and $\text{Na}_2\text{S}\cdot 9\text{H}_2\text{O}$ (54 g, 0.22 mol) were refluxed for 48h in 1 L of DMF. **Caution:** a wide condenser and vigorous reflux must be employed to prevent sublimed Na_2S from plugging

the condenser and causing a pressure build-up. The mixture was allowed to cool to 23°C and then 2 L of NaOH (0.75M) were added with vigorous stirring. The mixture was allowed to settle down (48 h) and then centrifuged to separate the solid, which was redissolved in 300 mL of MeOH and refluxed for 3h with ZnO (8g) and NaOH (150 mL, 0.75M). The hot slurry was filtered and the solution was acidified to a neutral pH with H₂SO₄. A pale yellow precipitate was filtered and dried with an air stream in the filtration funnel. This product was extracted (Soxhlet apparatus) with Et₂O to remove a dark green insoluble material. The solvent was evaporated from the solution to leave 11.3 g of a yellow solid. This crude product was shown by EIMS to consist of a mixture of C₆Cl₅SH and C₆Cl₄-1,2-(SH)₂, M/Z (M⁺) = 280 and 282, respectively (approximate yield: 36%). Purification by recrystallization from toluene and sublimation (140°C, 50 μmHg) was attempted. In most cases the components were not completely separated. In the following preparations "C₆Cl₅SH" or "C₆Cl₄-1,2-(SH)₂" indicate a mixture in which one of the components is dominant.

6.11.4. Chlorination of C₆Cl₅SH and C₆Cl₄(SH)₂

A CH₂Cl₂ slurry of 11.3 g of the crude mixture of both thiols was treated with a vigorous stream of Cl₂ during 1h at 0°C. The brown slurry was filtered to separate an orange solution. The solvent was removed under vacuum and the residue was recrystallized from the minimum amount of pentane. The orange crystalline powder (9.1g) was dried under

vacuum and stored under nitrogen. The EIMS showed that both C_6Cl_5SCl and $C_6Cl_4(SCl)_2$ were present in the crude product.

6.11.5. Preparation of 4-CH₃C₆H₄C(NSC₆Cl₅)(N(SiMe₃)₂) (38b)

A slurry of C_6Cl_5SH (1.68 g, 5.95 mmol) in CCl_4 was treated with dry Cl_2 during 40 min. The solvent was removed under vacuum and the residue was redissolved in Et_2O (100 mL). This solution was slowly added to 4-CH₃C₆H₄CN₂(SiMe₃)₃ (**1b**) (6.0 mmol) in Et_2O . After stirring for 16 h, the solvent was evaporated and the solid residue was recrystallized from Et_2O to give pale yellow crystals of **38b** (yield 0.75g, 24%). ¹H NMR ($CDCl_3$): δ 7.62, 7.58, 7.14, 7.10 (A₂B₂ q, 4-CH₃C₆H₄, 4), 2.34 (s, 4-CH₃C₆H₄, 3), 0.26 (s, Si(CH₃)₃, 18). I.R.(cm⁻¹, Nujol): 1453 s, 1375 m, 1335 m, 1252m, 919 m, 902 m, 878 w, 760 m, 692 m, 681 m, 665 m, 648 m, 483 s, 411 s. Mp. 151°C. Anal. Calcd for C₂₀H₂₅N₂SCl₅Si₂: C, 42.98; H, 4.51; N, 5.01. Found C, 43.16; H, 4.44; N, 4.99.

6.11.6. Reaction of C₆Cl₄-5,6-(SCl)₂ with 4-CH₃C₆H₄CN₂(SiMe₃)₃

a) A solution of sublimed "C₆Cl₄-5,6-(SH)₂" (1.33 g, 4.7 mmol) in benzene was treated with Cl_2 for 25 min. The solvent was evaporated under vacuum to leave an orange residue. This was redissolved in Et_2O (60 mL) and decanted to remove a small amount of precipitated $(Cl_4C_6S_2)_2$, identified by EIMS. This solution was added dropwise to a solution of 4-CH₃C₆H₄CN₂(SiMe₃)₃ (1.65 g, 4.7 mmol) in 90 mL of Et_2O . After 2 days the solvent was evaporated to dryness leaving a foamy residue, which was rinsed with 10

mL of diethyl ether. Fractional recrystallization from diethyl ether afforded yellow prisms, which were identified as $\overline{\text{S}(\text{C}_6\text{Cl}_4)\text{S}(\text{NSiMe}_3)(4\text{-CH}_3\text{C}_6\text{H}_4\text{C})=\text{N}}$ (74) (0.528 g, 24%). $^1\text{H NMR}$ (ppm, CDCl_3): δ 7.47, 7.42, 7.20, 7.15 (A_2B_2 q, $4\text{-CH}_3\text{C}_6\text{H}_4$, 4), 2.38 (s, $4\text{-CH}_3\text{C}_6\text{H}_4$, 3), -0.02 (s, SiCH_3 , 9). I.R. (cm^{-1} , Nujol): 1332 m, 1317 m, 1304 m, 1286 m, 1254 m, 1172 m, 1105 m, 1091 m, 939 m, 835 s, 781 m, 636 m. Mp 110°C (dec.). EIMS: M/Z 482 (M^+), 292 ($\text{Cl}_4\text{C}_6\text{S}_2\text{N}^+$), 190 ($4\text{-CH}_3\text{C}_6\text{H}_4\text{NSiMe}_3^+$), 73 (SiMe_3^+). Anal. Calcd for $\text{C}_{17}\text{H}_{16}\text{N}_2\text{S}_2\text{Cl}_4\text{Si}$: C, 42.33; H, 3.34; N, 5.81. Found C, 40.89; H, 3.23; N, 5.53.

A second fraction was isolated and recrystallized twice from Et_2O to yield pale yellow flakes. $^1\text{H NMR}$ (ppm, CDCl_3): δ 7.52, 7.48, 7.41, 7.37, 7.15, 7.11, 7.09, 7.05 (2 A_2B_2 q, $4\text{-CH}_3\text{C}_6\text{H}_4$, 8), 3.47 (q, $^3\text{J}(\text{}^1\text{H}-\text{}^1\text{H}) = 7$ Hz, $(\text{CH}_3\text{CH}_2)_2\text{O}$, 4), 2.35, 2.31 (2 s, $4\text{-CH}_3\text{C}_6\text{H}_4$, 6), 1.20 (t, $^3\text{J}(\text{}^1\text{H}-\text{}^1\text{H}) = 7$ Hz, $(\text{CH}_3\text{CH}_2)_2\text{O}$, 6), 0.15 (s, SiCH_3 , 18). FABMS: M/Z 686 ($\text{Cl}_4\text{C}_6(\text{SNC}(4\text{-CH}_3\text{C}_6\text{H}_4)\text{NSiMe}_3)_2$). Anal. Calcd for $\text{C}_{34}\text{H}_{32}\text{N}_4\text{S}_4\text{Cl}_8\text{Si}_2\cdot\text{C}_4\text{H}_{10}\text{O}$: C, 43.94; H, 4.08; N, 5.39. Found C, 43.74; H, 4.14; N, 5.28.

The mother liquor was dried under vacuum. The $^1\text{H NMR}$ spectrum showed still a complex mixture of products.

- b) The trisilylated benzamidine $4\text{-CH}_3\text{C}_6\text{H}_4\text{CN}_2(\text{SiMe}_3)_3$ (1.88 g, 5.4 mmol) and a mixture of $\text{C}_6\text{Cl}_5\text{SCl}$ and $\text{C}_6\text{Cl}_4(\text{SCl})_2$ (1.88 g, 5.4 mmol of $\text{C}_6\text{Cl}_4(\text{SCl})_2$, assuming this is the main component) were each dissolved in 100 mL of Et_2O . The two solutions were added simultaneously to 600 mL of boiling Et_2O over a 2h period. After 16h of reflux, the volume of solvent was reduced to 50 mL by distillation under N_2 . The remaining solvent was removed by a gentle N_2 stream. In this way the formation of a foam, which

complicates the purification operations, is avoided. The ^1H NMR spectrum showed the crude product to consist mainly of **38c** and **74**. The residue was extracted with CH_3CN (2 x 20 mL) and hexanes (10 mL), leaving behind yellow microcrystals of **38c**, identified by its ^1H NMR spectrum. A viscous phase separated from the extract, and it was stored at -20°C 24 h. After this time crystalline **74**, tainted with a brown impurity, was decanted from the solution and recrystallized from $\text{THF}/\text{Et}_2\text{O}$. The identity of this product was verified by ^1H NMR spectroscopy.

6.11.7. Attempted Reaction of $\text{S}(\text{C}_6\text{Cl}_4)\text{S}(\text{NSiMe}_3)(4\text{-CH}_3\text{C}_6\text{H}_4\text{C})=\text{N}$ with PhSeCl

A solution of PhSeCl (0.10 g, 5.2 mmol) in 50 mL of Et_2O was added to a solution of **74** (0.25 g, 5.2 mmol) in 100 mL of Et_2O at ambient temperature. Stirring was continued for 16 h. The solvent was evaporated under vacuum. The ^1H NMR spectrum of the residue showed the presence of only the starting reagents. The same reaction was repeated in boiling THF . In this case NMR analysis of the products indicated decomposition of **74**; $(\text{Cl}_4\text{C}_6\text{S}_2)_2$ was identified in this mixture by EIMS ($M/Z = 556$).

6.11.8. Attempted Reaction of $\text{S}(\text{C}_6\text{Cl}_4)\text{S}(\text{NSiMe}_3)(4\text{-CH}_3\text{C}_6\text{H}_4\text{C})=\text{N}$ with $4\text{-CH}_3\text{C}_6\text{H}_4\text{SCl}$

The solid disulfide $(4\text{-CH}_3\text{C}_6\text{H}_4\text{S})_2$ (0.026 g, 0.1 mmol) was treated with Cl_2 during 5 min. Excess of halogen was removed under vacuum. The product $4\text{-CH}_3\text{C}_6\text{H}_4\text{SCl}$ was dissolved in 5 ml of Et_2O and added to a solution of **74** (0.102 g, 0.21 mmol) in 20 mL of Et_2O at -90°C . The mixture was allowed to reach room temperature and stirred for 1 h. The

solvent was evaporated and the solid residue was washed with Et₂O. The ¹H NMR spectrum of the residue corresponded to that of 74.

6.11.9. Reaction of S(C₆Cl₄)SN(SiMe₃)C(4-CH₃C₆H₄)=N with Cl₂

- a) A solution of 74 (0.200 g, 0.4 mmol) in 10 mL of THF was frozen and slowly allowed to melt. When melting was complete SO₂Cl₂ (0.059 g, 0.4 mmol) was added to this solution. The mixture darkened slowly. After 40 min it had a dark purple colour which turned to a dark brown after 1h. At this point an excess of SO₂Cl₂ (1 mmol) was added. The mixture became red, and upon standing small orange crystals were formed on the walls of the flask. After 14h the solvent was removed. It was observed that the orange crystals decompose to a dark brown powder. The ¹H NMR spectrum (CD₂Cl₂) of this material showed no signal other than that of the residual solvent. The EIMS spectrum displayed a pattern (M/Z = 292) which can be attributed to Cl₄C₆S₂N.
- b) A solution of 74 (0.15 g, 0.3 mmol) in 20 ml of THF was treated with Cl₂ gas. A change of colour to dark purple was observed, then the solution turned red and small orange crystals were formed on the walls of the vessel. The orange crystals decomposed to a brown solid upon attempted isolation and purification of the compound. However, it was shown that the orange compound is regenerated by bubbling Cl₂ gas into a solution of the brown residue. The instability of the product, in the absence of an excess of Cl₂, precluded the complete characterization of this species.

- c) A small amount of **74** was dissolved in 0.5 mL of CDCl_3 , This solution was exposed to Cl_2 and an orange solution was obtained. The ^1H NMR spectrum revealed that **74** had been completely degraded to 4- $\text{CH}_3\text{C}_6\text{H}_4\text{CN}$.

6.11.10. Reaction of $\text{S}(\text{C}_6\text{Cl}_4)\text{S}(\text{NSiMe}_3)(4\text{-CH}_3\text{C}_6\text{H}_4\text{C})=\text{N}$ with CsF

- a) A solution of **74** (0.31 g, 0.6 mmol) in 10 mL of THF was added to a slurry of CsF (0.09 g, 0.6 mmol) in 10 mL THF. The slurry changed colour from yellow to red to dark brown over 1 h. The solvent was removed under vacuum. The residue was redissolved in THF and filtered to remove unreacted CsF. Attempts were made to purify the product by recrystallization from different solvents; however, the material was extremely soluble in polar solvents such as THF while very insoluble in non-polar solvents like pentane. Mixed solvents afforded a powder or no solid at all. The ^1H NMR spectrum indicated that the trimethylsilyl groups had been removed, however this product was a mixture which contained unreacted starting material.
- b) A solution of 18-crown-6 (0.033 g; 0.12 mmol) in 10 mL of THF was dried over freshly baked molecular sieves for 1h. This solution was added to CsF (0.015g, 0.1 mmol) to make a slurry. A solution of **74** (0.030 g, 0.06 mmol) in 5 mL of THF was dried in the same way. The two solutions were mixed at $-78\text{ }^\circ\text{C}$. The mixture slowly acquired an orange colour. After 15h the solution was filtered, and the solvent was removed from the solution under vacuum to leave a brown solid, which was washed with Et_2O to give a pale brown species, identified on the basis of the ^1H NMR spectrum as

[4-CH₃C₆H₄CN₂S₂C₆Cl₄][Cs(C₁₂H₂₄O₆)] (**80**). ¹H NMR (CD₂Cl₂): δ 7.74, 7.78, 7.33, 7.37 (A₂B₂ q, 4-CH₃C₆H₄, 4), 3.59, (s, C₁₂H₂₄O₆, 24), 2.43 (s, 4-CH₃C₆H₄, 3).

6.11.11. Crystallization of (C₆Cl₄S₂)₂ (**81b**)

In an attempt to crystallize a sample of **75**, a concentrated solution in THF in a narrow tube was allowed to evaporate slowly in air, through a needle inserted into a rubber septum. After 10 days the pale yellow solution acquired a red colour and small yellow prismatic crystals were deposited at the bottom of the vessel; these were allowed to grow over 2 months. X-ray diffraction showed the crystal to correspond to the dimer (C₆Cl₄S₂)₂. EIMS: M/Z = 556 (M⁺). I.R.(cm⁻¹, Nujol): 1377 s, 1335 m, 1303 s, 1095 m, 869 m. Mp 290°C (d).

6.11.12. Preparation of 2,3,4,5-F₄C₆H(SH)

This procedure is based on the original method by Brooke et al. [142]. A solution of n-BuLi (27 mL, 2.5M, 6.7 mmol) was added slowly (1h) under vigorous stirring to a solution of 1,2,3,4-F₄C₆H₂ (10 g, 66.7 mmol) in 85 mL of THF at -78°C. **Note:** the reaction vessel must be completely immersed in the cooling bath to prevent contamination by a dark product of thermal decomposition. Solid sulfur (2.13 g, 66.6 mmol) was added under stirring and the mixture was transferred to an ice bath. After 16h, 10 mL of concentrated HCl were added at 0°C. The organic fraction was extracted with pentane and dried over MgSO₄. The solvents were removed and vacuum distillation (Bp: 37-43°C, water aspirator)

afforded 2,3,4,5-F₄C₆H(SH) as a colourless liquid (8.44g, 70%). ¹H NMR (ppm, CDCl₃): δ 6.93 (m, F₄C₆H, 1), 3.64 (s, SH, 1). ¹⁹F NMR (ppm, CDCl₃): δ -132.6 (m ABCD, F₄C₆H, 1), -139.6 (m ABCD, F₄C₆H, 1), -155.0 (m ABCD, F₄C₆H, 1), -159.0 (m ABCD, F₄C₆H, 1).

6.11.13. Preparation of 3,4,5,6-F₄C₆-1,2-(SH)₂

This procedure is based on the original method by Nyholm et al. [143]. This product was prepared by a process similar to the synthesis of 2,3,4,5-F₄C₆H(SH). It was isolated in 70% yield as a colourless liquid (Bp 60°C, 50 μmHg). Mp 50°C. ¹H NMR (ppm, CDCl₃): δ 3.82 (SH). ¹⁹F NMR (ppm, CDCl₃): δ -131.7 (m AA'XX', F₄C₆, 2), -158.5 (m AA'XX', F₄C₆, 2).

6.11.14. Attempted Chlorination of 3,4,5,6-F₄C₆-1,2-(SH)₂. Preparation of (C₆F₄S₂)₂ (81a)

A solution of the dithiol (0.30 g, 1.4 mmol) in 50 mL of benzene was treated with Cl₂ gas during 30 min. The solvent was removed by vacuum distillation. The residue was recrystallized from Et₂O to give 0.30 g of (C₆F₄S₂)₂ (81a). I.R.(cm⁻¹, Nujol): 1387 m, 1380 m, 1366 m, 1315 s, 1245 s, 1114 s, 1064 m, 1043 m, 876 s, 825 s, 485 m, 418 s. Mp 193°C. ¹⁹F NMR (ppm, CDCl₃): δ -131.0 (m AA'XX', F₄C₆, 1), -135.8 (m AA'XX', F₄C₆, 4), -148.2 (m AA'XX', F₄C₆, 4), -153.2 (m AA'XX', F₄C₆, 1).

7. Concluding Remarks and Suggestions for Future Research

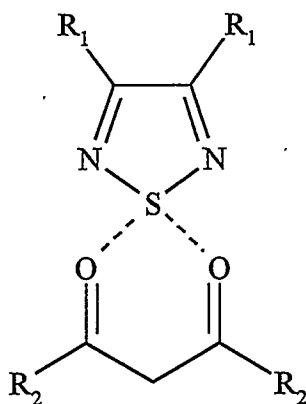
7.1. The $RSN=C(R')N=NC(R')=NR$ Diazenes and Related Close $D\cdots E$ ($D = O, N; E = S, Se, Te$) Contacts

7.1.1. Intermolecular Interactions

Intramolecular contacts are occasionally encountered in molecules which contain a chalcogen and an atom with available lone pairs, N or O. For a long time these weak interactions have either been neglected or they have been regarded as of little consequence. Currently "intramolecular coordination" is a feature of organochalcogen compounds that is receiving increasing attention. Our DFT investigation of the close $E\cdots N$ ($E = S, Se$) contacts observed in the diazenes of the type **28** provided an interpretation which emphasizes the role of the back-donation from a chalcogen lone-pair into the $\pi^*(N=N)$ orbital, especially in the case of low electronegativity substituents on sulfur. The derived bonding scheme can easily be extended to related systems that involve the heavy chalcogen tellurium, and to the donor oxygen.

It was shown that these interactions may be formed and broken reversibly. The calculated energetic magnitude of these interactions (< 30 kJ/mol) is comparable to that of some hydrogen bonds. It is then reasonable to expect that this type of interaction may also

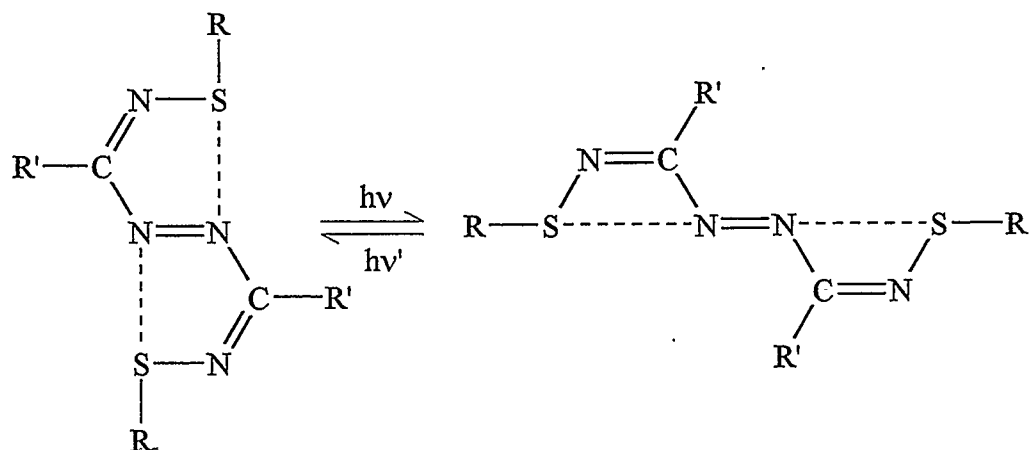
occur intermolecularly, i. e. to hold together two different molecules, and possibly be used in the construction of supramolecular assemblies. The simultaneous interaction of a chalcogen atom with two "donor" centers may stabilize an adduct. In order to minimize steric hindrance, oxygen "donors" should be preferred over the nitrogen systems, which require additional substituent groups. The chalcogen atoms have to be part of ring, to avoid the steric and conformational effects of an open chain. Based on these factors one could, for example, suggest an investigation of the "coordination" of a 1,2,5-dithiadiazole by carbonylic compounds (Scheme 7.1). The two nitrogen atoms attached to the chalcogen avoid the need of substituents on positions 2 and 5; at the same time they provide some σ acidity to the sulfur atom, which can be further enhanced by using strongly electronegative R_1 groups. The heavier chalcogen derivatives are also expected to form more stable adducts by enhancing both the σ and π interactions.



Scheme 7.1

7.1.2. Materials with Potentially Useful Optical Properties

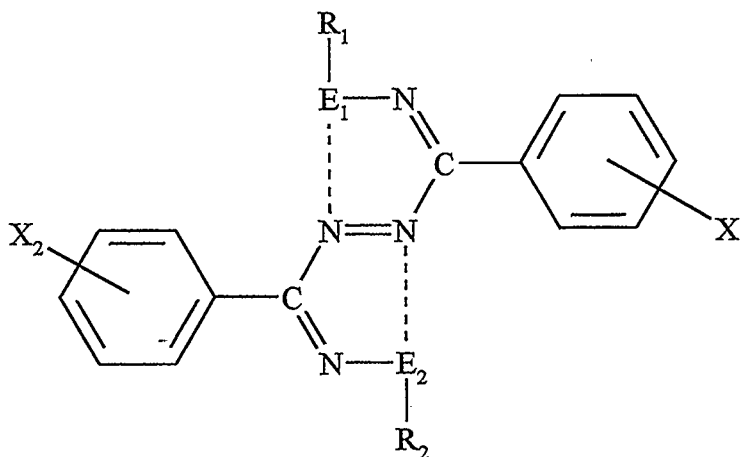
The properties of the diazenes of the type **28** suggest potential applications for these materials. Especially in consideration of their remarkable chemical stability; some derivatives are able to resist hydrolysis by concentrated KOH solutions in EtOH. The difference of colour between the *Z,E,Z* diazene with the shortest S...N distance ($\lambda_{\text{max}} \sim 550$ nm) and the other two isomers ($\lambda_{\text{max}} \sim 470$ nm) is remarkable. Although the geometric interconversion was observed upon temperature changes, it may also be expected that some diazenes will undergo this type of rearrangement in response to light (Scheme 7.2). Such derivatives could have application as optical switches. Preparation of such a device still requires research to establish the effect of the nature of the R and R' substituents on the structures, geometrical interconversion and colour of the diazenes. The current studies have included hydrogen and some substituted phenyl groups as R', but R has been restricted mainly to the phenyl and *p*-tolyl groups due to the limitations of the synthetic method. Synthesis of derivatives with strong electron-releasing (e.g. NMe₂) or electron-withdrawing (e.g. NO₂) groups attached to sulfur deserves attention since it can be anticipated that they will affect the S...N interaction. The goal is to identify a derivative which undergoes a reversible change of structure, and colour, upon light irradiation.



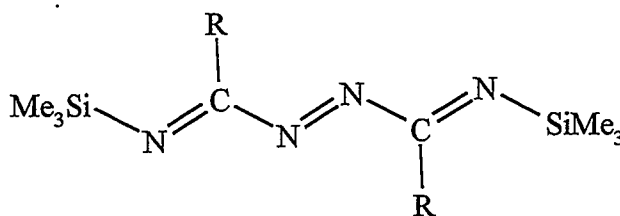
Scheme 7.2

Derivatives of the type **28** possess characteristics that may be useful in the preparation of materials with non-linear optical (NLO) properties [144]: (a) the presence the chalcogen-nitrogen linkages provides a polarizable π -system; (b) intense electronic transitions that are associated with large optical non-linearities.

It is known that the placement of substituents of different electronegativity on opposite ends of a π system induces non-linear optical (NLO) properties [145]. Two approaches may be envisioned (See Scheme 7.3). These involve the introduction of different substituents on either the C ($X_1 \neq X_2$) or S ($R_1 \neq R_2$) atoms. The preparation of the first type of derivative could be attempted by reaction of PhSCl with an equimolar mixture of two differently substituted benzamidines. This method would undoubtedly yield a mixture of the two symmetric diazenes and the asymmetric compound. Column chromatography may be used to separate the components of the mixture, since it has proven successful in the separation of a mixture of the rings **27** and **30**, the diazenes and phenyl disulfide [46].



Scheme 7.3

**82**

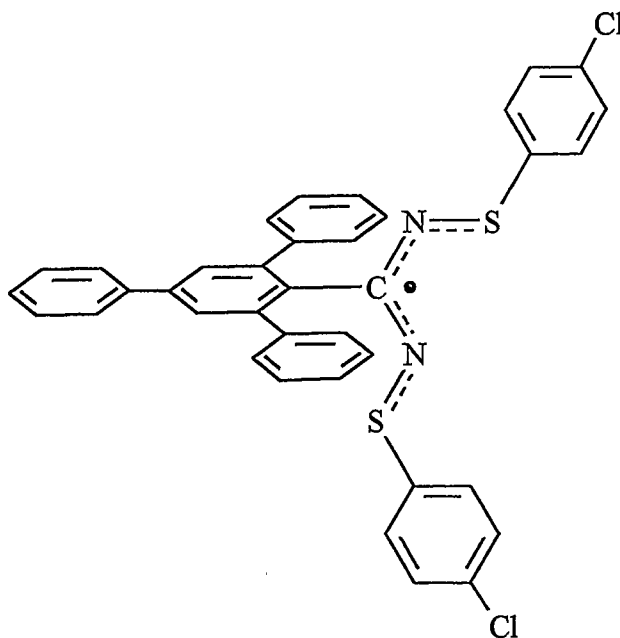
The preparation of a derivative with different substituents on the chalcogen may be approached from the diazene precursor **82**. A possible synthesis of this precursor, based on known procedures [146], is outlined in Scheme 7.4. The first step requires the formation of an imidate salt (**83**) [147]. A condensation reaction with hydrazine [148] followed by bromine oxidation [149] may produce the intermediate salt **84**. Neutralization and replacement of H by trimethylsilyl groups would produce **82**. The reaction conditions must be carefully adjusted to prevent the side reactions which yield 1,2,4-triazole derivatives and *s*-tetrazines, among other by-products [150].

7.2. Mechanism of Formation of the Diazenes of the Type 28. Properties of the RC(NPh)₂· (29) Radicals

7.2.1. Stable Radicals of the Type 29

The mechanistic studies have afforded an interesting conclusion regarding the decomposition of the tris(thiolato)substituted amidines. This process is driven by the availability of PhS· radicals, which are able to catalyze the decomposition by abstraction of PhS units. However, this does not facilitate the decomposition of other stable derivatives such as PhCN₂(SCCl₃)₃ (**31b**). The observation of the activity of PhS· radicals in the mechanism suggests that a similar process is involved in the decomposition of (PhS)₃N [95].

Radicals of the type RC(NPh)₂· (**29**) are unstable. However, even radicals of the type [RSNR']· have been stabilized by choosing the appropriate substituent groups. Good results have been obtained with R as a halogen-substituted aromatic ring and R' as 2,4,6-triphenylphenyl [80]. Based on that work the formation of a stable radical like **29e** can be proposed.



29e

7.2.2. Formation of Cyclic Products

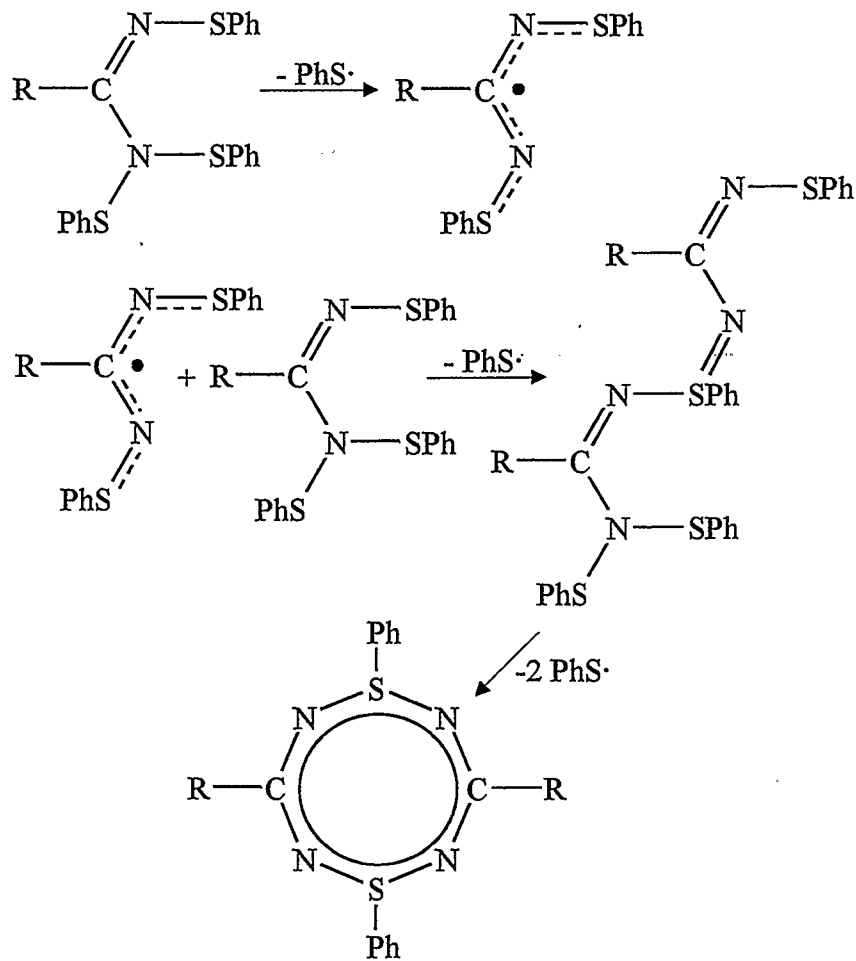
In this dissertation it has been shown that the radicals **29** decay to the corresponding diazenes **28** by second order kinetics, consistent with radical dimerization as the rate-determining step.

It has been observed that, in the case of $R = 4\text{-BrC}_6\text{H}_4$, the yields of the 8-membered ring (**27h**) and especially the 16-membered ring (**30**) are enhanced when the reaction mixture of trisilylated benzimidine and PhSCl is kept at low temperature for long periods of time [46]. It may reasonably be assumed that a radical of the type **29** is also involved in the formation of these rings, but the process of ring formation should be different from the production of diazenes. The radical **29** may react with another molecule of trisubstituted

benzamidine to form a longer chain intermediate (Scheme 7.6). Upon warming up to room temperature this molecule would quickly cyclize to form the 8-membered ring with loss of 2 PhS \cdot , by analogy with the production of **29**. This alternative pathway for the decay of **29** would be first order with respect to the radical. The concentration of the radical would be small enough to guarantee pseudo first order conditions. As a consequence, for most concentrations of the radical-**29**, the dimerization and diazene formation are the dominant processes. However, at very small radical concentration, which can be achieved at low temperatures or by using a large volume of solvent, the first order process becomes faster and the formation of cyclic products is favoured.

7.3. The (R'C) $_2$ N $_4$ (SR) $_2$ Rings

The theoretical study of (R'C) $_2$ N $_4$ (SR) $_2$ rings (**27**) has been successful in explaining the geometry and the photochemistry of these systems. The calculations suggest the preparation of a dianion [(R'C) $_2$ N $_4$ (SR) $_2$] $^{2-}$, in view of the predicted S-S transannular bond. This would require preliminary electrochemical experiments (e.g. cyclic voltammetry) of the eight-membered ring to establish the existence of the dianions. The two-electron reduction may have a large reduction potential. Reduction to the radical anion [(R'C) $_2$ N $_4$ (SR) $_2$] $^{\cdot-}$, which should also exhibit a S-S bond, may be easier to achieve. Either electrochemical or alkali metal reduction could be attempted to prepare anionic derivatives.

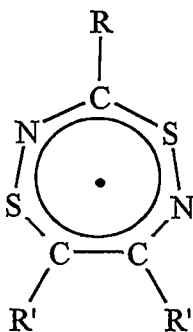
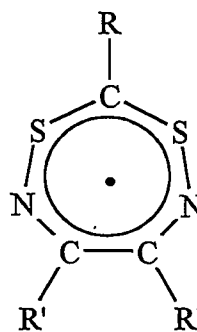


Scheme 7.6

7.4. The 1,4,5,7-Dithiadiazepinyl Radicals

The properties of 1,4,5,7-dithiadiazepinyl radicals have been modeled by DFT and compared to the properties of 1,3,2-dithiazolyl and 1,2,3,5-dithiadiazolyl radicals. It was concluded that the 1,4,5,7-dithiadiazepinyl radicals would provide solid state materials less prone to dimerization and with small electron-electron repulsions in the conduction band.

Experiments aimed at the synthesis of the 1,4,5,7-dithiadiazepinyl radicals have identified several practical problems. The cyclocondensation usually produces a mixture which probably contains cyclooligomers larger than the 7-membered rings. The polycondensation can be minimized by employing high dilution conditions. The silylated precursor $\overline{\text{S}(\text{C}_6\text{Cl}_4)\text{S}(\text{NSiMe}_3)(4\text{-CH}_3\text{C}_6\text{H}_4\text{C})=\text{N}}$ (**74**) was isolated and structurally characterized. Thermochemical calculations indicate that these rings are unstable as the cation and neutral radical, with respect to ring contraction by nitrile elimination. This precludes the use of such radicals as molecular conductors, since electron transfer may induce the decomposition. The same might be expected for a 1,4,2,5 isomer (**85**), since it may easily form a nitrile. However, the 1,3,4,7 isomer (**86**) could not eliminate a nitrile. As a consequence, radicals of the type **86** may constitute a better option for the preparation of 9 π -electron heterocyclic C-S-N rings.

**85****86**

References

1. J.E. Mark, H.R. Allcock, R. West, *Inorganic Polymers*, Prentice Hall, Englewood Cliffs, N. J., 1992.
2. A.W. Cordes, R.C. Haddon, R.T. Oakley, in *The Chemistry of Inorganic Ring Systems*, R. Steudel (Ed.), Elsevier, Amsterdam 1992, Chapter 16, p. 295.
3. M. Shakir, H.W. Roesky, *Phosphorus, Sulfur and Silicon*, **93-94**, 13, 1994.
4. a) A. Bernthsen, *Ann. Chem. Pharm.*, **184**, 321, 1876. b) A. Bernthsen, *Ann. Chem. Pharm.*, **192**, 1, 1878. c) A. Bernthsen, *Chem. Ber.*, **10**, 1235, 1877.
5. A.R. Sanger, *Inorg. Nucl. Chem. Lett.*, **9**, 351, 1973.
6. R.T. Boeré, R.T. Oakley, R.W. Reed, *J. Organomet. Chem.*, **331**, 161, 1987.
7. K. Dehnicke, *Chem. Ztg.*, **114**, 295, 1990.
8. F.T. Edelmann, *Coord. Chem. Rev.*, **137**, 403, 1994.
9. H.G. Heal, *The Inorganic Heterocyclic Chemistry of Sulfur, Nitrogen and Phosphorus*, Academic Press, London, 1980, p. 8.
10. L. Ouvrard, *Ann. Chim. Phys.* **2**, 212, 1894.
11. a) J. Passmore, M.J. Schriver, *Inorg. Chem.*, **27**, 2749, 1988. b) R.L. Patton, W.L. Jolly, *Inorg. Chem.*, **9**, 1079, 1970.
12. N.N. Greenwood, A. Earnshaw, *Chemistry of the Elements*, Pergamon Press, Oxford, 1984, p. 872.

13. T. Chivers, J.F. Richardson, N.R.M. Smith, Inorg. Chem., **25**, 47, 1986.
14. a) A. Baceiredo, G. Bertrand, J.-P. Majoral, G. Sicard, J. Jaud, J. Galy, J. Am. Chem. Soc., **106**, 6088, 1984. b) A. Baceiredo, G. Bertrand, J.-P. Majoral, F. El Anba, G. Manuel, J. Am. Chem. Soc., **107**, 3945, 1985.
15. S. Parsons, J. Passmore, X. Sun, M. Regitz, Can. J. Chem., **73**, 1312, 1995.
16. T. L. Gilchrist, Heterocyclic Chemistry, Pitman, London, 1985, p. 225.
17. T. Chivers, D.D. Doxsee, M. Edwards and R.W. Hiltz, in The Chemistry of Inorganic Ring Systems, R. Steudel (Ed.), Elsevier, Amsterdam, 1992, Chapter 15, p. 271.
18. J. Tejada, R. Réau, F. Dahan, and G. Bertrand, J. Am. Chem. Soc., **115**, 7880, 1993.
19. R. Réau, A. Baceiredo, G. Bertrand, Phosphorus, Sulfur, and Silicon, **93-94**, 1, 1994.
20. M. Herberhold, W. Jellen, Z. Naturforsch., **41b**, 144 (1986).
21. a) T. Chivers, X. Gao, M. Parvez. J. Chem. Soc., Chem. Commun., 2149, 1994. b) T. Chivers, X. Gao, M. Parvez. Inorg. Chem., **35**, 9, 1996.
22. E. Lork, G. Knitter, R. Mews, J. Chem. Soc., Chem. Commun., 1437, 1995.
23. T. Chivers, X. Gao, M. Parvez. J. Am. Chem. Soc., **117**, 2359, 1995
24. M. Amin, C.W. Rees, J. Chem. Soc., Chem. Commun., 1137, 1989.
25. U. Scholz, H.W. Roesky, J. Schimkowiak, M. Noltemeyer, Chem. Ber., **122**, 1067, 1989.
26. R.T. Boéré, K.H. Moock, S. Derrick, W. Hoogerduck, K. Preuss, J. Yip, M. Parvez, Can. J. Chem., **71**, 473, 1993.

27. T. Chivers, K.S. Dhathatreyan, S.W. Liblong and T. Parks, Inorg. Chem., **27**, 1305, 1988.
28. T. Chivers, D.D. Doxsee, M. Parvez, Inorg. Chem., **32**, 2238, 1993.
29. T. Chivers, D.D. Doxsee, J.F. Fait, J. Chem. Soc., Chem. Commun., 1703, 1989.
30. E. Hey, C. Ergezinger, K. Dehnicke, Z. Naturforsch., **44b**, 205, 1989.
31. T. Chivers, M.N.S. Rao, Phosphorus, Sulfur, and Silicon, **69**, 197, 1992
32. K. Dehnicke, C. Ergezinger, E. Hartmann, A. Zinn, K. Hösler, J. Organomet. Chem. **352**, C1, 1988
33. V. Chandrasekhar, T. Chivers, J.F. Fait, S.S. Kumaravel, J. Am. Chem. Soc., **112**, 5373, (1990).
34. V. Chandrasekhar, T. Chivers, S.S. Kumaravel, M. Parvez and M.N.S. Rao, Inorg. Chem. **30**, 4125, 1991.
35. P. Zoricak, M. Parvez, I. Vargas-Baca, T. Chivers. Phosphorus, Sulfur and Silicon, **93-94**, 455, 1994.
36. K.F. Preston, L.H. Sutcliffe, Mag. Reson. Chem., **28**, 189, 1990.
37. T. Ziegler, Can. J. Chem., **73**, 743, 1995.
38. T. Chivers, H. Jacobsen, R. Vollmerhaus, T. Ziegler, Can. J. Chem., **72**, 1582, 1994.
39. T. Chivers, I.H. Krouse, M. Parvez, I. Vargas-Baca, T. Ziegler, P. Zoricak, Inorg. Chem., accepted for publication.
40. N.N. Greenwood, A. Earnshaw, Chemistry of the Elements, Pergamon Press, Oxford, 1984, Chapter 17.

41. a) A. Kuszman, L. Kapovits, In Organic Sulfur Chemistry: Theoretical and Experimental Advances, I.G. Csizmadia, A. Mangini, Eds.; Elsevier, Amsterdam, 1985, pp. 191-245.
b) I. Hargittai, R. Rozsondai, In The Chemistry of Organic Selenium and Tellurium Compounds, Vol. 1, S. Patai, Z. Rappoport, Eds.; Wiley, 1986, pp. 63-156.
42. (a) S. Tomoda, Iwaoka, M. In Unusual Valency and Property of Organic Compounds of Main Group Elements; E. Akiba, Ed.; Hiroshima University Japan, 1993, p. 163. (b) S.R. Wilson, P.A. Zucker, R.-R.C. Huang, A. Spector, J. Am. Chem. Soc., **111**, 5936; 1989; (c) L. Engman, D. Stern, I.A. Cotgreave, C.M. Andersson, J. Am. Chem. Soc., **114**, 9737, 1992.
43. P.J. Dunn, C.W. Rees, A.M.Z. Slawin, D.J. Williams, J. Chem. Soc. Chem. Commun., 1134, 1989.
44. C. Bois, J. Armand, P. Bassinet, Acta Cryst., **B36**, 1731, 1980.
45. P.G. Jones, M.C. Ramirez de Arellano, Chem. Ber., **128**, 741, 1995.
46. P. Zoricak, M. Sc. Thesis, The University of Calgary, Calgary, 1996.
47. I.H. Krouse, M. Sc. Thesis, The University of Calgary, Calgary, 1996.
48. H. Hope, D. Victor, Acta Crystallogr., **B25**, 1849, 1969.
49. R. Allman, in The Chemistry of the Hydrazo, Azo and Azoxy Groups, S. Patai, Ed., John Wiley and Sons, New York, 1975, Chapter 2.
50. T. Ziegler, In Metal-Ligand Interactions: from Atoms, to Clusters, to Surfaces, D.R. Salahub, N. Russo, Eds.; Kluwer Academic Publishers, Amsterdam, 1992.

51. H. Jacobsen, H.B. Kraatz, T. Ziegler, P.M. Boorman, J. Am. Chem. Soc., **114**, 7851, 1992.
52. H.W. Roesky, K.L. Weber, U. Seseke, W. Pinkert, M. Noltemeyer, W. Clegg, G. M. Sheldrick, J. Chem. Soc., Dalton Trans., 565, 1985.
53. For examples of intramolecular Te--N coordination, see (a) N. Sudha, H.B. Singh, Coord. Chem. Rev., **135/136**, 469, 1994; (b) R. Kaur, H.B. Singh, R.J. Butcher, Organometallics, **14**, 4755, 1995.
54. R.E. Cobblestick, F.W.B. Einstein, W.R. McWhinnie, F.H. Musa, J. Chem. Res. (S), 145, 1979; (M), 1901, 1979.
55. a) N. Petragnani, L. Torres, K.J. Wynne, J. Organomet. Chem., **92**, 185, 1975. b) M.J. Dabdoub, V.B. Dabdoub, J.V. Comasseto, N. Petragnani, J. Organomet. Chem., **308**, 211, 1986.
56. (a) O. Gunnarsson, I. Lundquist, Phys. Rev., **B10**, 1319, 1974; (b) O. Gunnarsson, I. Lundquist, Phys. Rev., **B13**, 4274, 1976; (c) O. Gunnarsson, M. Johnson, I. Lundquist, Phys. Rev., **B20**, 3136, 1979.
57. E.J. Baerends, D.E. Ellis, P. Ros, Chem. Phys., **2**, 41, 1973.
58. E.J. Baerends, Ph.D. Thesis Frije Universiteit, Amsterdam, 1975.
59. W. Ravenek, In Algorithms and Applications on Vector and Parallel Computers, H.J.J. Riele, Th.J. Dekker, H.A. van de Horst, Eds.; Elsevier, Amsterdam, 1987.
60. G te Velde, Ph.D. Thesis, Vrije Universiteit, Amsterdam, 1990.

61. L. Versluis, T. Ziegler, J. Chem. Phys., **88**, 322, 1988.
62. T. Ziegler, A. Rauk, Theor. Chim. Acta, **46**, 1, 1977.
63. (a) J.G. Snijders, E.J. Baerends, P. Vernoijs, At. Nucl. Data Tables, **26**, 483, 1982; (b) P. Vernoijs, J.G. Snijders, E.J. Baerends, Slater Type Basis Functions for the Whole Periodic System, Internal Report; Frije Universiteit, Amsterdam, 1981.
64. J. Krijn, E.J. Baerends, Fitfunctions in the HFS Method, Internal Report, Frije Universiteit, Amsterdam, 1984.
65. S.H. Vosko, L. Wilk, M. Nusair, Can. J. Phys., **58**, 1200, 1990.
66. A.D. Becke, J. Phys. Rev. A, **38**, 2938, 1988.
67. (a) J.P. Perdew, Phys. Rev., **B33**, 8822, 1986; (b) J.P. Perdew, Phys. Rev., **B34**, 7406, 1986.
68. A.W. Cordes, S.H. Glarum, R.C. Haddon, R. Halford, R.G. Hicks, D.K. Kennepohl, R.T. Oakley, T.T.M. Palstra, S.R. Scott, J. Chem. Soc., Chem. Commun., 1265, 1992.
69. W.H. Mueller, J. Am. Chem. Soc., **90**, 2075, 1968.
70. T. Chivers, K. McGregor, M. Parvez, I. Vargas-Baca, T. Ziegler, Can. J. Chem., **73**, 1380, 1995.
71. T. Chivers, K. McGregor and M. Parvez, Inorg. Chem. **33**, 2364, 1994.
72. A.V. Zibarev, M.A. Fedorov and G.G. Furin, Izv. Akad. Nauk. S.S.S.R Ser. Khim. **4**, 829, 1989.
73. A.F. Wells. Structural Inorganic Chemistry. 5th Ed. Clarendon Press, Oxford, England, 1984.

74. F. Wasaki, H. Murakami, N. Yamazaki, M. Yasui, M. Tomura and N. Matsumura, *Acta Crystallogr.* **C47**, 998, 1991.
75. T. Chivers, B. McGarvey, M. Parvez, I. Vargas-Baca, T. Ziegler, *Inorg. Chem.*, **35**, 3839, 1996.
76. a) J.A. Baban, B.P. Roberts, *J. Chem. Soc., Perkin Trans. 2*, 678, 1978. b) J.E. Bennet, H. Sieper, P. Tavs, *Tetrahedron*, **23**, 1697, (1967). c) W.C. Danen, D.D. Newkirk, *J. Am. Chem. Soc.*, **98**, 516, 1976. d) B. Maillard, K.U. Ingold, *J. Am. Chem. Soc.*, **98**, 520, 1976.
77. J.A. Hunter, B. King, W.E. Lindsell, M. A. Neish, *J. Chem. Soc., Dalton Trans.*, 880, 1980.
78. K. Bestari, R.T. Oakley, A.W. Cordes, *Can. J. Chem.*, **69**, 94, 1991.
79. G. Brunton, J.F. Taylor, K.U. Ingold, *J. Am. Chem. Soc.*, **98**, 4879, 1978.
80. Y. Miura, A. Tanaka, *J. Chem. Soc., Chem. Commun.*, 441, 1990.
81. Y. Miura, A. Yamamoto, Y. Katsura, M. Kinoshita, S. Sato, C. Tamura, *J. Org. Chem.*, **47**, 2618, 1982.
82. Y. Miura, H. Asada, M. Kinoshita, *J. Phys. Chem.*, **87**, 3450, 1983.
83. Y. Miura, A. Yamamoto, K. Katsura, M. Kinoshita, *J. Org. Chem.*, **45**, 3875, 1980.
84. Y. Miura, H. Asada, M. Kinoshita, *Bull. Chem. Soc. Jpn.*, **53**, 720, 1980.
85. Y. Miura, M. Kinoshita, *J. Org. Chem.*, **49**, 2724, 1984.
86. R.S. Atkinson, B.D. Judkins, N. Khan, *J. Chem. Soc., Perkin Trans. 1*, 2491, 1982.

87. a) Y. Miura, H. Asada, M. Kinoshita, Bull. Chem. Soc. Jpn., **51**, 3004, 1978. b) Y. Miura, M. Kinoshita, J. Org. Chem., **51**, 1239, 1986.
88. Y. Miura, T. Kunishi, M. Kinoshita, J. Org. Chem., **50**, 5862, 1985.
89. H. Lecher, K. Köckerle and P. Stocklin, Chem. Ber., **58**, 423, 1925.
90. Y. Miura, N. Makita and M. Kinoshita, Tetrahedron Lett., **2**, 127, 1975.
91. Y. Miura, N. Makita and M. Kinoshita, Bull. Chem. Soc. Jpn., **50**, 482, 1977.
92. S.R. Harrison, R.S. Pilkington and L.H. Sutcliffe, J. Chem. Soc., Faraday Trans. 1, **80**, 669, 1984.
93. R. Mayer, D. Decker, S. Bleisch, G. Domschke, J. Prakt. Chem., **329**, 81, 1987.
94. R. Fleischer, S. Freitag, F. Pauer, D. Stalke, Angew. Chem. Int. Ed. Engl., **35**, 204, 1996.
95. D.H.R. Barton, I.A. Blair, P.D. Magnus, R. Norris, J. Chem. Soc., Perkin Trans. 1, 1031, 1973.
96. T.G. Back, R.G. Kerr, J. Chem. Soc., Chem. Commun., 134, 1987.
97. Y. Miura, A. Yamamoto, Y. Katsura, M. Kinoshita, Bull. Chem. Soc. Jpn., **54**, 3215, 1981.
98. B. Wrackmeyer, B. Distler, S. Gerstmann, and M. Herberhold, Z. Naturforsch., **48B**, 1307, 1993.
99. J.R. Carruthers, K. Prout, D.J. Watkin, Cryst. Struct. Commun., **10**, 1217, 1981.

100. a) Y. Drozdova, R. Steudel, Chem. Eur. J., **1**, 193, 1995. b) R. Steudel, Angew. Chem., Int. Ed. Engl., **34**, 1313, 1995. c) R.J. Suontamo, R.S. Laitinen, Main Group Chemistry, **1**, 241, 1996.
101. D. Griller, J.A. Martinho-Simões, D.D.M. Wagner, in Sulfur Centered Reactive Intermediates in Chemistry and Biology; C. Chatgililoglu, K.D. Asmus (ed.), Plenum Press, New York 1990.
102. E.S. Levchenko, T.N. Dubinina, S.V. Sereda, M.Yu. Antipin, Yu.T. Struchkov, I.E. Boldeskul, Zh. Org. Khim., **23**, 86, 1987.
103. M. Lazar, J. Rychlý, V. Klimo, P. Pelikán, L. Volko, Free Radicals in Chemistry and Biology. CRC Press, Boca Raton, Florida, 1989, Chapter 3.
104. a) M. Negareche, Y. Badrudin, Y. Berchadsky, A. Friedmann, P. Tordo, J. Org. Chem., **51**, 342, 1986. b) V. Malatesta, K.U. Ingold, J. Am. Chem. Soc., **95**, 6110, 1973. c) L. Lunazzi, K.U. Ingold, J. Am. Chem. Soc., **96**, 5558, 1974. d) V. Malatesta, K.U. Ingold, J. Am. Chem. Soc., **96**, 3949, 1974. e) V. Malatesta, D. Lindsay, E.C. Horseville, K.U. Ingold, Can. J. Chem., **52**, 864, 1974.
105. K. Raghavachari, R.C Haddon, J. Phys. Chem., **87**, 1312, 1983.
106. Y. Miura, N. Makita, M. Kinoshita, Bull. Chem. Soc. Jpn., **50**, 482, 1977.
107. a) M. Bonifacic, K.-D. Asmus, J. Phys. Chem., **88**, 6286, 1984. b) T.J. Burkey, D. Griller, J. Am. Chem. Soc., **107**, 246, 1985.

108. a) R. Laitinen, R. Steudel, R. Weiss, J.Chem.Soc. Dalton Trans., 1095, 1986. b) R. Minkwitz, V. Gerhard, R. Krause, H. Prenzel, H. Preut, Z.Anorg.Allg.Chem., **559**, 154, 1988. c) R. Minkwitz, R. Krause, H. Preut, Z.Anorg.Allg.Chem., **571**, 133, 1989.
109. C.R. Russ, I.B. Douglass, in Sulfur in Organic and Inorganic Chemistry, A. Senning, Ed., Marcel Dekker, Inc. New York, 1971, p. 248.
110. R.T. Oakley, Prog. Inorg. Chem., **36**, 299, 1988.
111. I. Ernest, W. Holick, G. Rihs, D. Schomburg, G. Shoham, D. Wenkert, R.B. Woodward, J. Am. Chem. Soc., **103**, 1540, 1981.
112. R. Gleiter, Angew. Chem., Int. Ed. Engl., **20**, 444, 1981.
113. J. Bojes, T. Chivers, A.W. Cordes, G. MacLean, R.T. Oakley, Inorg. Chem., **20**, 16, 1981.
114. a) N. Burford, T. Chivers, P.W. Coddling, R.T. Oakley, Inorg. Chem., **21**, 982, 1982. b) N. Burford, T. Chivers, J.F. Richardson, Inorg. Chem., **22**, 1482, 1983. c) T. Chivers, M. Edwards, M. Parvez, Inorg. Chem., **31**, 1861, 1992.
115. a) R. Gleiter, R. Bartetzko, D. Cremer, J. Am. Chem. Soc., **106**, 3437, 1984. b) J.P. Boutique, J. Riga, J.J. Verbist, J. Delhalle, J.G. Fripiat, R.C. Haddon, M.D. Kaplan, J. Am. Chem. Soc., **106**, 312, 1984. c) S. Millefori, A. Millefori, G. Granozzi, Inorg. Chim. Acta, **90**, L55, 1984.
116. T. Chivers, I. Vargas-Baca, T. Ziegler, P. Zoricak, J. Chem. Soc., Chem. Commun., 949, 1996.

117. C. Bessenbacher, W. Kaim, J. Chem. Soc., Chem. Commun., 469, 1989.
118. S.R. Harrison, R.S. Pilkington, L.H. Sutcliffe, J. Chem. Soc., Faraday Trans. 1, **80**, 669, 1984
119. E.T. Strom, G.A. Russell., J. Am. Chem. Soc., **87**, 3326, 1965.
120. J.M. Rawson, A.J. Banister, I. Lavender, Adv. Heterocyclic Chem., **62**, 137, 1995.
121. W.V.F. Brooks, N. Burford, J. Passmore, M.J. Schriver and .H. Sutcliffe, J. Chem. Soc., Chem. Commun., 69, 1987.
122. P.J Hayes, R.T Oakley, A.W. Cordes, W.T. Pennington, J. Am. Chem. Soc., **107**, 1346, 1985.
123. A.W. Cordes, H. Koenig, R.T. Oakley, J. Chem. Soc., Chem. Commun., 710, 1989.
124. A.W. Cordes, K.T. Bestari, R.T. Oakley, J. Chem. Soc., Chem. Commun., 1328, 1988.
125. S. Kagoshima, H. Nagasawa, T. Sambongi, One Dimensional Conductors, Springer Verlag, London, 1988.
126. J.M. Williams, J.R. Ferraro, R.J. Thorn, K.D. Carlson, U.Geiser, H.H. Wang, A.M. Kini, and M.H. Whangbo. Organic Superconductors (Including Fullerenes). Synthesis, Structure, Properties and Theory. Prentice Hall, Englewood Ciffs, N.J., 1992.
127. a) R.C. Haddon, Nature, **256**, 394, 1975. b) R.C. Haddon, Aust. J. Chem., **28**, 2343, 1975. c) A.W. Cordes, R.C. Haddon, R.T. Oakley, in The Chemistry of Inorganic Ring Systems, R. Steudel (Ed.), Elsevier, Amsterdam, 1992, Chapter 16.

128. a) R.T Oakley, *Can. J. Chem.*, **71**, 1775, 1993. b) C.D. Bryan, A.W. Cordes, R.M. Fleming, N.A. George, S.H. Glarum, R.C. Haddon, R.T. Oakley, T.T.M. Palstra, A.S. Perel, L.F. Schneemeyer, J.V. Waszczak, *Nature*, **365**, 821, 1993.
129. C.D. Bryan, A.W. Cordes, J.D. Goddard, R.C. Haddon, R.G. Hicks, C.D. MacKinnon, R.C. Mawhinney, R.T. Oakley, T.T.M. Palstra, A.S. Perel, *J. Am. Chem. Soc.*, **118**, 330, 1996.
130. A.W. Cordes, C.D. Bryan, W.M. Davis, R.H. de Laat, S.H. Glarum, J.D. Goddard, R.C. Haddon, R.G. Hicks, D.K. Kennepohl, R.T. Oakley, S.R. Scott, N.P.C. Westwood, *J. Am. Chem. Soc.*, **115**, 7232, 1993.
131. E.G. Awere, N. Burford, R.C. Haddon, S. Parsons, J. Passmore, J.V. Waszczak, P.S. White, *Inorg. Chem.*, **29**, 4821, 1990.
132. V. Chandrasekhar, T. Chivers, unpublished results, 1991.
133. V. Chandrasekhar, I. Vargas-Baca, T. Chivers, T. Ziegler, *Phosphorus, Sulfur and Silicon*, **93-94**, 445, 1994.
134. J. Sundermeyer, H.W. Roesky, M. Noltemeyer, *Can. J. Chem.*, **67**, 1785, 1989.
135. T. Chivers, S. Gamble, unpublished results.
136. M.J. Baker-Hawkes, E. Billing, H.B. Gray, *J. Am. Chem. Soc.*, **88**, 21, 1966
137. E.J. Wharton, J.A. McCleverty, *J. Chem. Soc. A.*, 2258, 1969.
138. J.L. Morris, C.W. Rees, *J. Chem. Soc., Perkin Trans. 1*, 211, 1987.
139. B. Dietrich, P. Viout, J.-M. Lehn, *Macrocyclic Chemistry*, VCH, Weinheim, Germany, 1993, p. 176.

140. a) M. Dobler, R.P. Phizackerley, Acta Crystallogr., Sect.B, **30**, 2748, 1974. b) S.B. Dawes, D.L. Ward, O. Fussa-Rydel, R.H. Huang, J.L. Dye, Inorg. Chem., **28**, 2132, 1989. c) R.H. Huang, D.L. Ward, M.E. Kuchenmeister, J.L. Dye, J. Am. Chem. Soc., **109**, 5561, 1987. d) N.E. Brese, C.R. Randall, J.A. Ibers, Inorg. Chem., **27**, 940, 1988. e) P.R. Mallinson, J. Chem. Soc., Perkin Trans. 2, 261, 1975. f) J. Hasek, D. Hlavata, K. Huml, Acta Crystallogr., Sect.B, **33**, 3372, 1977. g) S. Magull, B. Neumuller, K. Dehnicke, Z. Naturforsch., Teil B, **46**, 985, 1991. h) P.J. Dutton, T.M. Fyles, V.V. Suresh, F.R. Fronczek, R.D. Gandour, Can. J. Chem., **71**, 239, 1993. i) M. Clark, C.J. Kellen-Yuen, K.D. Robinson, H. Zhang, Z.-Y. Yang, K.V. Madappat, J.W. Fuller, J.L. Atwood, J.S. Thrasher, Eur. J. Solid State Inorg. Chem., **29**, 809, 1992. j) V. Muller, A. Ahle, G. Frenzen, B. Neumuller, K. Dehnicke, D. Fenske, Z. Anorg. Allg. Chem., **619**, 1247, 1993.
141. T. Shimizu, K. Iata, H. Murakani, N. Kamigata. Book of Abstracts, 17th International Symposium on the Organic Chemistry of Sulfur. The Chemical Society of Japan. Tsukuba, Japan, July 7-12, 1996. p. 96.
142. G.H. Brooke, B.S. Furniss, W.K.R. Musgrave, Md.A. Quasem, Tetrahedron Letters, 2991, 1965.
143. A. Callaghan, A.J. Layton, R.S. Nyholm, J. Chem. Soc., Chem. Commun., 399, 1969.
144. N.J. Long, Angew. Chem. Int. Ed. Engl., **34**, 21, 1995.
145. a) B.L. Davydov, L.D. Derkacheva, V.V. Dunina, M.E. Zhabotinskii, V.F. Zolin, L.G. Koreneva, M.A. Samokhina, Opt. Spectrosc. Engl. Trans., **30**, 503, 1971. b) B.L.

- Davydov, V.V. Dunina, V.F. Zolin, L.G. Koreneva, Opt. Spectrosc. Engl. Trans., **34**, 267, 1973.
146. S.R. Sandler, W. Karo, Organic Functional Group Preparations. 2nd Ed. Academic Press, San Diego, 1989, Chapters 6,8.
147. S.M. McElvain, C.L. Stevens, J. Am. Chem.Soc., **68**, 1917, 1946.
148. K.R. Huffman, F.C. Schaefer, J.Org. Chem., **28**, 1816, 1963.
149. G.W. Kenner, R.J. Stedman, J. Chem. Soc., 2089, 1952.
150. B. Stanovnik, in Comprehensive Organic Functional Group Transformations, A.R. Kutritzky, O. Meth-Cohn, C.W. Rees, J. Moody (ed.), Pergamon, Oxford, 1995, Chapter 5.21, pp. 847-850.